AMMRC CR 70-14(F)

INVESTIGATION OF THE APPLICATION OF COHERENT ACOUSTIC IMAGING TO NONDESTRUCTIVE TESTING

April 1971

W.R. Arndt and J.L. Kreuzer
The Perkin-Elmer Corporation
Optical Group, Research
Norwalk, Connecticut

Final Technical Report - Contract DAAG46-69-C-0010
Sponsored by
Advanced Research Projects Agency
ARPA Order No. 1245
Program Code No. 19D10

Prepared for

ARMY MATERIALS AND MECHANICS RESEARCH CENTER
Watertown, Massachusetts 02172

The findings in this report are not to be construed as an official Department of the Army position, unless so designated by other authorized documents.

Mention of any trade names or manufacturers in this report shall not be construed as advertising nor as an official indorsement or approval of such products or companies by the United States Government.

DISPOSITION INSTRUCTIONS

Destroy this report when it is no longer needed.
Do not return it to the originator.

UNCLASSIFIED

Security Classification

DOCUMENT CONTROL DATA - R&D

(Security classification of title, body of abstract and indexing annotation must be entered when the overall report is classified)

1. ORIGINATING ACTIVITY *(Corporate author)*

The Perkin-Elmer Corporation
Optical Group, Research
Norwalk, Connecticut 06856

2a. REPORT SECURITY CLASSIFICATION

Unclassified

2b. GROUP

3. REPORT TITLE

INVESTIGATION OF THE APPLICATION OF COHERENT ACOUSTIC IMAGING TO NONDESTRUCTIVE TESTING

4. DESCRIPTIVE NOTES *(Type of report and inclusive dates)*

Final Report - November, 1968 through August 1970

5. AUTHOR(S) *(Last name, first name, initial)*

Arndt, Walter R. and
Kreuzer, Justin L.

6. REPORT DATE	7a. TOTAL NO. OF PAGES	7b. NO. OF REFS
April 1971	126	13

8a. CONTRACT OR GRANT NO.	9a. ORIGINATOR'S REPORT NUMBER(S)
Contract DAAG46-69-C-0010	CR AMMRC [redacted] 70-14(F)
b. PROJECT NO. Program Code No. 19D10	
c. TASK	9b. OTHER REPORT NO(S) *(Any other numbers that may be assigned this report)*
d. ARPA Order No. 1245	10462

10. AVAILABILITY/LIMITATION NOTICES

Approved for public release; distribution unlimited.

11. SUPPLEMENTARY NOTES	12. SPONSORING MILITARY ACTIVITY
Prepared for Army Materials and Mechanics Research Center, Watertown, Mass. 02172	Advanced Research Projects Agency

13. ABSTRACT

The purpose of this research program was to analyze and perform experimental demonstrations of the application of ultrasonic holographic and ultrasonic light diffraction techniques to the detection, analysis, and examination of the interval structure of optically opaque materials. A holographic scanner, operated in several modes, was used to produce more than 130 holograms, which were illuminated with a laser to reconstruct visible acoustic images. Several configurations of a Bragg diffraction microscope were used to produce comparison images. Techniques for real time computer constructed images were demonstrated. This report includes details of the analyses and experiments and indicates design approaches for practical nondestructive testing systems.

Details of illustrations in this document may be better studied on microfiche

DD FORM 1 JAN 64 1473

UNCLASSIFIED

Security Classification

14. KEY WORDS	LINK A		LINK B		LINK C	
	ROLE	WT	ROLE	WT	ROLE	WT
Nondestructive Testing Ultrasonics Acoustics Holography Acoustic Holography Bragg Diffraction Fast Fourier Transforms Scanners Light Modulators						

INSTRUCTIONS

1. ORIGINATING ACTIVITY: Enter the name and address of the contractor, subcontractor, grantee, Department of Defense activity or other organization *(corporate author)* issuing the report.

2a. REPORT SECURITY CLASSIFICATION: Enter the overall security classification of the report. Indicate whether "Restricted Data" is included. Marking is to be in accordance with appropriate security regulations.

2b. GROUP: Automatic downgrading is specified in DoD Directive 5200.10 and Armed Forces Industrial Msnual. Enter the group number. Also, when applicable, show that optional markings have been used for Group 3 and Group 4 as authorized.

3. REPORT TITLE: Enter the complete report title in all capital letters. Titles in all cases should be unclassified. If a meaningful title cannot be selected without classification, show title classification in all capitals in parenthesis immediately following the title.

4. DESCRIPTIVE NOTES: If appropriate, enter the type of report, e.g., interim, progress, summary, annual, or final. Give the inclusive dates when a specific reporting period is covered.

5. AUTHOR(S): Enter the name(s) of author(s) as shown on or in the report. Enter last name, first name, middle initial. If military, show rank and branch of service. The name of the principal author is an absolute minimum requirement.

6. REPORT DATE: Enter the date of the report as day, month, year, or month, year. If more than one date appears on the report, use date of publication.

7a. TOTAL NUMBER OF PAGES: The total page count should follow normal pagination procedures, i.e., enter the number of pages containing information.

7b. NUMBER OF REFERENCES: Enter the total number of references cited in the report.

8a. CONTRACT OR GRANT NUMBER: If appropriate, enter the applicable number of the contract or grant under which the report was written.

8b, 8c, & 8d. PROJECT NUMBER: Enter the appropriate military department identification, such as project number, subproject number, system numbers, task number, etc.

9a. ORIGINATOR'S REPORT NUMBER(S): Enter the official report number by which the document will be identified and controlled by the originating activity. This number must be unique to this report.

9b. OTHER REPORT NUMBER(S): If the report has been assigned any other report numbers *(either by the originator or by the sponsor)*, also enter this number(s).

10. AVAILABILITY/LIMITATION NOTICES: Enter any limitations on further dissemination of the report, other than those imposed by security classification, using standard statements such as:

(1) "Qualified requesters may obtain copies of this report from DDC."

(2) "Foreign announcement and dissemination of this report by DDC is not authorized."

(3) "U. S. Government agencies may obtain copies of this report directly from DDC. Other qualified DDC users shall request through

_____."

(4) "U. S. military agencies may obtain copies of this report directly from DDC. Other qualified users shall request through

_____."

(5) "All distribution of this report is controlled. Qualified DDC users shall request through

_____."

If the report has been furnished to the Office of Technical Services, Department of Commerce, for sale to the public, indicate this fact and enter the price, if known.

11. SUPPLEMENTARY NOTES: Use for additional explanatory notes.

12. SPONSORING MILITARY ACTIVITY: Enter the name of the departmental project office or laboratory sponsoring *(paying for)* the research and development. Include address.

13. ABSTRACT: Enter an abstract giving a brief and factual summary of the document indicative of the report, even though it may also appear elsewhere in the body of the technical report. If additional space is required, a continuation sheet shall be attached.

It is highly desirable that the abstract of classified reports be unclassified. Each paragraph of the abstract shall end with an indication of the military security classification of the information in the paragraph, represented as *(TS), (S), (C), or (U).*

There is no limitation on the length of the abstract. However, the suggested length is from 150 to 225 words.

14. KEY WORDS: Key words are technically meaningful terms or short phrases that characterize a report and may be used as index entries for cataloging the report. Key words must be selected so that no security classification is required. Identifiers, such as equipment model designation, trade name, military project code name, geographic location, may be used as key words but will be followed by an indication of technical context. The assignment of links, rules, and weights is optional.

AMMRC CR 70-14(F)

INVESTIGATION OF THE APPLICATION OF COHERENT ACOUSTIC IMAGING TO NONDESTRUCTIVE TESTING

W.R. Arndt and J.L. Kreuzer
The Perkin-Elmer Corporation
Optical Group, Research
Norwalk, Connecticut

April 1971

Final Technical Report - Contract DAAG46-69-C-0010
Sponsored by
Advanced Research Projects Agency
ARPA Order No. 1245
Program Code No. 19D10

Approved for public release; distribution unlimited.

Prepared for

ARMY MATERIALS AND MECHANICS RESEARCH CENTER
Watertown, Massachusetts 02172

TABLE OF CONTENTS

TABLE OF CONTENTS (Continued)

LIST OF ILLUSTRATIONS

LIST OF ILLUSTRATIONS (Continued)

LIST OF ILLUSTRATIONS (Continued)

SECTION I

INTRODUCTION

A. BACKGROUND

This report is the Final Technical Report on Contract No. DAAG46-69-C-0010 with the U.S. Army Materials and Mechanics Research Center in Watertown, Massachusetts, and covers the period November 1968 through August 1970. This contract concerned a research program whose purpose was to analyze and perform experimental demonstrations of the application of ultrasonic holographic and ultrasonic light diffraction techniques to the detection, analysis, and examination of the internal structure of optically opaque materials. The program was funded by the Advanced Research Projects Agency, Washington, D.C.

Three semi-annual technical reports were prepared on the program covering the periods November 1968 through April 1969 (reference 1), May 1969 through October 1969 (reference 2) and November 1969 through April 1970 (reference 3). Although the essence of those reports is summarized in this Final Report, the interim reports should be referred to for additional details.

The research program under this contract follows the work accomplished by Perkin-Elmer during 1965-1968 under Contract Nos. DA-19-066-AMC-286(X) and DAAG46-67-0132(X). Under these earlier contracts Perkin-Elmer demonstrated the feasibility of the holographic technique in forming three-dimensional acoustic images of solid objects and their internal structure. The results of the earlier work are published in the contract technical reports, references (4) and (5), and in the technical literature, references (6), (7), and (8).

B. SUMMARY OF WORK ACCOMPLISHED

During this contract the breadboard electronic circuits for the holographic scanner were completely redesigned and rebuilt, so that the system would be more stable and reliable, and would have a greater operating flexibility. A new water tank, fabricated on a Perkin-Elmer IR&D program and loaned to this contract, contributed to the ease of operation of the system, and enabled some longer range testing to be accomplished. The mechanical scanner was also modified to permit off-axis holograms to be generated.

Upon completion of system modifications, the holographic scanner was used in several modes of operation to explore techniques for NTD, and to evaluate the capabilities and limitations of the holographic imaging process. Over 130 holograms were generated during this work, using combinations of transmission modes, types of specimens, and system operating parameters.

Development of the 35 mm hologram negatives was accomplished by a Versamat automatic processor instead of by hand, as had been done previously, and very uniform results were obtained. Image reconstruction was done with the same laser and optical bench as had been used before, but several methods of optical filtering were tried and evaluated. The effect of the sound-to-light wavelength scaling error on image reconstruction was also analyzed.

In order to compare the performance of the holographic technique with that of the Bragg diffraction technique, several configurations of a Bragg diffraction microscope were constructed, and their imaging capabilities evaluated. The ultimate configuration utilized a spherical mirror with cylindrical optics, and presented its output on a TV tube display. A theoretical analysis of the Bragg diffraction imaging relationships accompanied the experimental work.

Although the generation of acoustic holograms by means of a mechanical scanner is entirely adequate for experimental work in the laboratory, the length of time required to scan the required aperture mechanically might be prohibitive for many NDT applications. Therefore, an investigation was made of acoustic arrays for real-time imaging. Arrays were simulated by sampling available holograms. Images of simple objects were then constructed by means of a digital computer, using the Fast Fourier Transform (FFT) algorithm.

C. SUMMARY OF RESULTS ACHIEVED

The experiments performed on this program were aimed at improving the acoustic holographic system and evaluating its practicality for NDT applications. They accomplished this through the investigation of several system configurations and modes of operation, using representative simulated defects and a variety of test conditions. Over 130 holograms were generated and evaluated while performing the experiments.

Since it is very desirable that any test equipment made for NDT applications not require the mounting of a transducer on the specimen, or the alteration of the specimen in any way, one of the first series of tests conducted was a comparison of the contact and immersion techniques for "illuminating" the specimen. In the contact technique, the transmitting transducer is mounted on a relatively flat surface of the specimen, while in the immersion technique the transmitting transducer is placed in the water near the specimen. Most of the early work done with our system had been done using the contact technique.

The results of these experiments proved that the immersion technique was superior to the contact technique in every way, and this technique was used exclusively for the remainder of the tests. The immersion technique allows a higher gain transmitting transducer to be used for illumination, and enables the incident angle of the impinging wave to be easily changed and controlled. Illumination of any surface can be quickly accomplished by simply rotating or moving the specimen, and there is no coaxial transmitting cable to interfere with the scattered sound field.

The primary disadvantage of the immersion technique is also shared by the contact technique, and that is the difficulty in properly coupling through a curved surface of a specimen. For production testing, special curved transducers could be used in either case. However, for general purpose testing, the immersion transducer can always be oriented to produce an image, even though it may be somewhat distorted.

Another technique implemented and tested during this program was the monostatic mode of transmission used by conventional radar systems. In this transmission mode the transmitter and receiver are co-located so that the transmission and receiving paths to the target are essentially identical. All previous work on our system had made use of the bistatic transmission mode, in which the transmitter and receiver sites are separated by distances comparable to the transmitter-to-target distance. The transmission and reception paths are normally quite different in this mode.

It was expected that the use of monostatic, or two-way, transmission would greatly improve the performance of the holographic system operating with the immersion technique, since this configuration is essentially that used by side-looking sonars and side-looking airborne radars. The resolution of the system is theoretically double that of the bistatic mode for the same size aperture, and the difficulty of illuminating the entire volume of a specimen should not exist. By using a duplexer, it also should be possible to transmit and receive from a common antenna.

The results, however, were very disappointing. Although the top surfaces of the various specimens produced excellent holograms and reconstructed images, defects below the surface could barely be discerned. The reason for this lack of signal strength stems from the low gain receiving and transmitting transducers which must be used in the holographic scanning system if a high resolution and wide field of view are to be obtained. The gain of the transmitting transducer could have been increased somewhat without degrading the resolution too badly, and this would have been done had there been time. There is no question that this mode of transmission has many advantages and should be seriously considered for future holographic NDT systems.

The first holograms created by D. Gabor in 1948 utilized a coherent sample of the transmitted signal to interfere with the received signal and form a hologram. This mode of reference has continued to be employed on elementary holographic systems, both optical and acoustic, and was used in all of the basic work on this program. However, this technique has the disadvantage of superimposing the wanted image on top of the defocused conjugate image, and places both coincident with the zero-order undiffracted light. Improvements in the holographic system can be realized by modifying the reference signal. This modification, use of an off-axis reference signal, was incorporated in the holographic system, further enhancing its performance. The off-axis reference improves the reconstruction of images by separating the wanted image from its interfering conjugate image and from the zero-order light. Images from holograms generated with this reference had much less interfering background than those created from on-axis holograms. For this reason, complex images were more easily separated and identified.

During the course of the experiments outlined herein to evaluate and improve the ultrasonic holographic scanner, side investigations were also made of the Bragg diffraction imaging technique and real-time imaging by means of a computer. The latter study was accomplished on a related Perkin-Elmer IR&D study. Both studies produced fruitful results: the Bragg system study in pointing the way toward simplified non-scanning imaging systems, and the computer imaging investigation by advancing techniques for real-time imaging utilizing electronically-scanned arrays.

D. CONCLUSIONS

Based on the results obtained from the improvement and evaluation of the ultrasonic holographic system as reported on this contract, Perkin-Elmer is convinced that the ultrasonic holographic technique can be of value in nondestructive testing applications. Although this judgement relies on work carried out almost entirely with simulated defects of elementary shapes, the demonstrated performance of the system against those defects leads to the conclusion that the approach is sound, and that practical NDT equipment using this technique can be developed.

The experiments and tests performed with the system have shown that it has the sensitivity to detect small cracks and voids, and that adequate resolution can be attained for most applications with aperture sizes of less than a foot square. The work has also demonstrated that the illuminating transducer need not be mounted on the specimen, or the specimen modified in any way to accomplish NDT tests. This is important for the design of practical equipment.

The system has also been operated successfully with the transmitting and receiving transducers co-located on the scanning carriage, and also with an off-axis signal reference. Two-way (monostatic) transmission doubles the resolution of the system and provides for better illumination, leading to results such as are being obtained with side-looking sonar and airborne side-looking radar systems. Operation with the off-axis reference provides for higher signal-to-noise ratios in the reconstructed image and better image reconstruction through optical filtering.

Although only limited tests were performed in the two-way transmission mode, and the results were not as dramatic as had been expected, it is felt that with a slight increase in transmitting power and transmitting transducer gain, the expected increase in performance would be obtained.

Evaluation of the system on this contract has also demonstrated some of the disadvantages of the ultrasonic holographic system. These include the relatively long time required to generate a hologram with the present equipment, the fact that this requires a camera and film, the necessity for optical reconstruction as a separate operation after the specimen is scanned and, finally, the complications normally present with conventional pulse-echo testing. State-of-the-art developments in array technology and computer imaging will provide solutions to the first three of these problems: additional

testing with the present equipment, using actual samples of defects, is recommended to resolve the latter.

What kind of an ultrasonic holographic system would be practical for NDT testing? It is envisioned that the development of such equipment would be based on the immersion technique tested on this program, using a test tank with transmitting transducers installed in its walls and bottom. The specimen to be analyzed would be placed in the tank and holograms generated from several aspects, by use of the various transducers installed. The transducers could be switched manually or time-shared in more sophisticated systems. In this manner the entire volume of the specimen could be searched, and several views of the defect image presented. The excitation of logitudinal and transverse waves would have to be controlled, just as in present-day pulse-echo analysis.

In the early stages of such development, a simple mechanical scanner installed in the cover could be used, possibly adopted from some of the small automatic pen plotters now readily available. However, if the equipment is to reach the level of utility required, the mechanical scanner and camera attachment would have to be replaced by an electronic scan with cathode-ray tube or similar form of readout. Eventually, an all-computer system could probably be realized.

An attractive intermediate step would be the replacement of one scan dimension by a long strip array of point transducers. This strip array would be "push-broomed" mechanically in the orthogonal direction of scan, producing a hybrid electro-mechanical system which would be capable of scanning a hologram in a matter of seconds. Such acoustic transducer arrays have already been fabricated by edge-slicing strips of piezoelectric material. With integrated circuit techniques the transducer preamps and the scanning circuitry could be integrated with the array, as is now being done with optical photodiode and photo-transistor arrays.

The ultimate system would use a two-dimensional array sampled electronically, with the electrical signal outputting directly to a special-purpose computer. The computer would take the Fast Fourier Transform of the sampled acoustic field and produce an image. The results of the computer imaging experiment reported on this program indicate that such an imaging system is entirely feasible.

SECTION II

ULTRASONIC HOLOGRAPHIC SYSTEM

A. THEORY OF OPERATION

1. General

Basically, a hologram is a recording which, when illuminated from a monochromatic point source (i.e., a source of radiation which is both temporally and spatially coherent), reacts with the illuminating radiation in such a way as to create a multiplicity of new wavefronts corresponding both in strength and apparent source position to all points in the scene which was recorded. This is the operation which has been called "wavefront reconstruction." In order for a hologram to reconstruct wavefronts, it is necessary that the hologram store data on both the phase and amplitude of all wavefronts originally emanating from the coherently illuminated scene being holographed.

If suitably carried out, there is no restriction in holography as to the type of radiation chosen for creating the hologram, or to the type of radiation used for illuminating the hologram in performing wavefront reconstruction. Thus, synthetic aperture radar holograms are made of the surface of the earth with microwave radiation. These holograms, when illuminated by means of coherent light, reconstruct wavefronts which may be perceived by the human eye. Thus, images of the two-dimensional radar scattering properties of the earth may be visually observed and/or recorded. In an exactly similar fashion, holograms may be recorded using coherent sound waves, and then utilized to perform wavefront reconstruction in the visible. Here the viewer sees an image whose intensity corresponds to the three dimensional scattering properties of an object originally "illuminated" by coherent sound. Because of the fact that sonic radiation propagates in many materials which are opaque to light, acoustic holography provides us with an opportunity to "look inside" these materials and see their internal structure.

An example of one method of forming a synthetic aperture acoustic hologram is shown in Figure 1. Here a block of material containing a localized acoustic scattering center or "hole" is illuminated by means of coherent sound. The scatterer produces a spherical wave emanating in all directions. This spherical wave may be picked up by a transducer scanning in an acoustically flat plane. If the output of this transducer is connected to a homodyne detector operating at the original acoustic frequency, then it is possible to detect both the amplitude and phase of the scattered sound. To record the acoustic hologram, a small lamp is made to mechanically track the scanning transducer. The emission

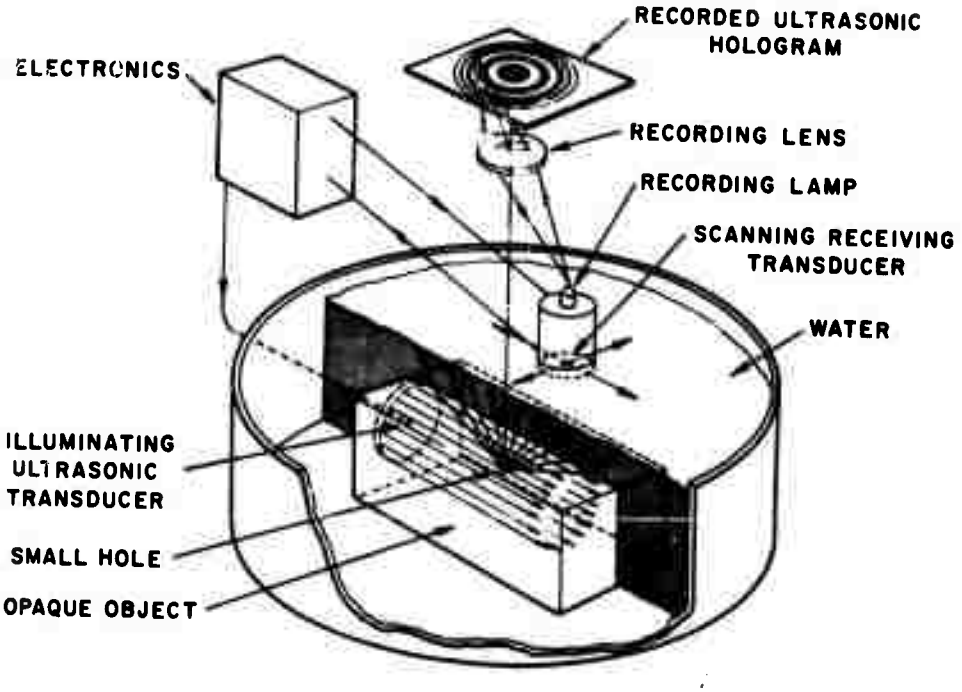

Figure 1. Ultrasonic Holographic Camera (Recording)

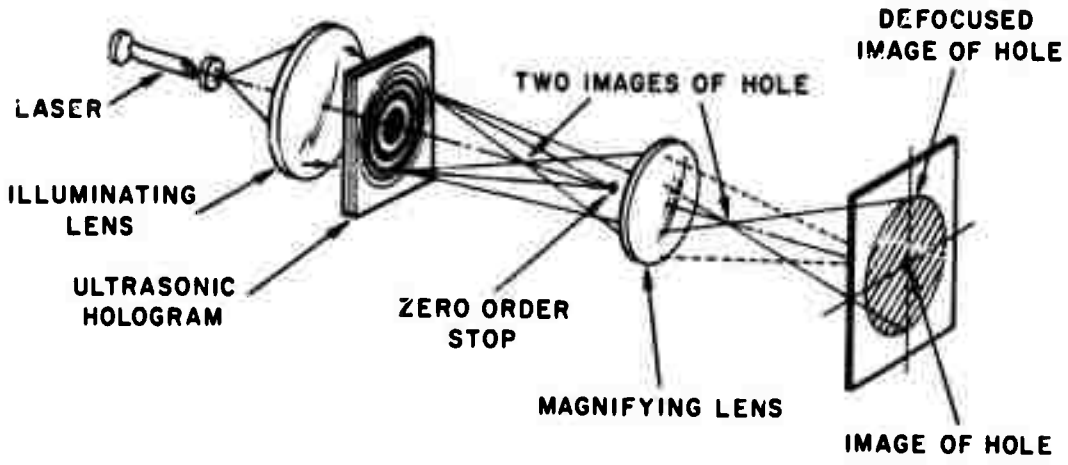

Figure 2. Ultrasonic Holographic Image Reconstruction (Imaging)

from the lamp is made to correspond on a point-by-point basis to the product of the sonic field amplitude with the cosine of the detected phase angle. When this is done for a point scatterer of sound (Figure 1), the resultant acoustic hologram is the well-known Fresnel zone plate.

The apparatus shown in Figure 2 shows how a hologram of a point scattering center may be used to reconstruct the original wavefront and, therefore, produce an image of the point scatterer which can be seen visually. The hologram is placed in a beam of coherent optical radiation (here produced by a laser). The zone plate has lens-like properties which cause it to focus some of the incident light to a point. A wavefront converging to a point is, of course, spherical and is the reconstruction (now by electromagnetic energy of optical wavelength) of the original acoustic wavefront. This optical wavefront produces a point image which may be viewed by an observer or recorded on photographic film. Note that the zone plate also reconstructs a diverging spherical wavefront yielding a second, or "virtual," image of the point scatterer. In acoustic holography light associated with the virtual image appears strongly defocussed in the plane of the real image and thus does not create an objectionable effect. Light which is not influenced by the hologram is removed from the imaging system by means of what is called a "zero-order stop" (see Figure 2).

An example of acoustic holography, illustrating its use in analyzing the internal structure of an object, is shown in Figure 3. Here a long slanted hole has been formed in an aluminum block. When coherent energy impinges on the hole, it is scattered and picked up by the scanning transducer. The type of hologram which results is shown schematically in Figure 3. An actual hologram made of an 8-cm long, one millimeter diameter hole in an aluminum block is shown in the upper portion of Figure 4. If this hologram is properly scaled in the recording process by the ratio of the acoustic wavelength used for holographing to the optical wavelength used for wavefront reconstruction, then the image produced at the optical wavelength would focus along a tilted line, now having a length in optical wavelengths as long as the original hole in acoustic wavelengths.

For an acoustic frequency of five megahertz, and a wavelength (in aluminum) of approximately 2 millimeters, the image of the hole is only 40 optical wavelengths long, or about 20 microns. Thus, the visible image formed is microscopic. As we view this image through the microscope we find that we have the usual depth-of-focus problems characteristic of any low f-number imaging system. This is amply illustrated in the left-hand image in Figure 5, which shows the holographic image of the slanted hole viewed at the upper end. As can be seen, only a portion of the image is in focus, whereas most of the image of the hole is in an extremely defocused position. In an attempt to solve the focusing problem, an experiment was performed wherein the viewing optical system was tilted so as to lie in the plane of the image of the hole. The resultant image is shown in the right-hand position of Figure 5, demonstrating how the image of the entire hole may be viewed at once.

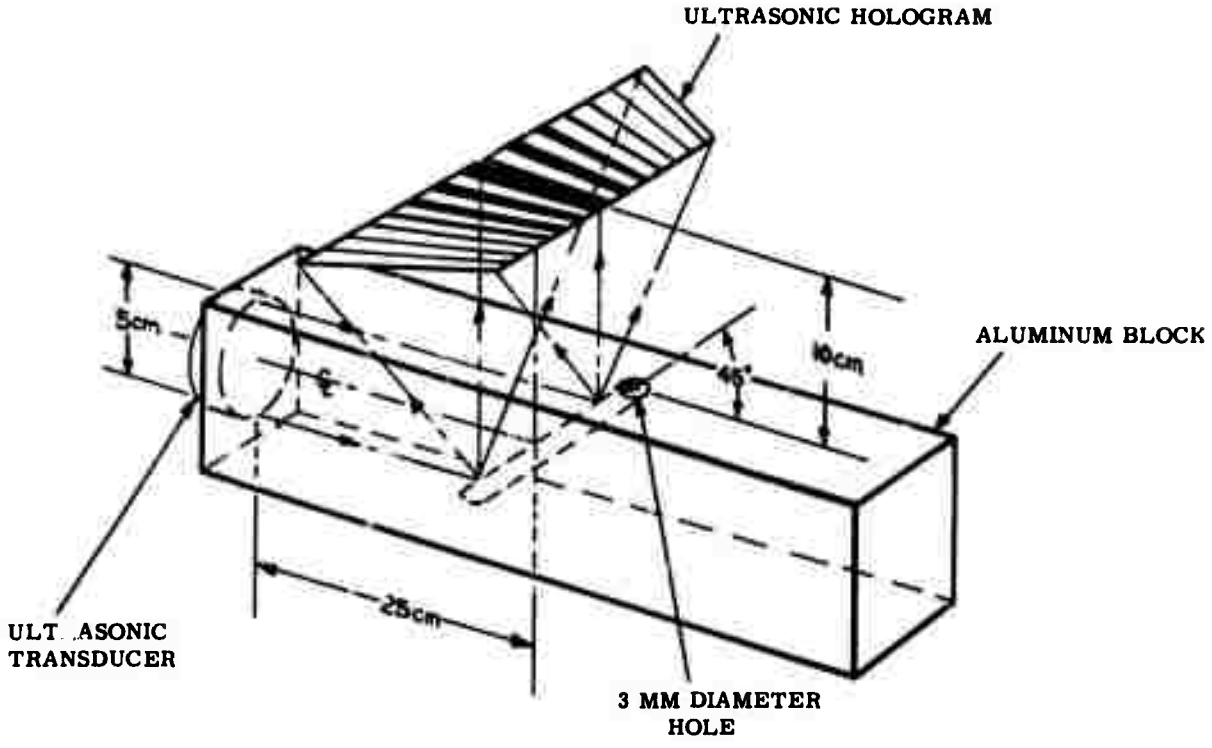

Figure 3. Recording an Acoustic Hologram of the Internal Structure of a Metal Block

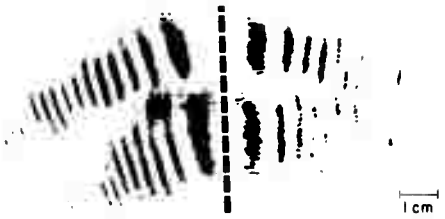

Figure 4. Actual Hologram of a Long Hole in an Aluminum Block

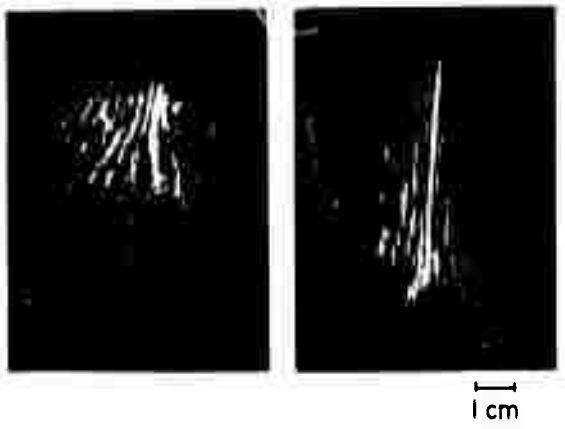

Figure 5. Images Formed from Figure 4 Using Two Different Imaging Techniques (Image Plane Parallel to Hologram vs Parallel to Hole)

2. Hologram Recording

The ultrasonic hologram formed using the ultrasonic holographic recorder is "range-gated", i.e., it is temporally sampled to eliminate undesired ultrasonic reflections such as those from the surfaces of the specimen and from the walls of the tank which contains the specimen. Without range-gating these reflections would completely mask scattering from the interior of the specimen. Range-gating produces a temporally and a spatially sampled ultrasonic hologram.

The following assumptions and notation are made to simplify this analysis. These assumptions do not appreciably reduce the applicability of the results.

(1) The analysis is presented in two dimensions.

(2) The transmitting and receiving transducers are assumed to be at the same location (i.e., scanning together).

(3) Phase and amplitude changes that are a function of the acoustic angle of incidence are ignored. The effect of these changes requires further study.

(4) The hologram reference is "on axis" (the hologram scan plane is the referenced phase plane).

(5) Acoustic attenuation due to energy absorbtion and spreading, and obliquity factors are ignored.

(6) Undefined constants will be denoted by C_i for $i = 0,1,2...$ as needed.

(7) The subscript ℓ stands for the ℓ^{th} pulse. τ will be used for variable time durations, and T for fixed time durations

The optical field transmittance $a_o(x)$ of an ideal ultrasonic hologram can be written as a weighted sum of sinusoidal zone plates. Each such zone plate of the sum can be written as

$$a_o(x) = C_o + C_1 \cos w_o \tau \tag{2-1}$$

where w_o is the ultrasonic temporal frequency and

$$\tau \equiv 2v^{-1}(x^2 + z^2)^{1/2} \tag{2-2}$$

is the time required for an ultrasonic pulse to travel at the velocity v from the transmitting transducer to an ultrasonic point scatterer and return to the receiving transducer. The spatial coordinates are (x.z). The point scatterer is located at (0,0). The hologram plane (line) is a distance $z > 0$ away from the point scatterer and parallel to the x axis.

The temporally sampled holograms are recorded to produce a spatially sampled optical field transmittance $a_1(x)$ of the following form

$$a_1(x) = \sum_{\ell} (b_\ell + C_2)s(x - x_\ell) \qquad (2\text{-}3)$$

where b_ℓ is the hologram sample produced by pulse number ℓ of L pulses; C_2 is a bias constant that satisfies the condition $b_\ell + C_2 \geq 0$ in order to keep the optical field transmittance positive; $s(x - x_\ell)$ is the recording point-spread function, or spatial optical field transmittance produced by the recording light exposure and includes the effect of the recording camera optics on the hologram centered at the point $x = x_\ell$.

The ultrasonic hologram recorder computes the hologram sample b_ℓ by the operations shown in Figure 6 and discussed next. The numerical subscripts on voltages (V) refer to the points circled in Figure 6.

The electrical reference voltage is

$$V_1 = \cos w_o t \qquad (2\text{-}4)$$

where t is time. The output voltage of the receiving transducer amplifier in response to ultrasonic pulse number ℓ can be written as the product

$$V_{2,\ell} = f(t-\ell T_1-\tau_\ell)\cos w_o(t-\tau_\ell) \qquad (2\text{-}5)$$

where f(t) is the "received pulse envelope function", including phase, at the output of the ultrasonic receiver transducer amplifier, and T_1 is the time between pulses. The ultrasonic pulse propagation delay is τ_ℓ, in analogy to Equation (2-2). In order to record a satisfactory hologram we require that f(t) be band-limited to frequencies less than w_o (i.e., have no energy for temporal frequencies greater than the ultrasonic temporal frequency). The received pulse envelope function includes the transmitted ultrasonic "pulse" frequencies as received through the temporal frequency response of the receiving transducer and the electrical amplifiers which follow. Only the composite envelope function is important.

Next we form the "heterodyne" product of the reference and the amplified received ultrasonic signal

$$V_{3,\ell} = V_1 V_{2,\ell} \qquad (2\text{-}6)$$

The low-pass filter temporally filters $V_{3,\ell}$ to retain temporal frequencies less than the ultrasonic frequency, but included in the band-limited received pulse envelope function. The filtered voltage $V_{4,\ell}$ can be idealized as the convolution integral

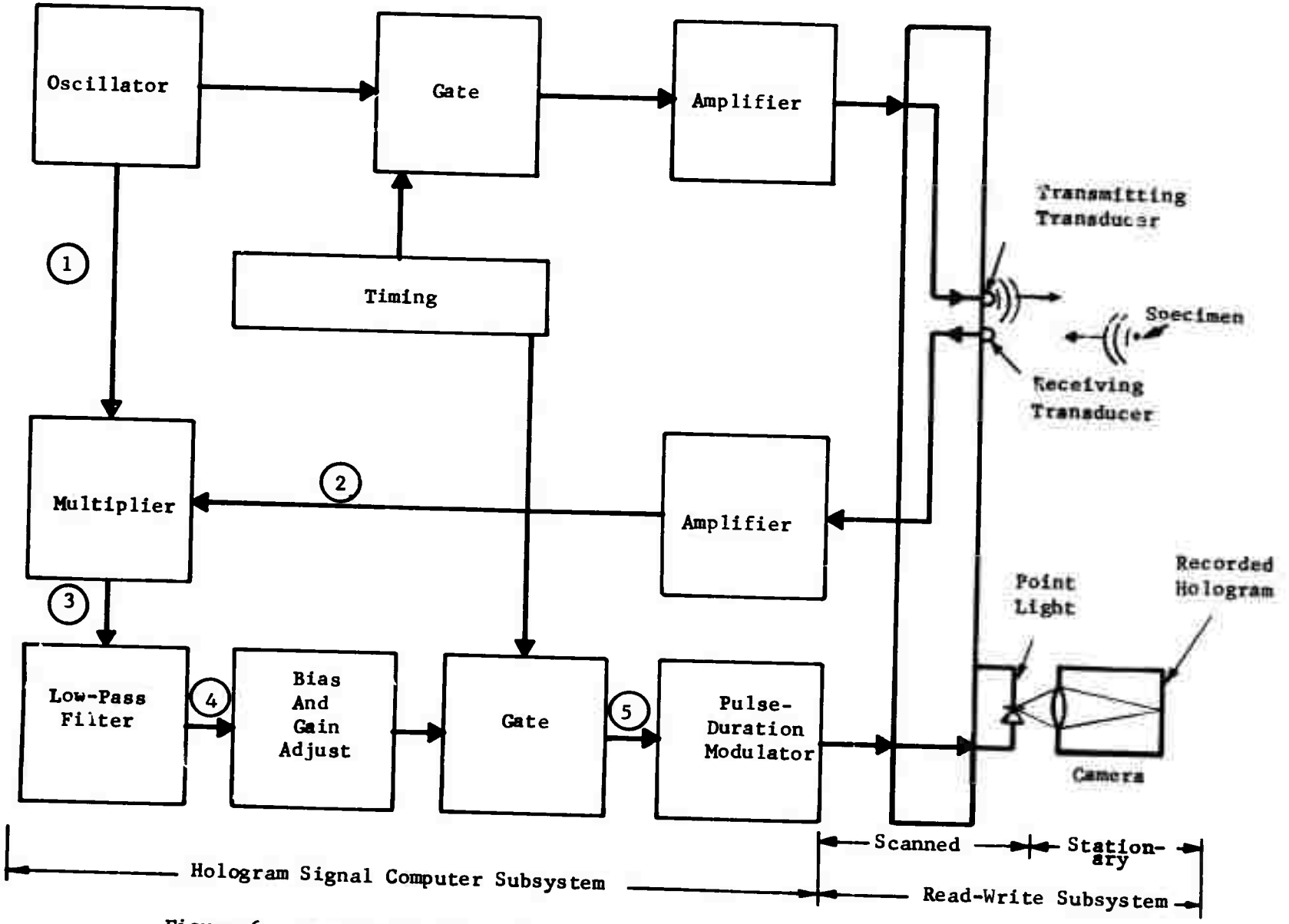

Figure 6. Functional Block Diagram - Ultrasonic Holographic Camera Recorder

$$V_{4,\ell} \int V_{3,\ell}(t-u)\frac{\sin w_o u}{\pi u}\,du \tag{2-7a}$$

$$\therefore f(t-\ell T_1-\tau_\ell)\cos w_o \tau_\ell \tag{2-7b}$$

We then adjust the gain, and add a bias to expose the photographic film over a linear range. We will ignore the gain and bias at this point.

We time gate the voltage $V_{4,\ell}$ to accomplish ultrasonic range gating which eliminates undesired echoes. The result of this time gating is

$$V_{5,\ell} = V_{4,\ell} g(t-\ell T_1-T_2) \tag{2-8}$$

where g(t) is the multiplicative receiver temporal gate function, and T_2 is the receiver delay time (separation between the transmitted pulse and the receiver gate function).

The ultrasonic hologram sample b_ℓ (and hence exposure) is proportional to the time integral of the voltage $V_{5,\ell}$. Our actual exposure is given by a constant brightness for a time proportional to b_ℓ, plus the bias constant. The exposure time for the ℓ^{th} hologram sample is

$$\tau_{1,\ell} = C_3\int V_{5,\ell}(t)\,dt + C_4 \tag{2-9a}$$

$$= C_3 h_\ell \cos w_c \tau_\ell + C_4 \tag{2-9b}$$

where

$$h_\ell = \int f(t+T_2-\tau_\ell)\, g(t)\,dt \tag{2-9c}$$

and

$(T_2-\tau_\ell)$ is the time difference between the ultrasonic pulse propagation delay time and the receiver gate delay time.

The correlation function (h_ℓ) is (the integral of) the coincidence time between the received ultrasonic pulse, which occurs at the varying ultrasonic pulse propagation delay times τ_ℓ as the transducers scan, and the fixed receiving delay gate time function. Equation (2-9c) shows that the role of the received pulse envelope and the receiver gate functions are interchangeable, and that the time between pulses, T_1, need not be constant from pulse to pulse.

The sampled hologram optical field transmittance can be written by combining Equations (2-3) and (2-9b) to yield a recorded zone plate transmittance of

$$a_1(x) = \sum_\ell (C_2 + C_5 h_\ell \cos w_o \tau_\ell) s(x-x_\ell). \tag{2-10}$$

This can be seen to be essentially a sampled version of the continuous sinusoidal zone plate given by Equation (2-1), except for the gate coincidence function (h_ℓ) which causes part (or all) of the zone plate to be absent if the received pulse envelope and gate functions do not coincide. It is normally desirable for h_ℓ to be a "smooth function." That is, the magnitude of the Fourier transform of h_ℓ should be small for frequencies greater than the reciprocal duration of h_ℓ. This means that both the received pulse envelope and the receiver gate function also should be smooth functions. The requirement for h_ℓ to be a smooth function will be apparent from the next section on image formation.

3. Image Formation

The visible image is formed by placing the recorded hologram transparency with the optical field transmittance given by Equation (2-10) in the optical system shown in Figure 2. If the sample spacings (x_ℓ) are very small and equal, the sum in Equation (2-10) becomes the convolution integral

$$a_2(x) = \int (C_2+C_5 h(u)\cos w_o\tau)\ s(x-u)du \tag{2-11a}$$

where Equation (2-9c) is replaced by

$$h(x) = \int f(t-T_2-\tau)g(t)dt \tag{2-11b}$$

and τ is a function of x(x=u in Equation (2-11a)). Equation (2-11a) can be written in complex notation as

$$a_2(x) = a_3(x) + a_3^*(x) + C_6 \tag{2-12}$$

where the star (*) denotes the complex conjugate. and

$$a_3(x) = C_7\int h(u)e^{jw_o\tau}\, s(x-u)du. \tag{2-13a}$$

We can expand the exponent as

$$w_o\tau \approx C_8+u^2B \tag{2-13b}$$

where

$$B = \frac{w_o}{vz} \tag{2-13c}$$

The real image is formed by $a_3(x)$, the virtual image by $a_3^*(x)$, and the zero order by C_6. In the appropriately scaled focal plane, the real image intensity $i(x)$ is given by the square of the optical field $u(x)$.

$$u(x) \quad \int a_3(v) e^{-jBv^2} e^{jvx} dv \tag{2-14a}$$

and

$$i(x) = |u(x)|^2. \tag{2-14b}$$

Equations (2-13a) through (2-14b) can be combined to yield

$$u(x) = C_9 \int H(x-2Bv) s(v) e^{j(xv-Bv^2)} dv \tag{2-15}$$

where

$$h(x) \leftrightarrow H(v) \tag{2-16}$$

are a Fourier transform pair.

We can neglect the phase term in Equation (2-15) because in a well designed system, both $H(v)$ and $s(v)$ are non-zero only for $v \approx 0$. This is true because the desired spatial extent of $h(x)$ is large and $s(x)$ small. This leads to the following two forms for the image optical field:

$$u(x) = C_{10} \int H(x-v) s\left(\frac{v}{2B}\right) dv \tag{2-17a}$$

$$= C_{11} \int h(w) S(2Bw) e^{jwx} dw \tag{2-17b}$$

We will discuss Equations (2-17a) and (2-17b) in some detail. The extent of the zone plate is determined by the spatial extent of the gate coincidence function $h(x)$. Equation (2-17a) gives the optical field image as the convolution of the scaled recording point-spread function and the Fourier transform of the zone plate extent. Equation (2-17b) gives the optical field image as the Fourier transform of the product of the zone plate extent and the Fourier transform of the scaled recording point-spread function. It is common to call $u(x)$ the coherent point-spread function. The Fourier transform $U(w_x)$ of $u(x)$ (where x and w_x are the Fourier transform variables. and w_x is the radian spatial frequency) is called the coherent modulation transfer function. From Equation (2-17b) we see that the coherent modulation transfer function is $h(w_x)S(2Bw_x)$.

The extent of $u(x)$ is small for a high resolution image. This implies that $h(x)$ should be a smooth function (as previously defined) of large extent, and $s(x)$ small in extent to record a zone plate of uniformly high modulation over a large extent. Once the extent of $s(x)$ is small enough there is no gain in making it smaller. However, $s(x)$ should not be too small, or else the linear dynamic range of the photographic record of the hologram will be reduced because the dynamic range of the film is a function of the area exposed.

Figure 7 shows the decrease in resolution for too large a recording point-spread function. The low resolution image (a) when s(x) is too large in extent is the image produced by a zone plate lens of smaller diameter than the zone plate for s(x) of smaller extent (b).

Next, we will examine the point image as a function of h(x) for s(x) sufficiently small to achieve high resolution. To do this we will approximate s(x) by a delta or impulse function, so that Equation (2-17b) becomes

$$u(x) = C_{11}\int h(w)e^{jwx}dw \qquad (2\text{-}18)$$

Figure 8A shows the effect of identical short gates [f(t) = g(t)]. Short gate times are times much less than the receiver delay time T_2. The corresponding spatial extent of f(t) and g(t) are shown. Five acoustic point scatters are shown at various distances from the receiving transducer. The receiver delay is optimized for the cross-hatched region centered at point (c). The gate coincidence function h(x) for these five points determines the fraction of the energy used to record the zone plate, as shown. Sound propagating within the marked angles is recorded. No hologram is recorded from point (a), because a real transducer will accept only sound within a certain acceptance angle (its antenna radiation pattern). The sound from (a) that corresponds to the non-zero values of h(x) is not recorded (shown as dashed lines), because the sound is assumed to be outside this acceptance angle. The three zone plates recorded (b,c,d) form images (at the appropriate distance) as shown magnified below their respective acoustic points. These images are enlarged and exaggerated to emphasize their different diffraction detail. These three points are the conventional point images for:

Example b - a conventional apodized or shaded zone plate lens with a large central obscuration. It exhibits high resolution with large amplitude side lobes.

Example c - a conventional apodized zone plate lens. It exhibits high resolution with small amplitude side lobes.

Example d - a conventional apodized zone plate lens of small extent. It exhibits low resolution.

Figure 8B shows images as a function of the received pulse envelope duration and the receiver gate duration for a point centered in the receiver gate. All other variables are held constant. The three cases show:

Example f - both gates short. It exhibits a low-resolution image.

Example g - either gate short and the other gate long. It exhibits a high-resolution image with side lobes, typical of a conventional zone plate lens.

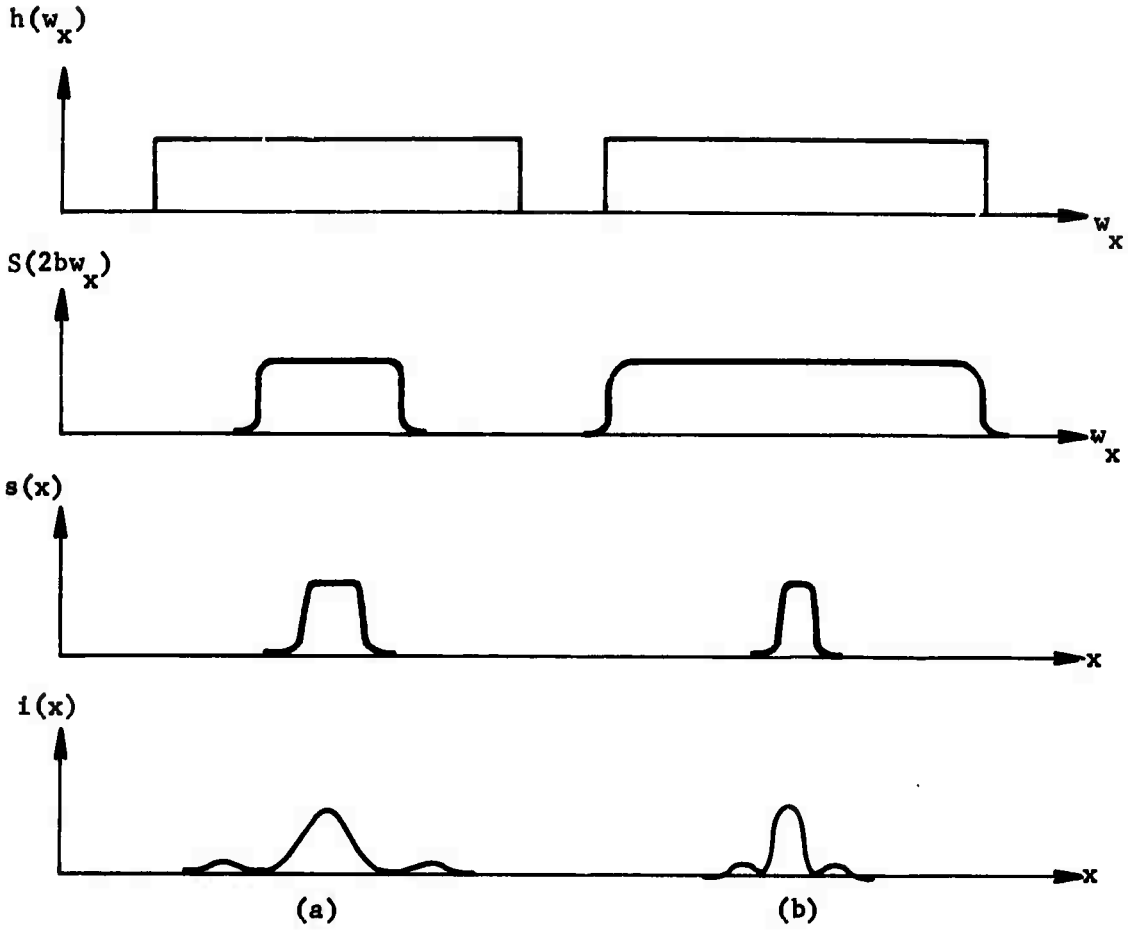

Figure 7. Point Images as a Function of the Recording Point-Spread Function

(a) Poor resolution caused by a recording point-spread function of too large an extent.

(b) Better resolution not limited by the recording point spread function.

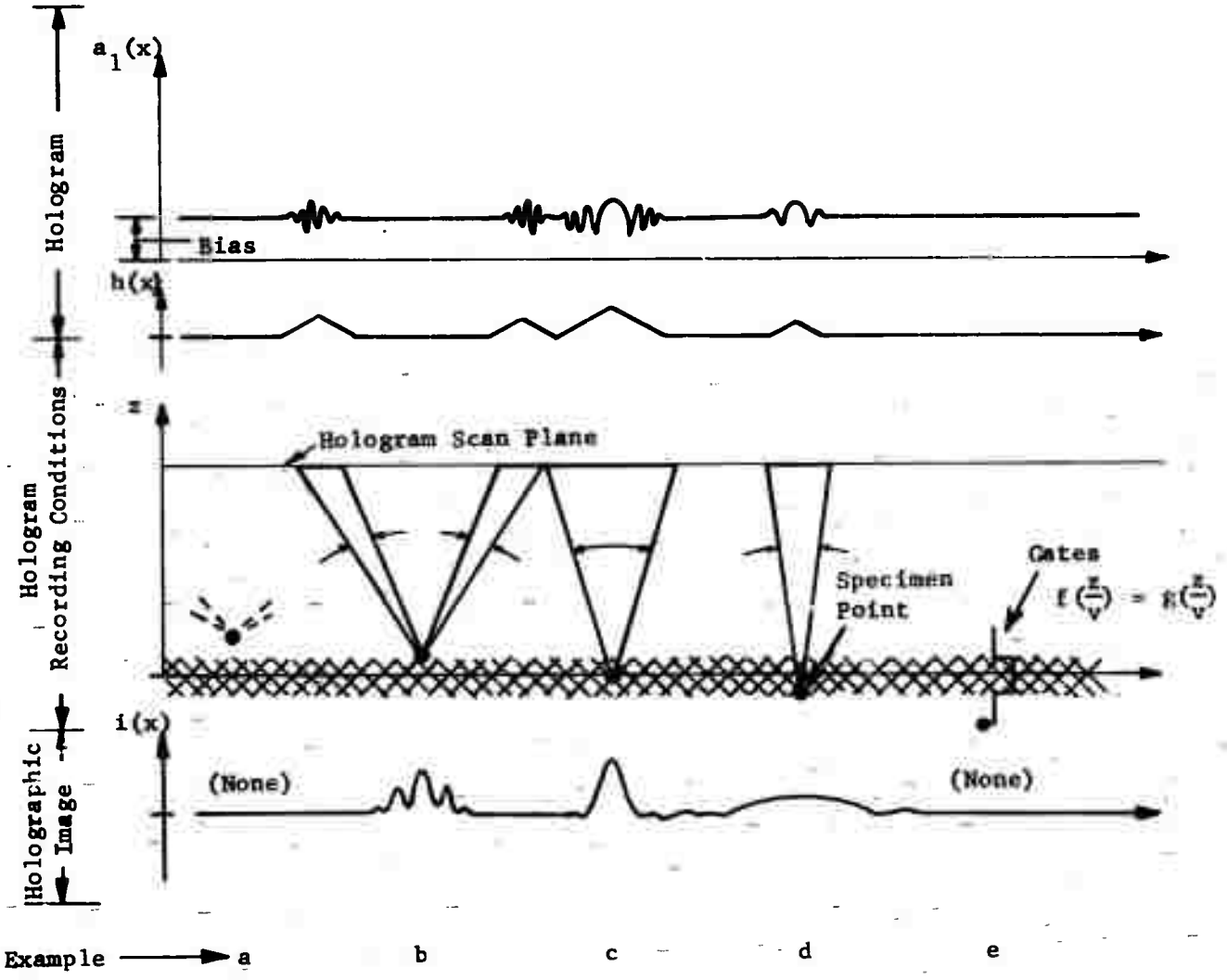

Figure 8A. Point Images as a Function of Range For Short Gates

Example h - both gates long. It exhibits a brighter high-resolution image with low amplitude side lobes, typical of an apodized zone plate lens.

The actual choice of available gate durations depends upon sample geometry and location, echo isolation and signal-to-noise considerations. Acoustic dispersion and attenuation inside a sample with high attenuation and/or scatter could be an important factor in some cases. A more detailed basis for the selection of gate durations must await further experimentation.

4. Summary

This section has described a simple set of parameters that yields a satisfactory holographic image. There is a fair degree of freedom in the detailed design of the system described. Certain other systems will also yield satisfactory ultrasonic holograms. At this time, these other variations seem to offer no apparent advantage. Violations of the conditions described to record a temporally sampled ultrasonic hologram will generally result in an inferior ultrasonic holographic image. The image may be degraded in two general ways (1) linearly and (2) nonlinearly.

Linear degradations include errors such as phase shifts and amplitude weighting over the hologram zone plates. In principle, linear degradation can be corrected in the recorded hologram by the use of inverse linear holographic spatial filtering, but one would like to avoid this. Factors which can contribute to linear degradation arise from all portions of the system, including the electrical circuits, the optical paths and the photographic film. Two areas requiring further study are (1) the amplitude and phase transmittance as a function of the acoustic angle of incidence through the water-to-specimen interface, and (2) the transmitting-receiving transducer phase and amplitude response as a function of angle.

Nonlinear degradation is not correctable, in general. However, nonlinear degradation can be considered within two classes: (1) nonlinearities uncorrelated to the desired hologram signals, and (2) nonlinearities correlated to the desired hologram signal. Basically, uncorrelated nonlinearities add a random background, or noise, to the image, while correlated nonlinearities add a nonrandom background. Nonlinearities correlated with the image are most undesirable.

There are many nonlinear system degradations which can affect overall system performance. It is important that the basic set of system parameters outlined earlier not be violated, and that excessive noise, time-dependent parameter changes (drift), electrical nonlinearities, limited dynamic range, photographic nonlinearities, and mechanical scanner motion irregularities be minimized.

Design tolerances for linear and nonlinear degradation factors are difficult to specify because of the lack of detailed ultrasonic holographic image data. However, these data are currently being collected. In the absence of this detailed information, conventional optical tolerances have been used for linear

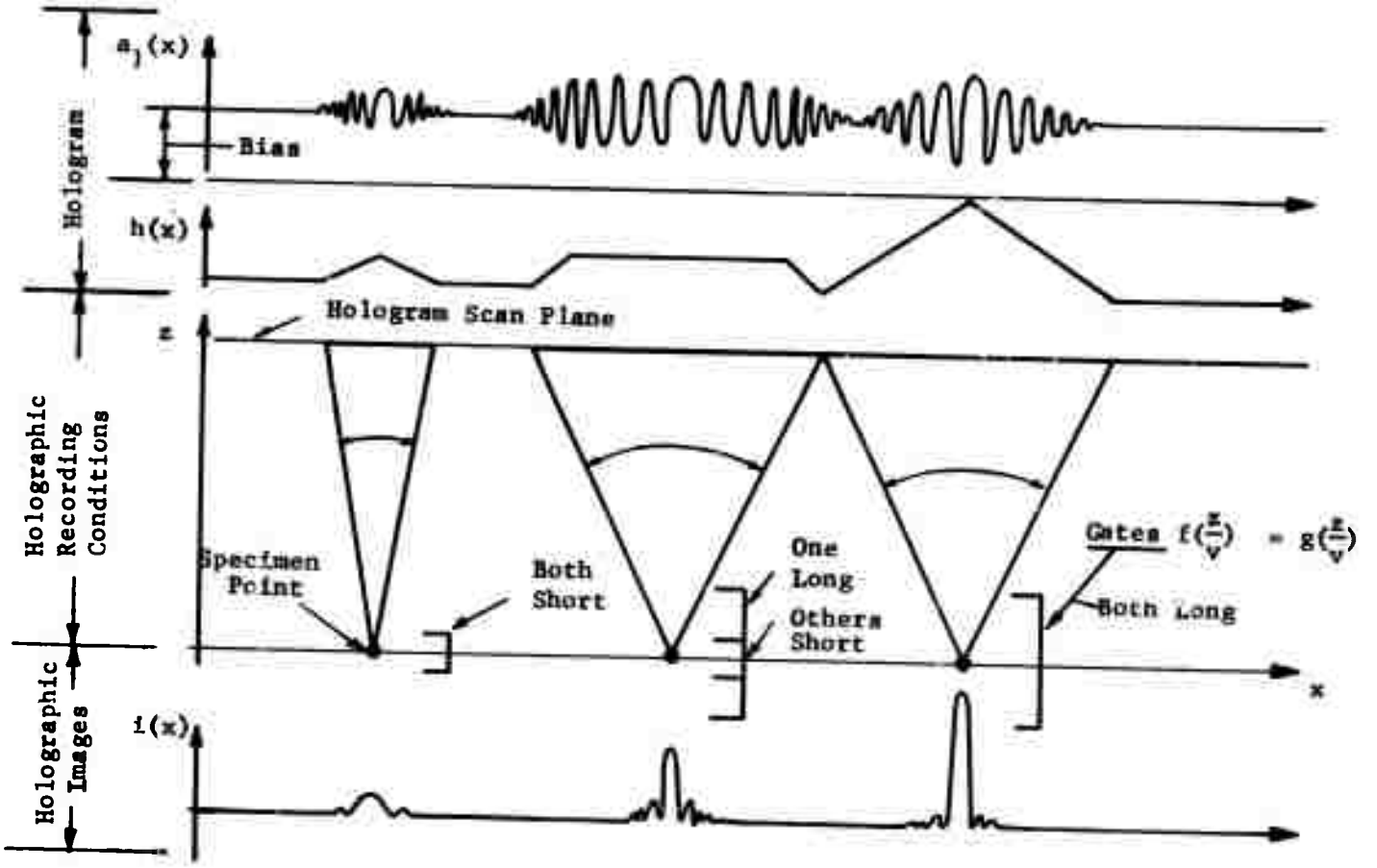

Figure 8B. Point Images as a Function of Gate Durations

and nonlinear degradation tolerances. In this regard, the tolerances for correlated nonlinearities have caused the most difficulty. Often, very rigid initial conditions are assumed to be necessary. This leads to design tolerances that cannot be met, but the system works anyway. Although the original design tolerances are clearly too rigid, it is not known how much, or in which direction, they can be relaxed. Further ultrasonic holographic image experience should reduce this uncertainty of the design tolerances. For this reason, the linearity and noise properties of our system should be measured.

B. SYSTEM DESCRIPTION

1. General

In the original ultrasonic holographic system, the processing of the received and reference signals to produce a hologram (according to the theory outlined in the last section) was accomplished by summing, squaring, and adding a constant (bias) before integrating, range-gating and modulating the recording light. Although theoretically sound, the analogue operations required to instrument this approach were difficult to implement without introducing nonlinearities, scale factor changes, instabilities and long-term drifts. Although of no consequence in the production of holograms, the system also was not completely coherent, the phase of the carrier frequency (5MHz) being completely random with respect to each transmitted pulse. It was difficult in such a system to maintain the proper timing relationships when transmitter pulse widths, pulse repetition rates and other parameters were changed.

By using the carrier frequency (5MHz) as the master timing waveform, the entire system was made phase coherent, and a much simpler implementation used. The summing and squaring operations were replaced by simple coherent mixing (multiplication), and the constant added by controlling the average brightness of the recording light. This is the basic implementation of the new transmitter, receiver and light modulator design.

A fundamental block diagram of the new system is shown in Figure 9. The timer unit generates all of the gating waveforms and synchronizes the entire system. The transmitter gates a portion of the 5MHz carrier frequency and amplifies the pulsed carrier to drive the transmitting transducer. The receiving transducer is integral with its preamplifier, and is mounted on the carriage of the scanner.

The receiver multiplies the received signal by the 5MHz reference signal, filters the mixed output, and integrates a selected portion of the return signals. The output of the receiver is a dc voltage proportional to the integral of the multiplied signals. This voltage is used by the light modulator to control the "on time" of a pulsed light-emitting diode, also mounted on the scanner carriage.

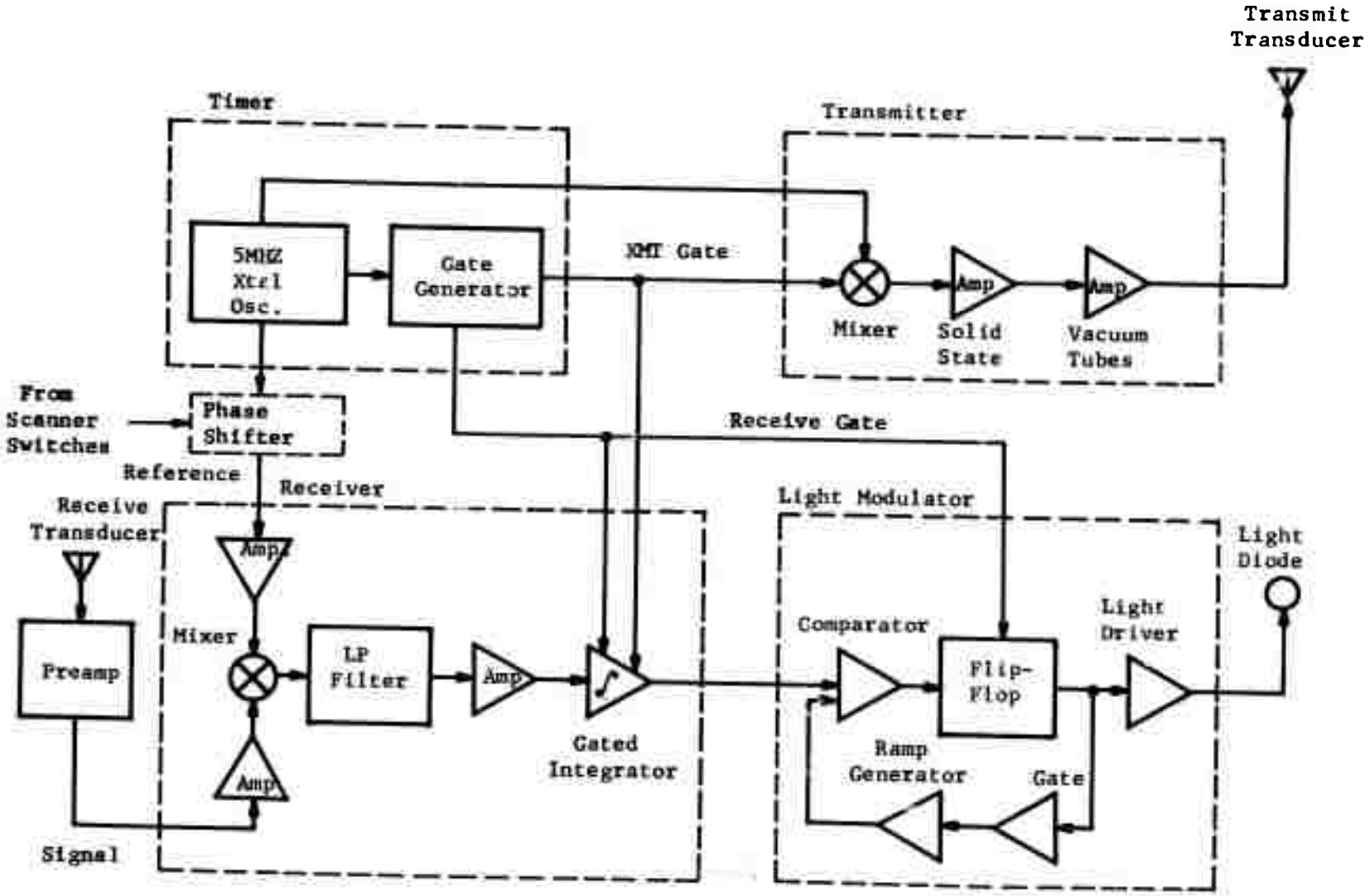

Figure 9. Block Diagram - Ultrasonic Holographic Recorder

The phase-shifter, shown between the timer and the receiver, is used to shift the phase of the reference signal at each scanning line when off-axis holograms are made.

Figure 10 is a photograph of the complete ultrasonic holographic scanner with the new tank installed. The tank is constructed of one-half inch thick plexiglass material, is 18x18x60 inches in size, and holds 70 gallons of water. A small circulating pump with a filter is used to keep the water clean. An aluminum block being tested can be seen in the tank at the left-hand side below the mechanical scanner.

A very brief description of the circuit blocks in Figure 9 will be given at this point. Detailed information, including circuit diagrams are contained in reference (2).

2. Timer

The timer unit provides timing signals for the entire system which are phase-locked to the carrier frequency of the transmitted pulses. (Although a 5MHz carrier frequency is being used for present tests, other frequencies can be used by changing the crystal oscillator and retuning the transmitter.) Convenient thumb switches on the front panel of the unit permit instant change of pulse repetition rate, transmitter pulse width, and receiver gate start and stop times.

The timing diagram of Figure 11 illustrates the timing intervals available from the timer unit. Starting from a 5MHz input from the crystal oscillator, the unit provides transmit and receive gates at any repetition interval from 1 to 999.999 microseconds. The first output in time is a synchronizing pulse used for test purposes. It is followed several microseconds later by the transmit gate which is variable in width from 1 to 999,999 microseconds. Note that the transmit gate is phase coherent with the reference signal and the transmitter carrier (5MHz) from pulse to pulse. A receive gate of any width and located at any time interval after the transmit pulse is provided by adjustment of the receive gate start and stop times.

During most of the NDT evaluation a transmitted pulse width of 1 to 20μsec was used at a pulse repetition rate of 1000 pps. Receiver gate widths of 5-100μsecs were used, delayed by 100-200μsecs after the transmitted pulse.

3. Transmitter

The transmitter puts out a pulsed carrier which maintains the same phase relationship between the pulse envelope and the carrier for every transmitted pulse. As may be seen in the overall block diagram, Figure 9, this is accomplished by combining the carrier and the phase-locked transmitter gate in a balanced mixer and then amplifying the resultant pulsed rf. The mixer is a Hewlett-Packard Type 10534B double-balanced (ring) modulator, used as a pulse amplitude modulator. The peak power output of the transmitter is several watts.

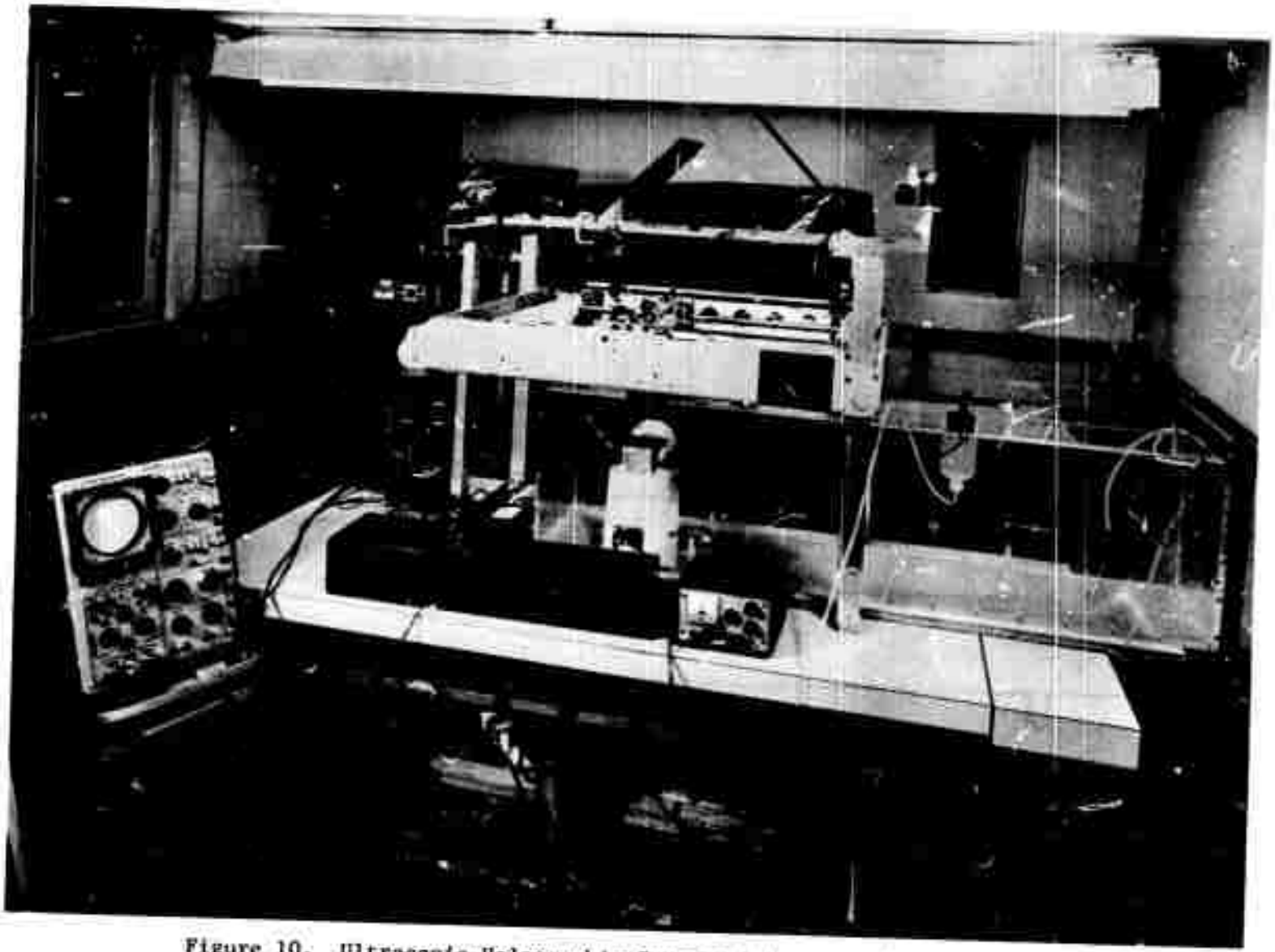

Figure 10. Ultrasonic Holographic Scanner Laboratory Setup

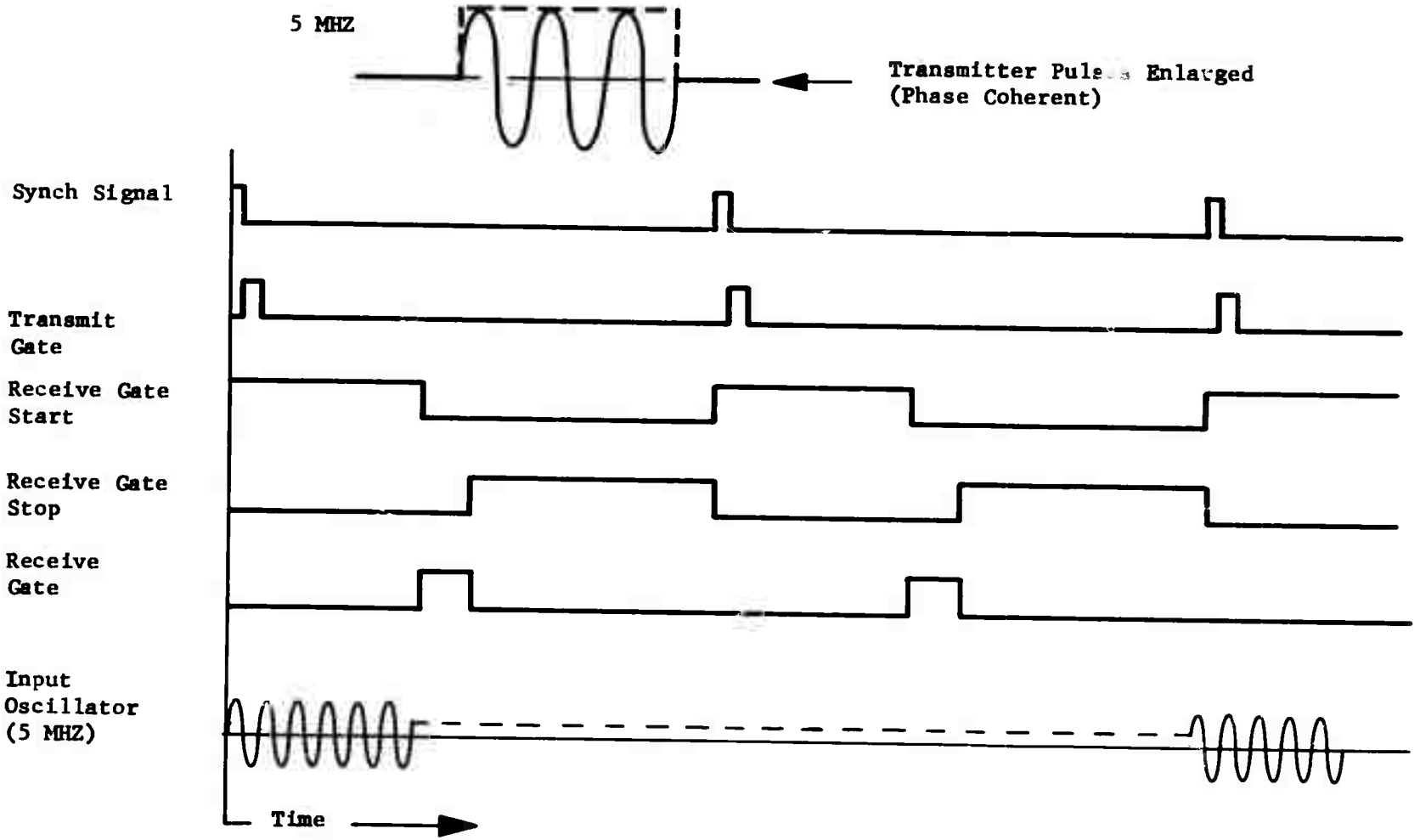

Figure 11. Timing Diagram of the Timer Unit

4. Receiver (See Figures 12, 13, and 14)

The requirements for the receiver portion of the system are that it multiply the 5MHz reference sine wave by the pulsed sine wave received signal and integrate the product over a preselected range-gated interval. The value of the integrated product must be sampled at the end of the integration time and used to control the intensity of the light-emitting diode which exposes the film to construct the hologram. The receiver consists of two blocks in Figure 9, the receiving transducer preamp, and the receiver itself.

The receiving transducer preamp is the same one used in the early phases of this program. It is mounted with the point-source receiving transducer in a plastic shall on the scanning carriage. Its gain is controlled by varying the 0 to -12 Volts dc supply voltage.

The receiver proper used a Hewlett-Packard type 10534 balanced mixer to multiply the 5MHz reference since wave by the 5MHz received signal (pulsed) scattered from the specimen. The components of the mixer output which are of use in generating the hologram are the dc term and frequency components up to approximately 1MHz necessary to reproduct a microsecond pulse. These are filtered from the mixer output by a low-pass filter.

Figure 12 illustrates the rf signal into the receiver mixer from a wire target, and the output after filtering.

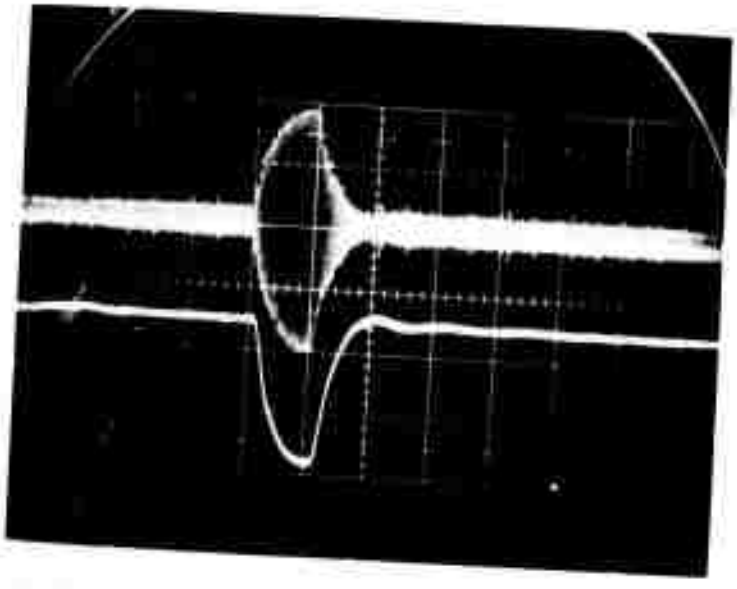

Figure 12. Waveform Photographs:

Upper - Signal From Wire at Input to Receiver Mixer
Lower - Output of Receiver After Multiplication with Reference and Low-Pass Filtering

Time Scale 10μsec/cm

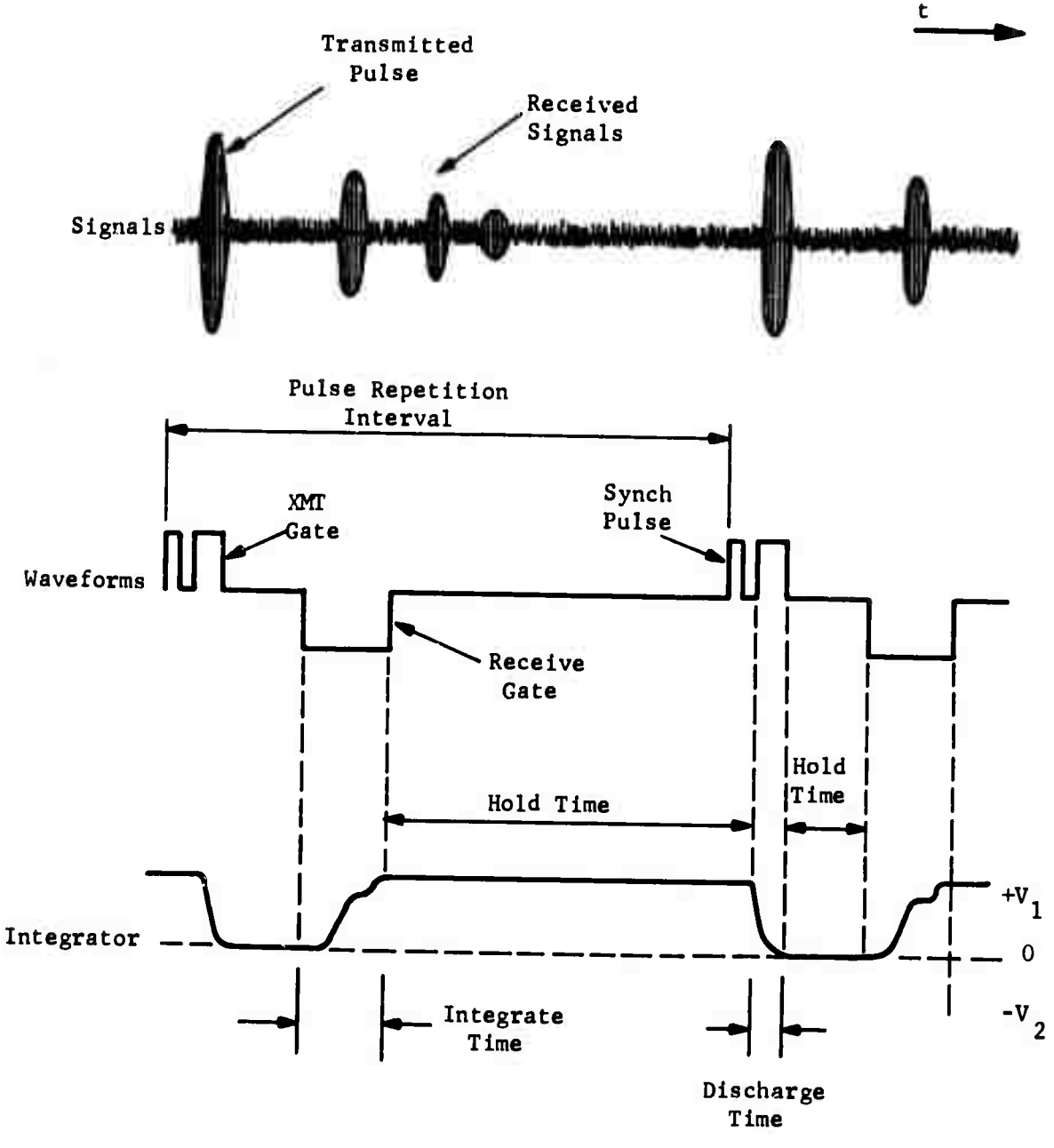

Figure 13. Timing Diagram - Gated Integrator

The integrator is the heart of the holographic receiver, and considerable care had to be spent in its design and construction. The requirements for this circuit are that it integrate the product of the received signal and the 5MHz reference signal over a preselected range-gate interval, and then "hold" the integrated value until it can be "sampled" by the light modulator which follows. Upon completion of the sampling, the integrating capacitor must be discharged prior to the initiation of the next cycle. The circuit must be capable of recycling at repetition rates of 10 to 10m000 Hz, and for combinatory values of transmitted pulse width, receive-gate delay, and receive-gate width.

The timing relationship for the functions of the gated-integrator is illustrated in the timing diagram of Figure 13 along with the corresponding timing of the overall system. As shown on the diagram, integration to either positive or negative values of voltage ($+V_1$ or $-V_2$) takes place during the duration of each receive gate, and the integrated value held for sampling. The sampling hold time extends until the next transmit pulse, at which time the integrator capacitor is discharged back to zero volts. Note that the hold circuit must maintain the integrator capacitor at zero volts from the time it is discharged up to the next integrating interval, as well as holding the integrated value for sampling immediately following the integration time. Figure 14 shows the output of the gated integrator compared with a received signal at the output of the receiver preamp. Note the integration of the signal (negative), and the subsequent "hold".

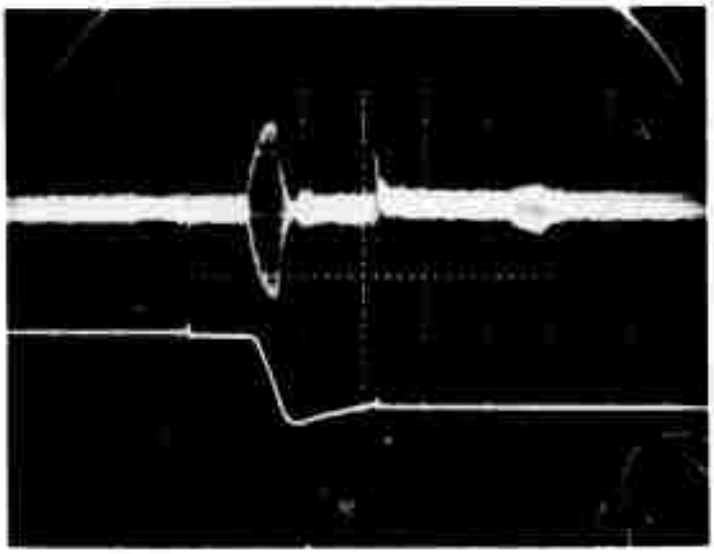

Figure 14. Waveform Photographs:
Upper - Received Signal Out of Preamp.
Lower - Output of Gated Integrator

Time Scale - 20μsec/cm

5. Light Modulator

The light modulator varies the duration of the pulse applied to the light-emitting diode (LED) which exposes the film to generate the hologram. Its input is the integrated output signal from the receiver which has been sampled and "held".

The timing sequence of the light modulator with relation to the other important system waveforms is shown in the timing diagram of Figure 15. In this diagram it may be seen that the light is turned on at the end of the receive gate (line 5 of Figure 15) and turned off before the start of the next transmission cycle. The turn-off time is made proportional to the integrator output by comparison of the integrator output with a time ramp, as indicated at point A on lines 3 and 4 of the timing diagram. The modulator is calibrated by setting the integrator output to zero volts and biasing the time ramp to produce a 250 micro-second long output pulse for the light, as indicated at point B on lines 3 and 4. As the integrator output voltage swings positive and negative around zero, the light is modulated about the 250 microsecond nominal value, as shown in the bottom line of Figure 15.

6. Mechanical Scanner

Since the mechanical scanning mechanism being used to make the acoustic holograms for this program was underpowered, and was suspected of introducing a grating-like striation in the holograms orthogonal to the fast-scan direction, a new motor drive system was designed early in the program. It was expected that the new drive would not only eliminate the nonuniformities in scan, but also that it would permit recording in each direction of scan, thus halving the hologram recording time, and would enable off-axis holograms to be produced by phase-shifting of the reference signal at the start of each scan line.

Unmodulated raster scans made with the new motor drive system showed that the vertical striations were not eliminated by the change to the constant-speed drive for the fast scan. It is probable, therefore, that small displacements of the carriage resulting from cyclic variations in the worm gear-worm nut interface, are causing the striations, rather than speed variations caused by non-uniform loading of the drive motor.

The worm gear-worm nut combination on the scanner also caused a gradual displacement of the carriage across the direction of scan as a line was scanned. The amount of this cross displacement was approximately equal to the interval between lines, so that one scan line merged into another toward one end of the scan. This fault was remedied by mechanically blocking the light-emitting diode during one direction of scan. However, when making off-axis holograms, the scanner had to be scanned in both directions. This scanning defect therefore appears in those holograms.

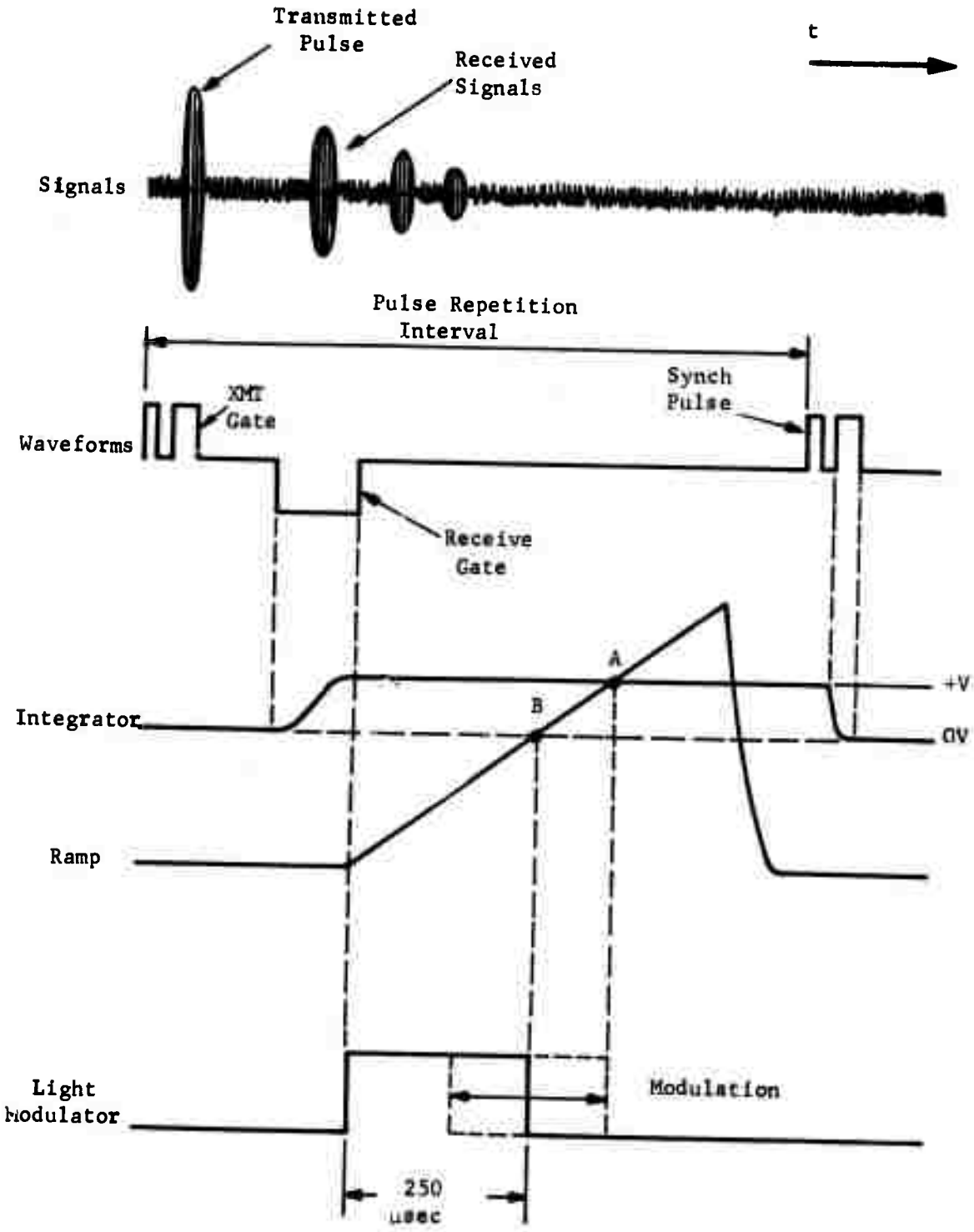

Figure 15. Timing Diagram - Light Modulator

Although the scanning defects just described still remain in the system, they have not prevented the generation of satisfactory holograms or hindered the evaluation of the holographic recording system for nondestructive testing applications.

7. Phase-Shifter

Off-axis holograms were produced on this program by shifting the phase of the reference signal at the start of each scan line. This introduces a spatial frequency across the scanned aperture which displaces the image and its conjugate on each side of the optical axis when the hologram is reconstructed.

The phase shifter was placed in series with the reference signal to the receiver, as may be seen in Figure 9, and is actuated by microswitches installed at the ends of the mechanical scanner. A schematic diagram of the phase-shifter system is shown in Figure 16. A 90° phase shift of the 5MHz reference signal is produced by means of a small inductance and capacitor, L-C, as shown in the schematic. The additional 180° phase shift needed to advance the phase continuously is obtained by using a small transformer with a center-tap on the secondary winding. The microswitches were arranged so that the 90° phase shift was switched at the start of each line, and the 180° phase shift switched at the start of every other line. Thus, the phase advanced 0-90-180-270-360 degrees, or one cycle in 4 lines.

8. Optical Reconstruction

The images reproduced in this report were made in the optical system shown schematically in Figure 17. Approximately 1 milliwatt of the fundamental transverse laser mode of wavelength 0.633μm is used to illuminate the hologram transparency in plane H_1. The hologram transparency is wetted with tetrahydronaphthalene and sandwiched between two optical flats (not shown) to minimize photographically induced optical path (phase) variations and scatter. The holographic image in plane O_1 is relayed and magnified in plane O_3 by lenses ℓ_2 and ℓ_3. The holographically formed image is photographed in plane O_3 on Polaroid film along with a transparent scale placed in plane O_1 to determine the magnification between planes O_1 and O_3. A typical magnification is 25 times. The image plane O_1 and the corresponding specimen plane may be determined by measuring the distance z_1 by simultaneously focusing on the transparent scale and the holographic image. Plane S_1 contains the "zero order" stop that blocks the undiffracted light, and a circular aperture to block light corresponding to spatial frequencies higher than the maximum recorded 1.4 cycles/mm, or lower as required.

Other typical parameters of the holographic imaging system follow: the area of illumination was 2 cm. The distances are z_1 = 10 to 30 cm and f = 100 cm. Lens ℓ_2, which is primarily a relay lens, is an inexpensive telescope objective of focal length 25 cm and diameter 5 cm. Lens ℓ_3, which provides most of the optical magnification, is a standard times-10 microscope objective. The circular aperture in plane S_1 is about 3 cm in diameter. The "zero order" stop is a 0.25-mm-diameter wire placed at 45 degrees to the fast scan lines in the hologram.

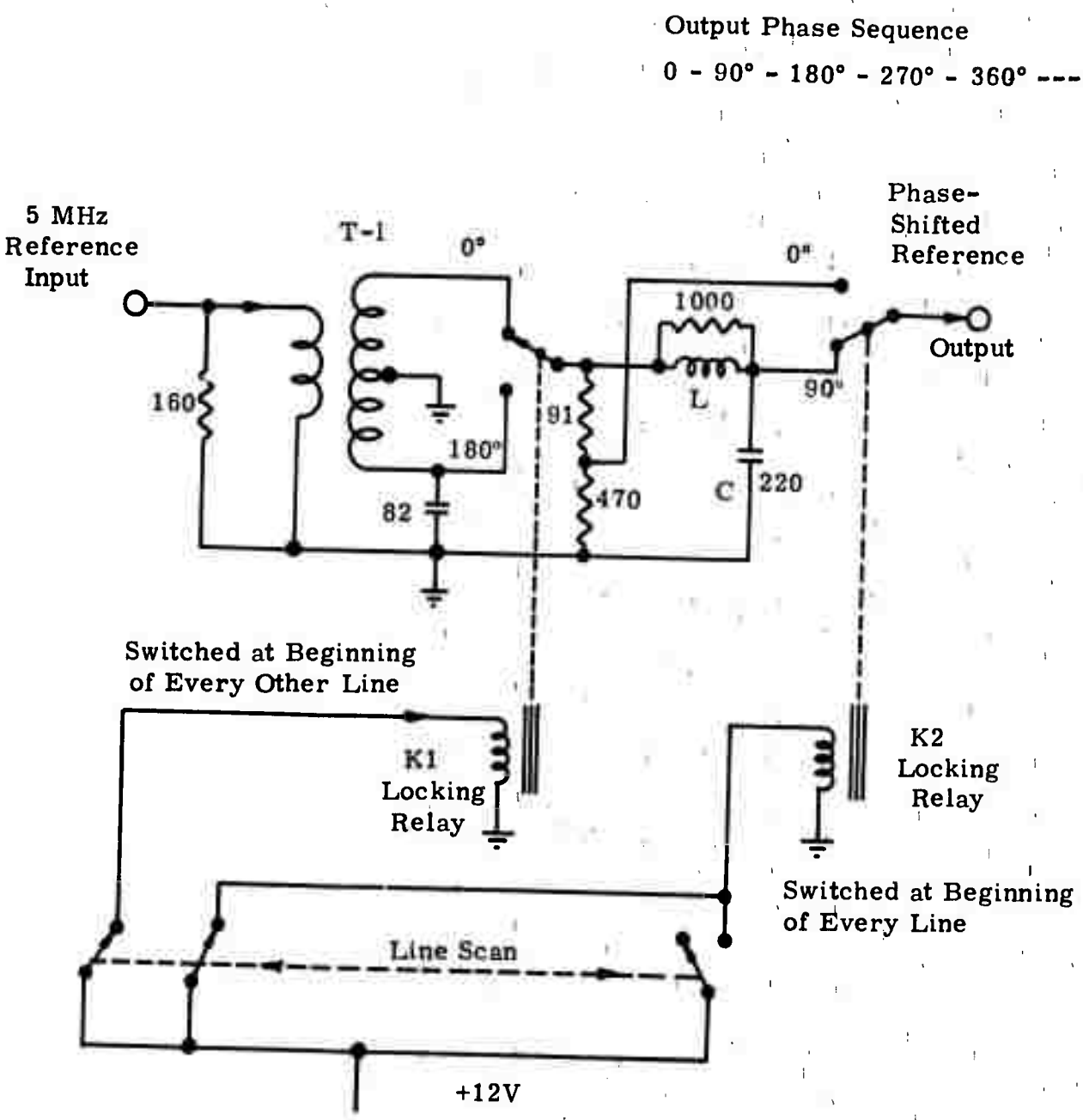

Figure 16. Phase Shifter for Off-Axis Reference

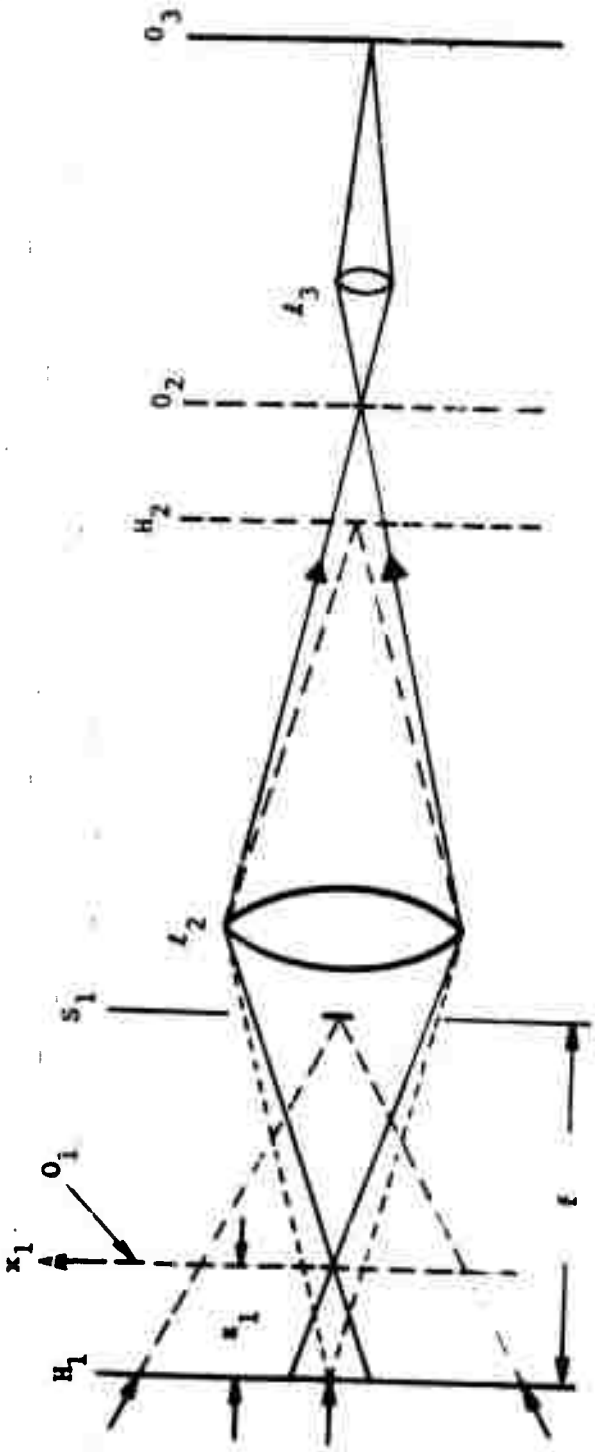

Figure 17. Optical System Used to Reconstruct Images

The location and size of defects in test specimens were determined from the reconstructed images by formulas derived in an earlier report on this program. see Reference (5). By using an optical scaling technique to locate and measure the optical magnification of the reconstructed image, it was possible to obtain the geometrical data needed in these formulas from measurements of only a few key dimensions in the tank, on the film negative, and on the optical bench. Figure 18 illustrates the basic principles involved, along with four formulas from the previous work.

In Figure 18, an object of size X_o at a distance Z_o in water is imaged by the lens action of a hologram to a size X_1 and distance Z_1, on the optical bench. However, the size of the hologram is m times smaller than the size of the acoustic aperture at the surface of the water, and the image at X_1 is enlarged M times to X_2 by the viewing or photographing optics. The value of m is determined by the ratio of the size of the scanned area to the size of the hologram film negative, and the focal length, f, is measured directly on the optical bench. The dimension, Z_1, and the magnification M, between X_1 and X_2 are determined after the hologram is focused by positioning a transparent scale along the Z axis of the optical system until it also focuses at the output X_2. Finally, if the object, X_o is inside a specimen in the water, one other dimension is needed, the distance Z_w between the hologram plane at the water surface and the top surface of the specimen.

To determine the location of a flaw, Z_o is calculated from equation(1) on Figure 18, using measured values of m, Z_1 and f. The depth in the specimen is then found by subtracting the value of Z_w (measured in the tank) from Z_o and using equation (4) on Figure 18 to obtain Z'.

Since the values of m and f remained constant for the experiments described in this report, a curve of equation (1) on Figure 18 was plotted to allow Z_o to be determined conveniently without calculation for any observed value of Z_1.

The linear size of an object, X_o, is given in terms of the image, X_1, by formula (2) on Figure 18. The additional magnification, M, used in photographing the image was measured, as described earlier, so that the flaw dimension in terms of the photographed dimension is given by

$$X_o = \frac{m}{M}\left(\frac{f}{f-Z_1}\right) X_2 \qquad (2\text{-}5)$$

In our system, the value of m was 15.5 times, and f was 113.5 centimeters. Since the ratio $\left(\frac{f}{f-Z_1}\right)$ was about 1-1/2, a magnification, M, of about 20 to 25 produced a full scale image of the hole in the block ($X_o = X_2$ in equation (2-5)).

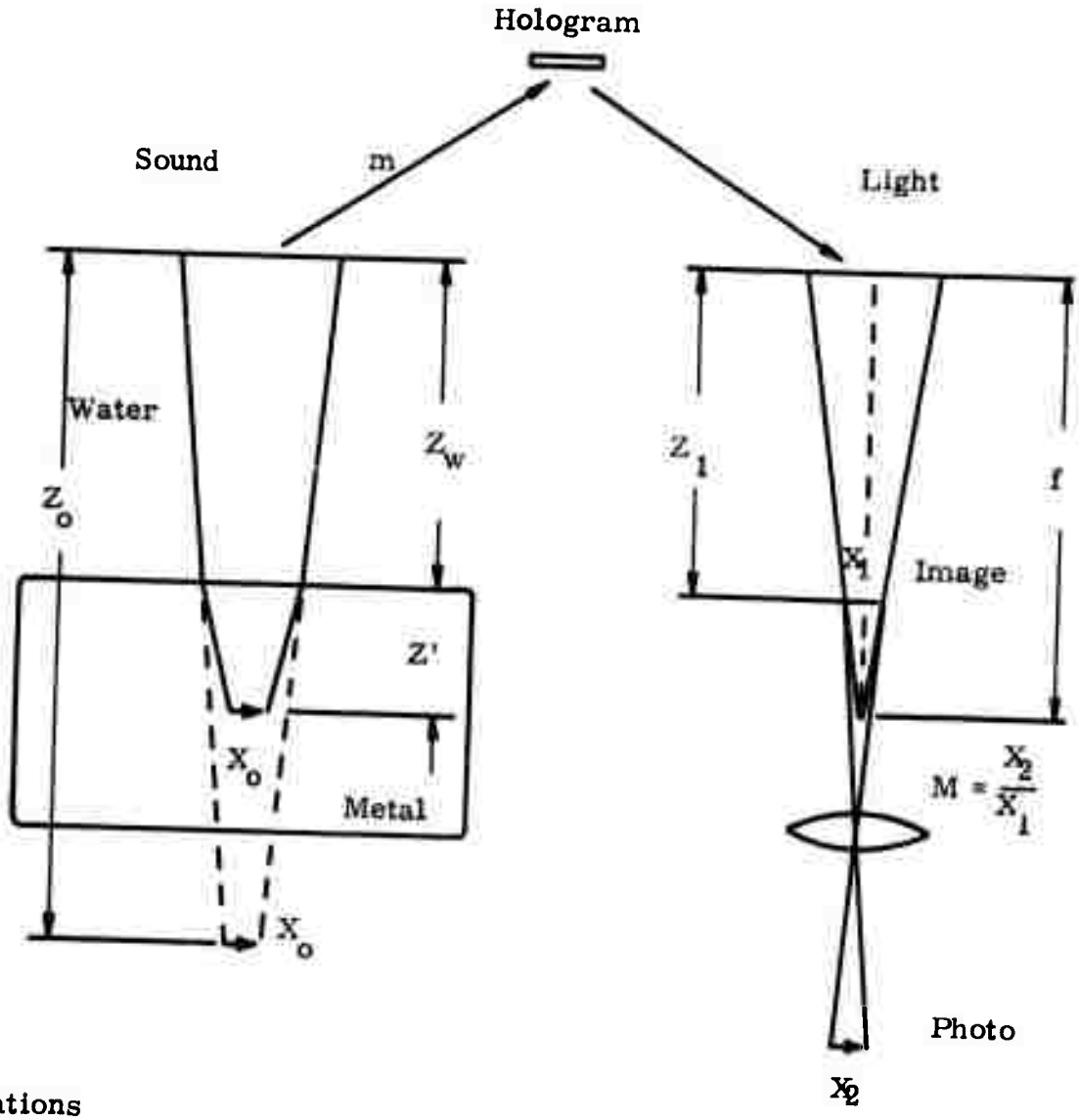

Equations

$$Z_o = c\left(\frac{fZ_1}{f-Z_1}\right) \quad (1) \qquad c \equiv m^2 \frac{\lambda}{\Lambda} \quad (3)$$

$$X_o = m\left(\frac{f}{f - Z_1}\right) X_1 \quad (2) \qquad Z' = (Z_o - Z_w)\frac{\Lambda}{\Lambda'} \quad (4)$$

Wavelengths: Water - Λ
Light - λ
Metal - Λ'

Figure 18. Scaling Between Optical and Sound Wave Fields

SECTION III

EXPERIMENTAL PROGRAM

A. GENERAL

In order to evaluate the capabilities of the acoustic holographic system for NDT applications, several system configurations and modes of operation were used to make holograms of representative types of defects in metal test specimen blocks.

The simulated defects were oriented and located in the test specimens as they might be under actual NDT applications. This provided a variety of test combinations as depicted in the flow chart of Figure 19.

By following the flow chart of Figure 19 from top to bottom, it may be seen that two basic NDT techniques were investigated (contact and immersion techniques), using two modes of signal transmission (monostatic and bistatic), and two modes of introducing the reference signal (on-axis and off-axis). Defects were considered to be of four basic types: cracks, voids inclusions and (poor) bonds, and were incorporated in the specimens in such a way as to test the sensitivity, resolution, field-of-view and other characteristics of the system. Operating parameters of the system could be changed in a number of ways, as indicated at the bottom of the flow chart.

B. TEST PROGRAM

1. NDT Techniques

The contact and immersion techniques are basic methods of "illuminating" the interior of a test specimen in conventional pulse-echo NDT applications, and refer to the position of the transmitting/receiving transducer(s) relative to the specimen. If the transducer is placed directly on a surface of the specimen (coupled through a thin layer of oil or water), the specimen need not be immersed in a fluid. If the transducer(s) is not in close contact with the specimen, both the transducers and specimen must be immersed in a fluid to obtain the acoustic coupling. Since in the holographic system it is desirable to map the acoustic field over a relatively large aperture, one of the transducers (receiving or transmitting) cannot be in contact with the specimen, and the specimen must be immersed in a fluid. The contact and immersion techniques in this case refer to the relative locations of the transmitting transducer, as illustrated in Figures 20a and 20b.

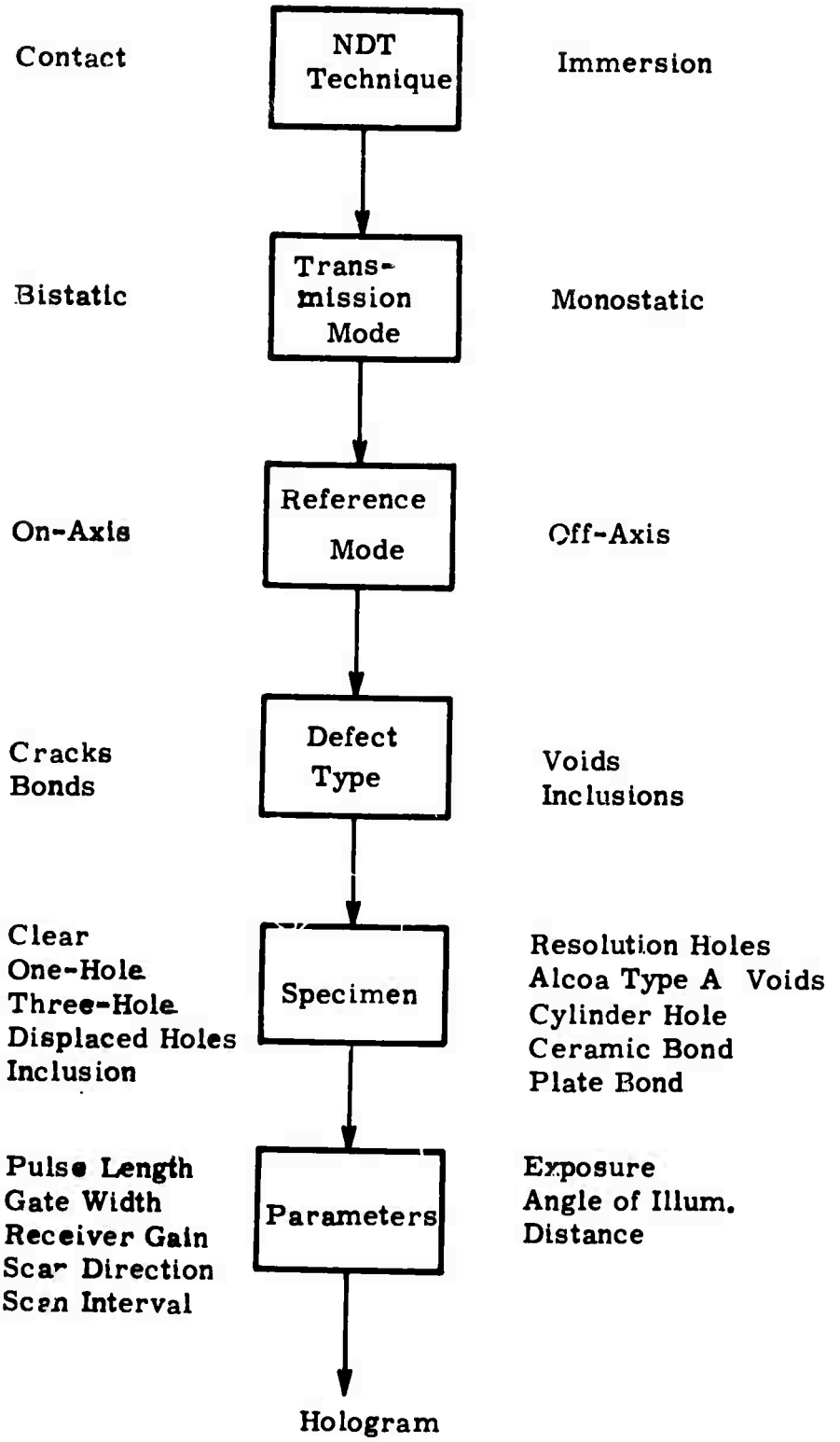

Figure 19.. Flow Chart for Holographic Testing Program

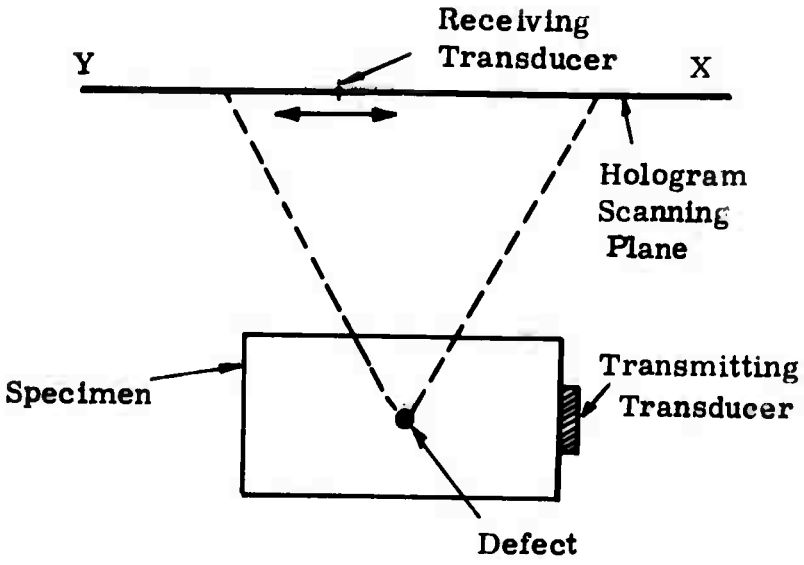

a. Contact Technique

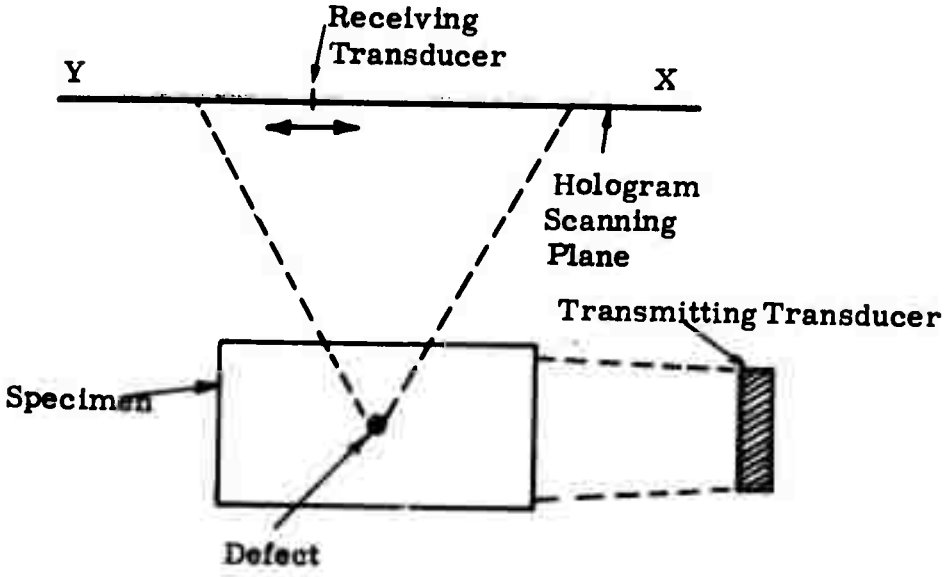

b. Immersion Technique

Figure 20. Ultrasonic Nondestructive Testing Techniques

Although the first ultrasonic holograms made in this program were made by fastening the transmitting transducer to the specimen, according to Figure 20a, it would be much more convenient in practical NDT applications if the transmitting transducer did not have to be fastened to the specimen. One of the first series of tests conducted, therefore, was a comparison of these two methods of illuminating the specimen.

2. Transmission Mode

The monostatic and bistatic modes of transmission are conventionally used to classify radar and sonar system configurations according to the number of stations used. When the transmitter and receiver are co-located, the system is called monostatic. In this mode of transmission the transmitter and receiver are always "looking" in the same direction, and the transmitting and receiving transmission paths from the station to the target are essentially the same. When the receiver is not located in close proximity to the transmitter, the system is bistatic, and the transmitting and receiving paths from the stations to the target are not the same. In the monostatic mode the signal received from an illuminated target is entirely backscatter, whereas in the bistatic mode most of the received signal is derived from forward or side scatter from the target, and very little from backscatter.

Diagrams illustrating the mono- and bistatic transmission modes used with the holographic system are presented as Figures 21a and 21b, respectively. In the monostatic case, Figure 21a, a small transmitting transducer was mounted alongside the small receiving transducer and scanned with it to generate the hologram. The advantages of this mode are the ease with which the entire volume of the specimen can be illuminated, the doubling of the theoretical angular resolution attainable, and the ability to search the volume in parallel strata by range-gating. The disadvantages of this mode are the additional circuit complexity required to transmit and receive from the same transducer (or from transducers very close to each other), and the fact that a high-gain transmitting transducer cannot be used if a large scanning aperture is used for purposes of achieving high resolution.

The biastatic mode, shown in Figure 21b, was used for most of the testing. It simplifies transmission problems by separating the transmitter and receiver, but makes it difficult to illuminate all of the interior volume of the specimen. Note that either the contact or immersion techniques may be used with this mode, while only the immersion technique can be employed with the monostatic mode.

3. Reference Mode

Since a hologram is an interferogram generated by recording the interference between a desired optical or acoustic field and a corresponding reference field, it is possible to modify the hologram by altering the reference signal. When the reference signal is simply a sample of the transmitting signal, its amplitude and phase are constant across the aperture, and upon reconstruction of the image (by taking the optical diffraction pattern) it is found that the

(a) Monostatic Transmission

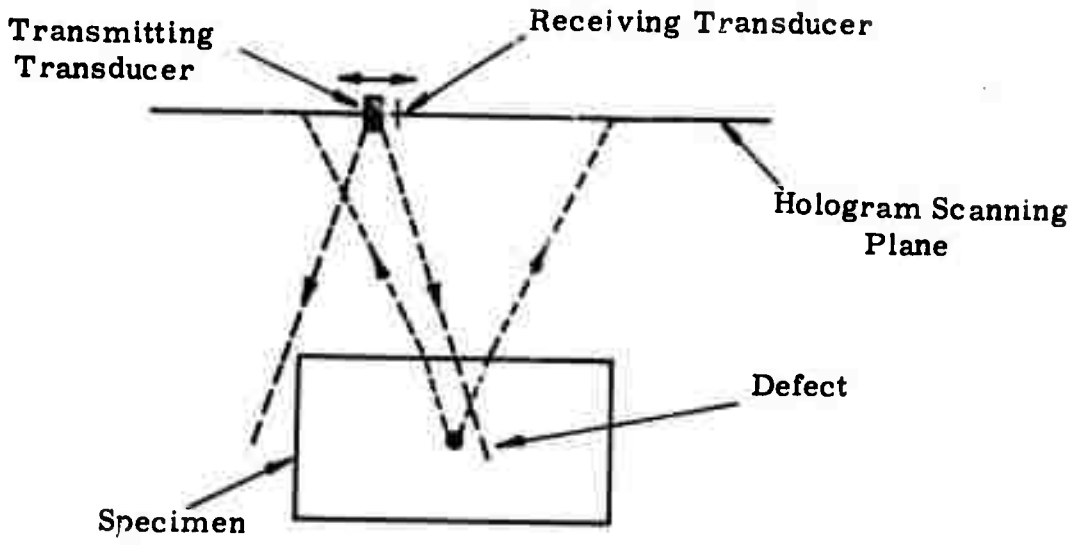

(b) Bistatic Transmission

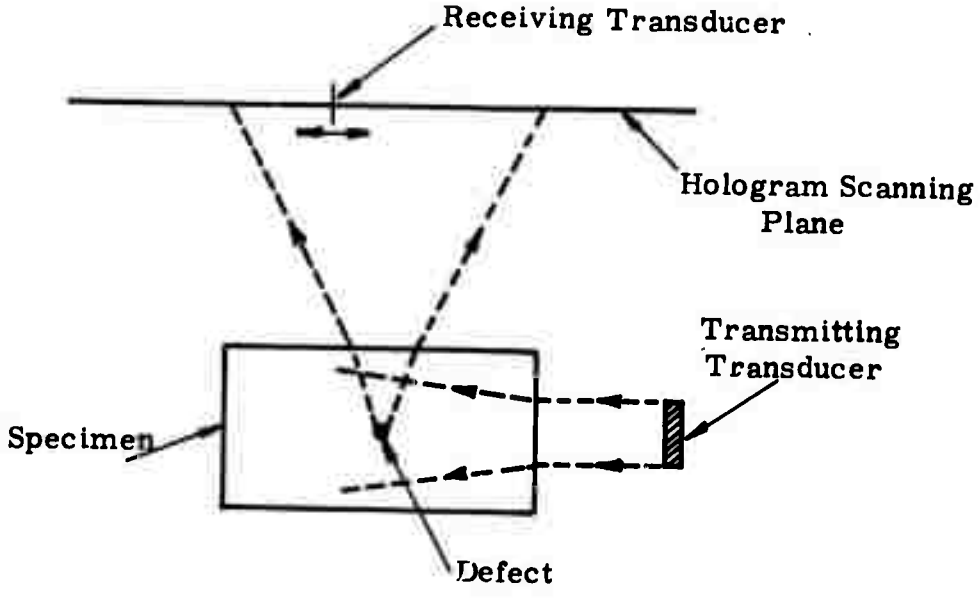

Figure 21.. Ultrasonic Transmission Modes

image and its interfering conjugate image are centered directly on-axis of the optical output. The first holograms constructed by D. Gabor[9] were made in this manner, and an on-axis referenced hologram is often called a Gabor hologram. From an optical approach, the image and its conjugate are centered on the zero-order term of the diffraction pattern. From an electrical signal analogy, the output spectrum and its conjugate spectrum are centered at zero frequency.

Just as the spectrum of two interfering electrical signals may be separated by heterodyning or beating the input signal against a reference signal of a different frequency, so can the optical images produced upon reconstruction of the hologram be separated. Off-axis images are produced by using a reference signal having a spatial frequency across the aperture which differs from zero.

Since the frequency of a spatial wave is the rate of change of phase of that wave with respect to distance,

$$f = \frac{d\phi}{dx} \approx \frac{\Delta\phi}{\Delta x} \qquad (3\text{-}1)$$

a spatial frequency across the aperture may be formed by changing the phase of the reference signal at each scan line as the aperture is scanned. If a 90° change in phase were introduced into the reference signal at the start of each scan line, for example, a spatial frequency of 1 cycle per 4 scan lines would be introduced into the reference signal. This would separate the reconstructed image from the reconstructed conjugate image and place them on either side of the output optical axis. Thus, the desirable image would be separated from the interfering conjugate and from the interference of the undiffracted light at the zero-order.

Off-axis holograms were generated by shifting the phase of the reference signal as described above. Microswitches were installed at the ends of the mechanical scanner to actuate a phase shifter in series with the reference signal to the receiver. A schematic diagram of the phase-shifting system was shown in Figure 16 under the System Description.

4. Representative Defects

Almost any type of defect in an opaque specimen can generally be classified as some sort of a crack, a void, an inclusion, or a defective bond. Grain structure within a metallic specimen is essentially a field of microscopic cracks. Gradual changes of refractive index, or similar discontinuities, within a nonmetallic specimen may be considered to be of the same general nature as a bond. In this investigation, most of the work was done with simulated defects, using long thin drilled holes broadside to represent cracks, and flat-bottomed holes on-end to represent voids. A broken-off drill point imbedded in an aluminum block was available as a form of inclusion, and two specimens, one of teflon bonded to aluminum and the other of teflon bonded to glass, were available as bond defects.

5. Test Specimens

The specimens made to evaluate the holographic system incorporated the simulated cracks or voids in aluminum blocks. The simulated cracks were distributed in six of the blocks (one block was clear), and were used to evaluate the various modes of operation, as well as to check system performance in the areas of resolution and coverage. Oblique drawings of these test blocks are shown in Figure 22a through 22f with their important dimensions.

The clear block, Figure 22a, was used as a control in the experiments and proved to be extremely useful in setting up the experiments, identifying signal paths, and otherwise clarifying the results. The block with the single hole, Figure 22b, was used in the majority of tests of equipment and techniques since it provided a single strong signal, well isolated from extraneous "noise". The three-hole block, Figure 22c, provided a complex array of simulated cracks from which problems of shadowing, range resolution, and optical focusing could be evaluated.

The test block of Figure 22d was made to test system resolution and had three pairs of 0.040-inch diameter holes, 1.375 inches deep. One pair of holes was 1/16 inches apart, the next 1/8 inches apart, and the last pair 3/16 inches apart. The coverage block, Figure 22e, was made to check the ability of the system to detect cracks near the corners, while the cylindrical block, Figure 22f, was made to check the effects of surface curvature. The coverage block, Figure 22e, also had an imbedded drill point in the center, as shown, which was available as a form of inclusion.

The remaining test specimens used in the experiments are illustrated in Figures 23a, b, and c. Figure 23a shows the dimensions of a set of 4 ALCOA Series A aluminum test blocks used to simulate voids of varying sizes. These blocks were made for pulse-echo testing, and have smoothly ground, flat-bottomed holes drilled up from the bottom and plugged with wax. The hole diameters range from 1/64 to 1/16 inches in diameter, as indicated in the table on Figure 23a. When illuminated from the top, these blocks provide simulated voids of various diameters (the flat bottoms), located at a fixed depth (3-1/4 inches) from the top of the block.

The bonded plate, illustrated in Figure 23b, was a sheet of teflon material 1/4 inch thick bonded onto a sheet of aluminum 1/16 inch thick. The only information available on the plate claimed that is had defects in the bond, but of unknown size and location. The bonded teflon-glass specimen, Figure 23c, was a portion of a lens casting with ribbed walls of teflon hexagonal honeycomb construction bonded to a 1/2-inch thick piece of glass. It also was purported to have bonding defects at the cell boundaries.

6. Parameter Variations

Throughout the generation of acoustic holograms with the holographic system, many changes of system parameters were made, as outlined at the bottom of the flow chart, Figure 19. In general it was not found that system characteristics, such as pulse length, gate width, receiver gain and others, were very critical in the holographic system.

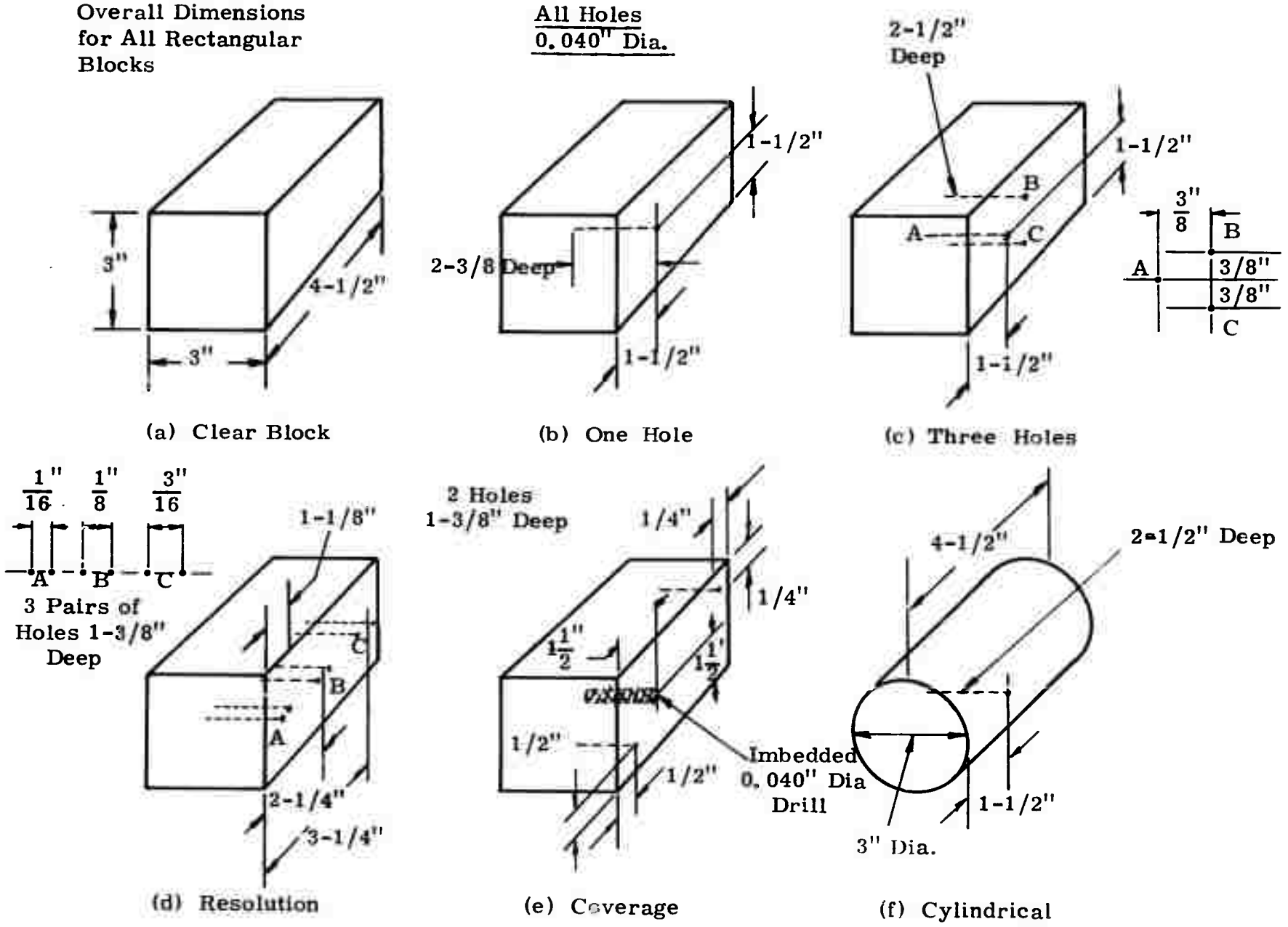

Figure 22. Aluminum Test Specimens with Simulated Cracks

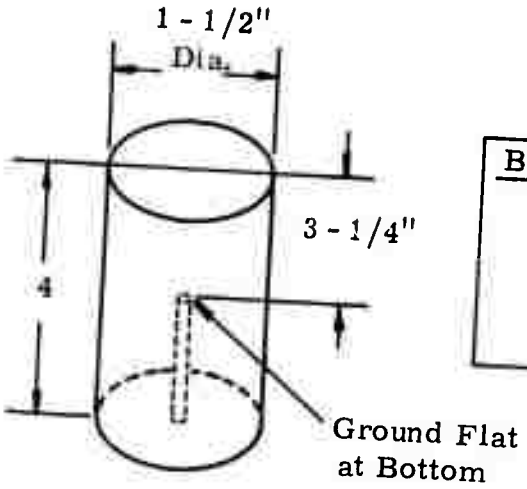

Block No.	Hole Dia.
1	1/64"
2	1/32
3	3/64
4	1/16

(a) Alcoa Series A Test Blocks

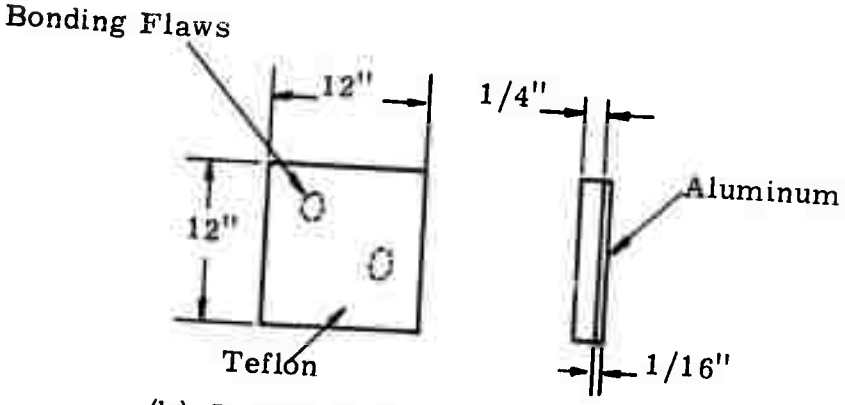

(b) Bonded Plate Specimen

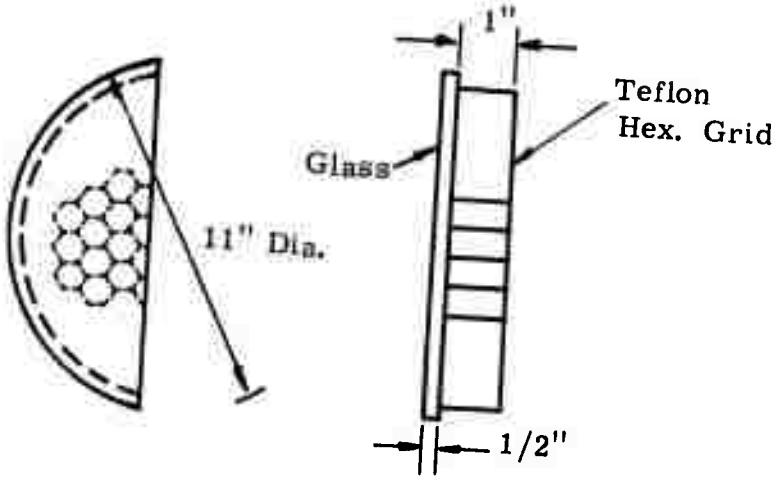

(c) Bonded Lens Honeycomb

Figure 23. Test Specimens for Voids and Bonds

7. Hologram Film Processing

The film negative upon which the acoustic hologram is recorded in our system is used as a square-law detector as well as a spatial storage device. Ideally, the intensity of the sum of two spatially modulated coherent wave fronts incident on the film is to be recorded in such as way as to obtain linearity between this intensity and the amplitude transmittance of the recording. Thus, upon reconstruction in a coherent optical system, the amplitudes of the incident waves can be faithfully recreated from the stored data.

If A_1 and A_2 are the complex amplitudes of the coherent wavefronts, then we want

$$\bar{A} = A_1(x,y) + A_2(x,y). \tag{3-2}$$

To obtain this linearity in amplitude it is necessary that

$$I(x,y) = |\bar{A}|^2 \quad KT_a(x,y) \tag{3-3}$$

where I is the incident intensity

T_a is the necessary amplitude transmittance

K is a constant of proportionality

Since the exposure E is the intensity, $I(x_1y)$, multiplied by time, T, equation (3-3) may be written

$$E(x.y) = K'T_a(x,y)$$

To obtain a faithful reconstruction, therefore, it is desirable to operate over a linear portion of the exposure vs amplitude transmittance transfer function of the film.

Since the negatives of the 35-mm hologram film for this program were developed on an automatic processor (VERSIMAT), accurate control of the processing could be obtained by changing the speed of the film through the solution. However, since film development is monitored by a densitometer using the D-log E curve (H-D or Hurter-Driffield curve), a conversion from that data to the amplitude transmittance vs exposure curve had to be made in order to select the exposure which provided the best linearity. The method of determining and monitoring the best exposure is outlined here.

Before developing any hologram negatives on the VERSIMAT automatic developer, several runs were made using standard test wedges exposed on the film type being used (SO-243 high-definition aerial film). The densities of the steps on the wedge were measured on a densitometer and the H-D curve plotted. Figure 24 is a typical plot for a film speed of 19 feet per minute. A print of the step wedge is shown on the right-hand side of the figure.

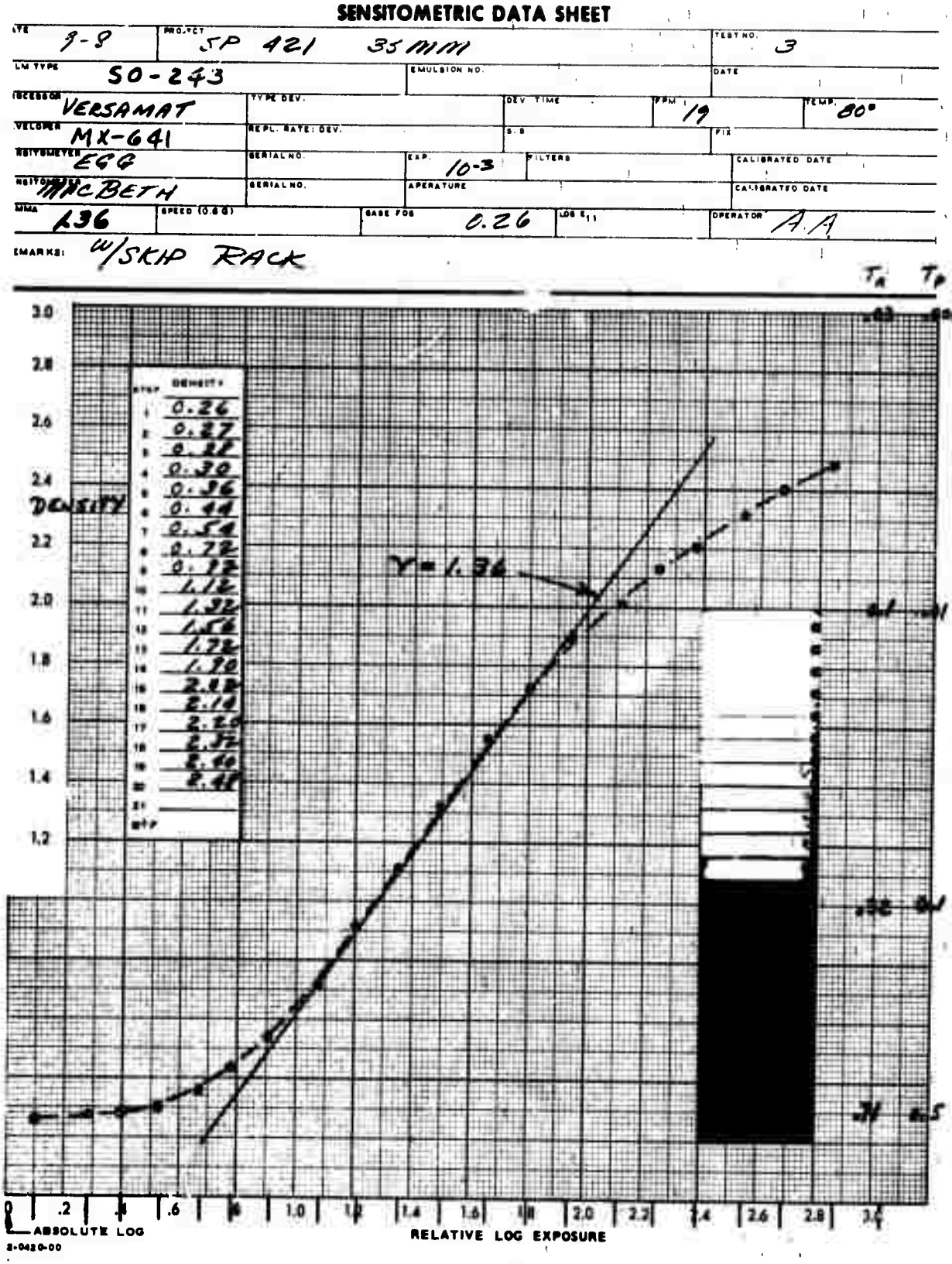

Figure 24. D-Log E Plot of SO-243 Hologram Film Negative

The D-log E curves were then converted to amplitude transmittance versus exposure curves by using the relationship between density and transmittance.

$T_p = 10^D$ -- power transmittance

$T_A = \sqrt{10^D}$ -- amplitude transmittance

Figure 25 illustrates E-T_a curves made for several film speeds on the VERSIMAT. When these curves are compared with the D-log E curve of Figure 24 for the same film, it will be noted that the linearity region on the E-Ta curve does not coincide with the linear region of the D-log E curve, but corresponds more with the toe and lower part of the linear region of the D-log E curve. In general, therefore, the hologram film which is optimally recorded appears to be underexposed by conventional standards.

Based on the results of Figure 25, a machine speed of about 20 fpm was used in developing the 35 mm hologram negatives, and film exposures were used to place the operating bias somewhere near the center of the linear portion of the curve, point A in Figure 25. The results achieved by this method are illustrated by the example of Figure 26, which is a microdensitometer recording made by taking one cut across an acoustic hologram. The hologram was that obtained from a steel-ball target in the tank, and consists of a series of dark and light rings typical of a Fresnel zone plate. Since the microdensitometer output is plotted as power transmittance, T_p, the square root of the plot must be taken in order to relate it to Figure 25. This was done by placing an amplitude transmittance calibration scale on the tape, as shown. Note that the negative is underexposed by conventional standards, and has a Ta range of 83-95. By marking this range on Figure 25, it may be seen that a slightly more dense negative (increased exposure) is needed to place the modulation range closer to the center of the linear portion of the curve, point A.

It is necessary to point out that the method described here for establishing the exposure and development of the film holograms is not completely accurate because of the difference in wavelength and spectra of the illuminations used. The step wedges were exposed with white light, while the holograms are illuminated with coherent light at 633 nm wavelength. Also, the hologram itself is made at a wavelength of 700 nm from a light-emitting diode. However, it is not felt that a correction for these differences would significantly alter the calibration achieved.

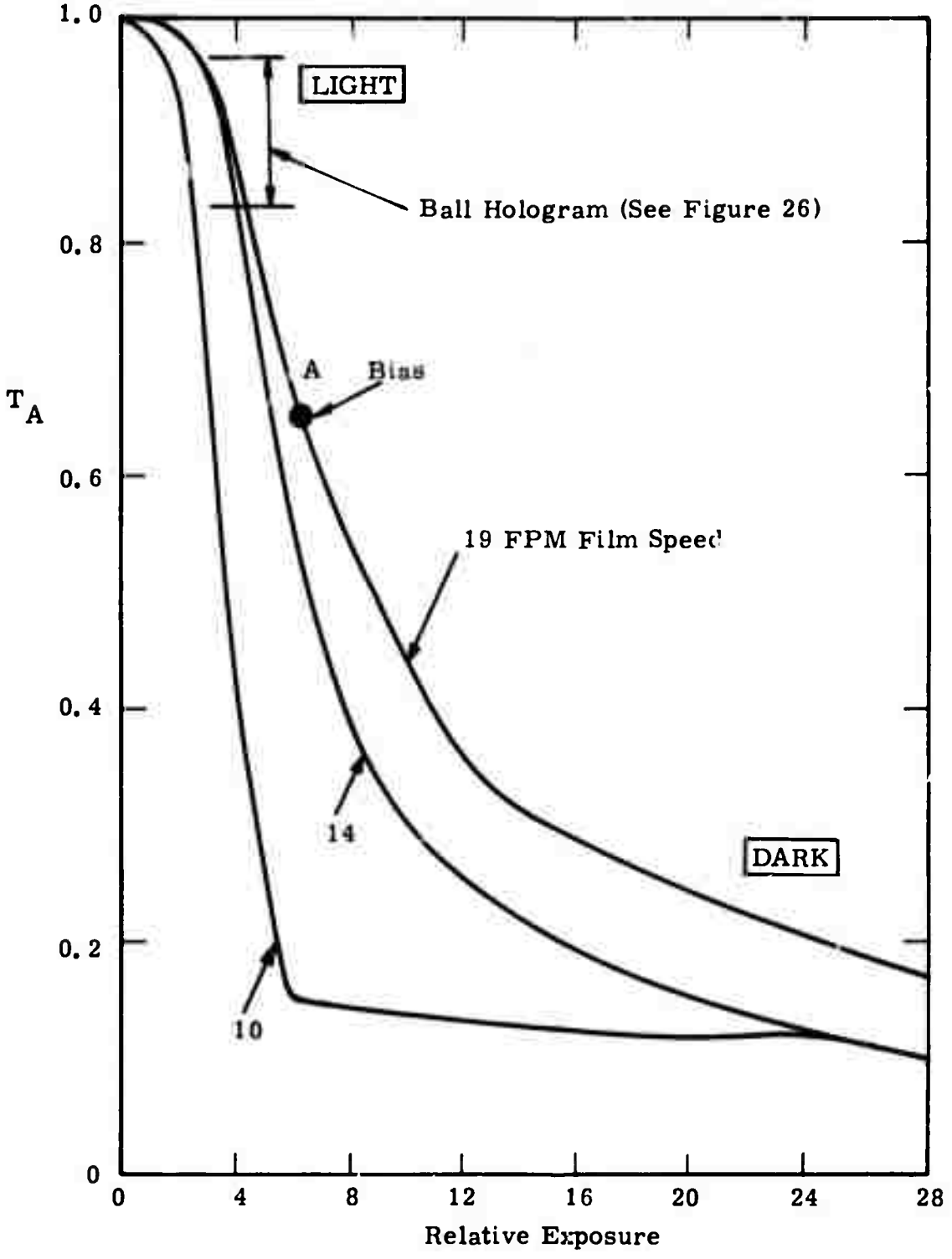

Figure 25. Exposure - Transmittance (Amplitude) versus Film Speed

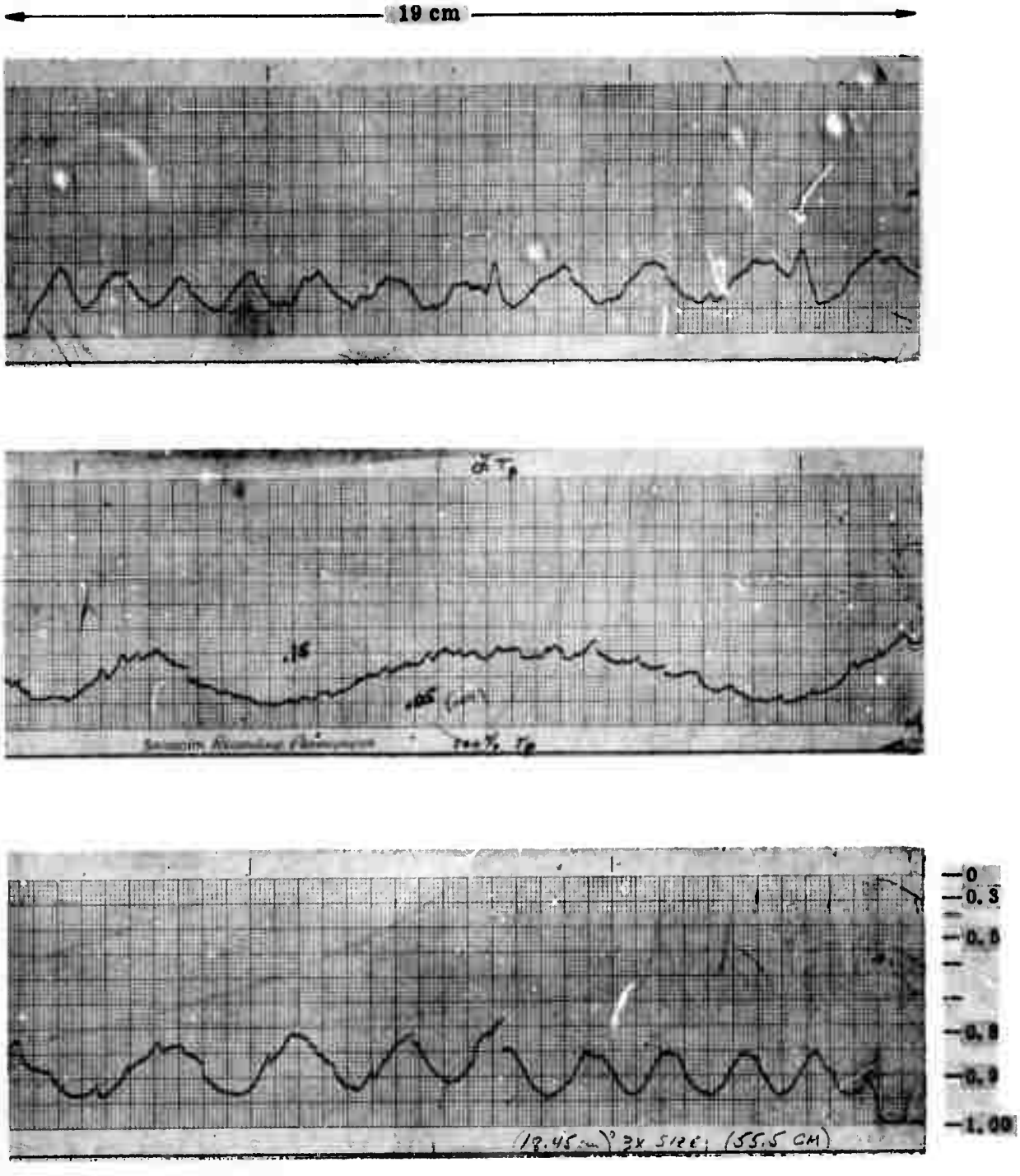

Figure 26. Transmittance (Power) Across Ball Hologram Film Negative

SECTION IV

EXPERIMENTAL RESULTS

A. GENERAL

The experimental tests carried out on this program were aimed at optimizing the ultrasonic holographic system and evaluating its use for NDT applications. They were accomplished by investigating the combinations of techniques, operating modes and simulated defects outlined under the Experimental Program, Section III, of this report. Over 130 holograms were made and analyzed during these experiments

B. HOLOGRAMS GENERATED

The holograms generated during the course of this program are tabulated on the 21 pages of Table 1, and illustrated by small photographs on the six pages of Figure 27. The tabulation and photographs are chronological according to the order in which they were made. As may be noted in Table 1, each 35mm film loading was labeled by a letter from A through U, and contained from 1 to 16 exposures.

The headings at the top of Table 1 list the system parameters of interest to the evaluation. An explanation of their meaning is given below.

SERIES - Letter from A through U identifying roll of film exposed. Number from 1 through 16 identifying the exposure.

TECHNIQUE - Immersion (IMM) or Contact (CONT) method of illuminating the specimen.

MODE - BISTATIC (1-way) or MONOSTATIC (2-way) modes of transmission used.

REFERENCE - ON-AXIS reference signal or OFF-AXIS reference signal (using the phase-shifter).

XMTTR - Transmitter characteristics
PL - Pulse length in microseconds
PRI - Pulse repetition interval in microseconds

RECEIVER - Receiver characteristics
GATE - Receive gate limits in microseconds
GAIN - Receive gain 0 to -12 volts dc on preamp, highest gain = - 12 volts.

SCAN - Mechanical Scanner Characteristics
MODE - 1 = light blanked during return trace
2 = no light blanking during return trace, equals 2-way scan
INT - Size of stepping interval on step scan
Each integer equals 0.015 inches per step
TIME - Total time of scan and exposure

f-NO - Camera f-stop (with time exposure)

SPECIMEN - Description of Specimen according to Figures 22 and 23 in Section III.

REMARKS - Additional Comments.

Inspection of Table 1 shows that most of the experimental work was done with the very simple simulated defects discussed earlier under the test program. This was based on the decision to evaluate the fundamental behavior of the system and evolve the basic NDT techniques first, before spending a great deal of time and effort in obtaining and testing real defects. Although the real defects would possibly be more representative of NDT problems, they would also be considerably more complex than the simple drilled holes, and data on their precise characteristics would be difficult to obtain. Representative real defects would be more useful in evaluating a completely defined prototype system.

Therefore, a considerable effort was spent in trying to arrive at an optimum system using the clear, single-hole, and three-hole blocks. It was hoped that the ultimate system would not require a modification of the specimen, or the mounting of a transducer on the specimen itself. By limiting the tests to these elementary simulated defects it was possible to investigate the differences between the contact and immersion techniques, and arrive at a better understanding of their possibilities. Over 50 separate photographs of reconstructed holograms were made of these three specimens on this particular problem.

C. TESTS PERFORMED

Before discussing the experimental results in detail, a general review of the holograms in Table 1 would be helpful. The series A and B holograms were made in a small tube of water immediately upon completion of the revised system. Since no images of the single hole could be obtained in the reconstruction, a single wire target was used in the C, D, and E series of holograms. Excellent images were reconstructed from the wires (see reference 2, page 47, Figure 31), thus verifying that the new receiver, light modulator and other electronic circuits were functioning properly.

The F series holograms were made just after the installation of the larger water tank, and were made at a range of approximately 40 inches, from target to receiving transducer, the longest range known to have been used at that time at a frequency of 5MHz. The long range experiments covering holograms

TABLE I

TABULATION OF HOLOGRAMS GENERATED ON PROGRAM

First Holograms New Electronics

SERIES	TECHN.	MODE	REF.	AMTTR		RECEIVER		SCAN			F NO.	SPECIMEN	REMARKS
				PL	PPI	GATE	GAIN	MODE	INT.	TIME			
A-12	Cont.	1-way	On-Axis	10	1042	60-85	-8			30	5.6	1-Hole Block	200 Scan Lines small xducer end of block.
-15	↓	↓	↓	↓	↓	↓	↓			30	8	↓	
-16	↓	↓	↓	↓	↓	↓	↓			30	11	↓	
			None of Holograms Produced Reconstructed Image Gated Integrator Not Holding Properly										

TABLE I, Cont.

SERIES	TECHN.	MODE	REF.	XMTR		RECEIVER		SCAN			F NO.	SPECIMEN	REMARKS
				PL	PRI	GATE	GAIN	MODE	INT.	TIME			
Reduced Receiver Gain to Prevent Bad Limiting													
B-11	Cont.	1-Way	On-Axis	10	1041	65-95	-7			30	5.6	1-Hole Block	Xducer on other end.
-14	↓	↓	↓	2	1040	65-96	-6			30	8	↓	RCVR Gain Reduced
-15	↓	↓	↓	10	↓	↓	-5			30	8	↓	"
-16	↓	↓	↓	10	↓	↓	-5			30	5.6	↓	"
	B14-15 Some Scan Lines Missing												
	Not Getting Good Reconstruction												

TABLE I, Cont.

Went to Single Wire Target

SERIES	TECHN.	MODE	REF.	XMTR		RECEIVER		SCAN			P NO.	SPECIMEN	REMARKS
				PL	PRI	GATE	GAIN	MODE	INT.	TIME			
C-3	IMM	1-Way	On-Axis	5	1042	190-285	-5			30	8	Small Dia Wire	Large Xducer
			Get Image of Wire But Receiver Gain Too Low to Get Fine Fringes on Hologram.										

TABLE I , Cont.

SERIES	TECHN.	MODE	REF.	XMTTR		RECEIVER		SCAN			F NO.	SPECIMEN	REMARKS
				PL	PRI	GATE	GAIN	MODE	INT.	TIME			
Modified Gated Integrator to Prevent Limiting													
D-1	Imm.	1-Way	On-Axis	5	1K	190-285	-8			30	5.6	1.6MM Dia Alum.Wire	Dud-Shutter Didn't Operate
-2	↓	↓	↓	↓	↓	↓	↓			↓	8	↓	
-3	↓	↓	↓	↓	↓	↓	↓			↓	5.6	↓	
		Obtained Very Good Images of Wire											
		Some Scan Lines Missing D1 and D3.											

TABLE I , Cont.

SERIES	TECHN.	MODE	REF.	XMTR		RECEIVER		SCAN			F NO.	SPECIMEN	REMARKS
				PL	PRI	GATE	GAIN	MODE	INT.	TIME			
E-1	Imm.	1-Way	On-Axis	10	1K	190-285	-8			30	5.6	Single Wire	Repeat of D-4
-2	↓	↓	↓	↓	↓	↓	↓			↓	↓	2 Wires Vertical	
-4	↓	↓	↓	↓	↓	↓	↓			↓	↓	2 Wires Oblique	
			Good Images of Wires										

TABLE I , Cont.

First Holograms with Long-Range Tank - New Automatic Development

	SERIES	TECHN.	MODE	REF.	XMTTR		RECEIVER		SCAN			F NO.	SPECIMEN	REMARKS
					PL	PRI	GATE	GAIN	MODE	INT.	TIME			
	F-1	Imm.	2-Way	On-Axis		2K	1340-1400	-7			20	5.6	0.25" Dia Alum Rod	Reversed Scan Direction
X*	-2	↓	↓	↓		↓	↓	-8			30	↓	↓	Also Reversed DUD
	-3							↓			32			Lens Set Wide Open by Error
	-4										30	5.6		
	-5										30	4		
	-6										30	4		
X	-7										31	5.6		Hologram Missing
X	-8	↓	↓	↓		↓	↓	↓			32	5.6	↓	Ditto

* X indicates photograph not provided.

TABLE I , Cont.

Long Range Test with Steel Ball Target

	SERIES	TECHN.	MODE	REF.	XMTTR		RECEIVER		SCAN			F NO.	SPECIMEN	REMARKS
					PL	PRI	GATE	GAIN	MODE	INT.	TIME			
	G-1	Imm.	2-Way	On-Axis	40	2K	1330-1440	-8			63	4	1" Dia Steel Ball	
X	-2													DUD
	-3										54	4	3 Slots in Alum. Plate	
X	-4													DUD
	-5				20	2.5 K	1400-1460				63	4	3 Slots in Alum. Plate	
	-6				20						65	2.8		
	-7				10						67	2.8		
		G-1 Gave Perfect Fresnel Zone Plate Hologram Which Was Used for Computer Imaging Work.												

TABLE I , Cont.

Continued Long Range Tests - 51.5" Range (131 CM)

SERIES	TECHN.	MODE	REF.	XMTTR		RECEIVER		SCAN			F NO.	SPECIMEN	REMARKS
				PL	PRI	GATE	GAIN	MODE	INT.	TIME			
H-1	Imm.	2-Way	On-Axis	40	2K	1420-1570	-8			60	4	Egg	
-2	↓	↓	↓	20	↓	↓	↓	↓	↓	60	↓	Egg	In Tank Over Night
-3	↓	↓	↓	↓	↓	↓	↓	↓	↓	65	↓	Knot in 3/4"Plywood	
-4	↓	↓	↓	↓	↓	↓	↓	↓	↓	55	↓	Allen Screw in Plywood	
			Egg Gave Point Image from Surface;Highly Astigmatic										
			Focusing Because of Ellipsoidal Shape										

TABLE I , Cont.

Long Range Tests

SERIES	TECHN.	MODE	REF.	XMTTR		RECEIVER		SCAN			F NO.	SPECIMEN	REMARKS
				PL	PRI	GATE	GAIN	MODE	INT.	TIME			
I-1	Imm.	2-Way	On-Axis	40	2K	1420-1550	-9			65	4	Wire Letters P-E	
-2	↓	↓	↓	↓	↓	↓	-8			60	↓	↓	Ditto I-2 Lower Gain
-3	↓	↓	↓	↓	↓	1440-1510	↓			65	↓	French Coin	
-4	↓	↓	↓	↓	↓	↓	↓				↓		DUD No Vert Scan
-5	↓	↓	↓	↓	↓	↓	↓			60	↓	0.5" Dia Ball	
-6	↓	↓	↓	↓	↓	1440-1520	↓			63	↓	2-0.5" Dia Balls 1.5CM Apart	1 Ball Fell Off During Run
			Excellent Images from All - Specular Reflection from										
			Coin and Letters										

X

TABLE I, Cont.

Long Range Tests - Rough Sandpaper Illuminator

SERIES	TEST IN.	MODE	REF.	PMT		RECEIVER		SCAN			P NO.	SPECIMEN	REMARKS
				PL	PRE	GATE	FAIL	MODE	INT.	TIME			
J-1	Imm.	1-Way	On-Axis	30	2K	1160-1220	-8			62	4	3 Slots in Alum.Plate	Illum By Bounce from Sandpaper
-2	↓	↓	↓	40	↓	1160-1235	-8			63	↓	↓	Ditto J-1 Diff. Geometry
-3	↓	↓	↓	40	↓	↓	-9			58	↓	↓	Ditto J-2 Higher Gain
-4	↓	↓	↓	60	↓	↓	-8			60	↓	Large Medallion	
		Provided No Solution to Specular Reflection Problem.											

TABLE I, Cont.

Tests Placing Targets on Acoustic Reflector

SERIES	TECHN.	MODE	REF.	XMTR		RECEIVER		SCAN			F NO.	SPECIMEN	REMARKS
				PL	PRI	GATE	GAIN	MODE	INT.	TIME			
K-1	Imm.	1-Way	On-Axis	20	2K	830-900	-8V			58	4	Illum. Xducer	41" Range
-2				20						58		3-Bar Plate on Mirror	Ditto K-1
-3				30						63		Coin on Mirror	
-4				30			-9			60		Coin on Mirror	
-5				40		1180-1240	-8			60		3-Bar Plate on Mirror	1"Dia Ball as Illuminator
-6				40						58		Medallion on Mirror	Ditto
-7										60		Sandpaper Letters on Mirror	
-8						1200-1255				58		Sandpaper Reflector	

TABLE I , Cont.

Signal to Noise Ratio Experiments Ball Target Reduced Power

SERIES	TECHN.	MODE	REF.	TR		RECEIVER		SCAN			F NO.	SPECIMEN	REMARKS
				PL	PRI	GATE	GAIN	MODE	INT.	TIME			
L-1	Imm.	2-Way	On-Axis	40	2K	1200-1260	-8	1		57	4	2 0.5" Dia Balls 1.6 CM Apart	
-2										30			Increased Vert Scan Rate
-3										30		East Ball Removed	
-4										35		One Ball	Atten. In No Discern. Sig.
-5													On Scope Weak Holos.
-6													
-7													Very Faint
-8													Very Faint

TABLE I , Cont.

NDT Experiments													Fast Scan Along Hole
SERIES	TECHN.	MODE	REF.	XMTR		RECEIVER		SCAN			F NO.	SPECIMEN	REMARKS
				PL	PRI	GATE	CAL.	MODE	INT.	TIME			
M-1	Imm.	1-Way	On-Axis	5	1000	260-305	-8			44	4	1-Hole	
-2				10						44			Atten. In XMTTR Line
-3				3						44			
-4				3									DUD No Vert Scan
-5				5		250-325				46			Avg. Sig Went to 150μsec Found Bad Joint
-6				5						40			
-7				10									
Results	- First 3 have sharp lines.			M-2 appears best, M5,6,7 Not Good - Appear Fuzzy - No									
	sharp lines; may have to go back to contact method; tilted Xducer to remove Backscatter												
	into Xducer.												

X

TABLE I, Cont.

	SERIES	PATTERN	MODE	REF.	TRANSMITTER PRF	TRANSMITTER PW	RECEIVER GATE	RECEIVER GAIN	SCAN MODE	SCAN INT.	SCAN TIME	F NO.	SPECIMEN	REMARKS
	Rubber Absorbers Put On Edges of Blocks - Fast Scan Along Hole													
X	N-1	1mm.	1-Way	On-Axis	8	1K	242-325	-8V			45	4	3-Hole	
X	-2	↓	↓	↓	10	↓	↓	↓			45	4	↓	Blank Raster Fet Socket Bad
X	-3	↓	↓	↓	10	↓	↓	↓			45	4	3-Hole	
	-4	↓	↓	↓	10	↓	↓	↓			45	4	Clear	
	-5	↓	↓	↓	10	↓	↓	↓			45	4	1-Hole	
	-6	↓	↓	↓	10	↓	234-305	↓			45	4	1-Hole	Xducer Normal to Block
				Fine Rectangular Pattern in Holograms										
				N1-2-3 Holograms Missing										

TABLE I , Cont.

NDT Experiments													Fast Scan Across Hole from No. 4 and After
SERIES	TECHN.	MODE	REF.	XMTTR		RECEIVER		SCAN			F NO.	SPECIMEN	REMARKS
				PL	PRI	GATE	GAIN	MODE	INT.	TIME			
0-1	Imm.	1-Way	On-Axis	5	1K	214-264	-8V			44	4	1-Hole	
-2	Imm.			10		220-264				42			
-3				5		105-128				45			DUD No Vert. Scan
-4	Cont.			5		105-128				41			Rubber Over All But Hole
-5				5		105-128				41			Repeat 0-4 Rubber Removed
-6				10		105-133				40			Atten. in. XMTTR Line
-7				10		110-133				45			Atten. in. Rubber Over All but Hole
		Switched to Fast Scan Across Hole 0-4,5,6											
		First Signs of Good Reconstruction											

X

TABLE I , Cont.

New Scanner Motors Step Scan in Vert. Scan - Blanker still being used up to P-6
#6 Posit = 45 Min.

	SERIES	PATTERN	MODE	REF.	FILTER PL	FILTER PRI	RECEIVER GATE	RECEIVER GAIN	SCAN MODE	SCAN INT.	SCAN TIME	F NO.	SPECIMEN	REMARKS
X	P-1	Blank Raster				1K			1	6	45	4	None	250µsec
X	-2								1	6	45	4		225µsec
	-3								1	6	45	4		150µsec too light
	-4	Cont	1-Way		3		100-132	-8V	1			4	One Hole	
	-5				3				1			5.6		Too light
	-6				6				1			5.6		
	-7				6				2	12	23	5.6		Scan in Two Directions
	-8				3				2	8	35	5.6		Scan in Two Directions
			Water Pump on for Whole Series											
			Modulation Weak - will go to 2000µsec PRI											

TABLE I , Cont.

	SERIES	TECHN.	MODE	REF.	ATTR PL	ATTR PRI	RECEIVER GATE	RECEIVER GAIN	SCAN MODE	SCAN INT.	SCAN TIME	F NO.	SPECIMEN	REMARKS
	Attempt to Improve Contrast													
X	Q-1	Blank Raster				1K			2	8		4	450µsec	50,150,250,350, Lamp Durations
X	-2					1K			2			5.6	Ditto	Q-1
X	-3					2K			2			4	Ditto	Q-1
X	-4					2K			2			5.6	Ditto	Q-1
	-5	Cont.	1-Way	On-Axis	3	2K	95-130	-9V	2	8	33	4	1-Hole	Raised RCVR Gain More Jitter on Lamp
	-6	↓	↓	↓	3	↓	↓	-10	2	8	33	4	↓	Now +25µsec Noise Jitter
	-7	↓	↓	↓	8	↓	↓	-9	2	8	33	↓	↓	Atten. in Line
	-8	↓	↓	↓	3	↓	↓	-8	2	8	34	↓	Clear	
			Q1-2-3-4 Test Strips to Check Exposures											

TABLE I , Cont.

	SERIES	TECHN.	MODE	REF.	FILTER PL	FILTER PRT	RECEIVER GATE	RECEIVER ATN	SCAN MODE	SCAN INT.	SCAN TIME	F NO.	SPECIMEN	REMARKS
	Return to Immersion Technique - Monostatic (2-Way) Transmission R-5 on													
X	R-1	Imm.	1-Way	On-Axis	3	1K	162-178	-10	2	8	35	5.6	1-Hole	
X	-2	↓	↓	↓	6	↓	162-182	-9	↓	↓	34	↓	↓	Ditto R-1 with 6-μsec Pulse
	-3	↓	↓	↓	9	↓	162-185	-8	↓	↓	36	↓	↓	Motor Fan Not On.
	-4	↓	↓	↓	12	↓	160-196	-8	↓	↓	35	5.6 8.0	↓	
	-5	↓	2-Way	↓	3	↓	168-205	-10	↓	↓	↓	5.6	↓	
	-6	↓	↓	↓	6	↓	170-205	-10	↓	↓	↓	↓	↓	
	-7	↓	↓	↓	6	↓	160-205	-8	↓	↓	↓	↓	↓	
X	-8	↓	↓	↓	6	↓	162-205	-8.6	↓	↓	↓	↓	↓	DUD No Vert. Scan
	-9	↓	↓	↓	6	↓	162-205	-8.6	↓	↓	↓	↓	↓	Atten. In
	-10	↓	↓	↓	6	↓	172-188	↓	↓	↓	↓	↓	Clear	Atten. In
	-11	↓	↓	↓	6	↓	174-188	↓	↓	↓	↓	↓	3-Hole	No Atten.

TABLE I, Cont.

Phase Shifter for Off-Axis Holograms S-2,3,4.

	SERIES	TECHN.	MODE	REF.	XMTR		RECEIVER		SCAN			F NO.	SPECIMEN	REMARKS
					PL	PRI	GATE	GAIN	MODE	INT.	TIME			
	S-1	Imm.	2-Way	On-Axis	20	1K	190-299	-11	2	6	44	5.6	1-Hole	
	-2	↓	1-Way	Off-Axis	6		162-182	-9			↓		↓	
X	-3		↓	↓	6		160-190	-9					3-Hole	
X	-4			↓	6		163-190	-10					1-Hole Cyc.	Heard Vert. Scan Miss - will Put Diode Phase Relay
X	-5			On-Axis	6		160-190	-10		8	34		Clear	
	-6			↓	6		160-190	-9		6	45		3-Hole	
	-7				3		160-190	-10			46		↓	
	-8	↓	↓	↓	3		164-200	-10			45		Glass Block	
			Using Higher Receiver Gain											
			Step Scan Being Triggered by Phase-Shifter Relay											

TABLE I, Cont.

Off-Axis Holograms

SERIES	TECHN.	MODE	REF.	FILTER PL	FILTER PCI	RECEIVER GATE	RECEIVER GAIN	SCAN MODE	SCAN INT.	SCAN TIME	F NO.	SPECIMEN	REMARKS
T-1	Imm.	1-Way	Off-Axis	3	1K	160-200	-9	2	6	45	5.6	3-Hole	
-2	↓	↓	↓	↓	↓	↓	-9.25	2	3	90	↓	↓	Very Fine Scan-Water Pump Off
-3	↓	↓	↓	↓	↓	↓	↓	↓	6	35	↓	1-Hole	Flattened Bottom of Hole-Pump Off
-4	↓	↓	↓	↓	↓	↓	↓	↓	↓	45	↓	↓	Ditto R-3
-5	↓	↓	↓	↓	↓	↓	↓	↓	↓	↓	↓	↓	
-6	↓	2-Way	On-Axis	↓	↓	79-97	↓	↓	↓	↓	↓	↓	
		No Recognizable Echo from End View of Hole in T-3.											

X

TABLE I, Cont.

Other Test Specimens

SERIES	LENGTH	MODE	REF.	TRANSMITTER		RECEIVER		SCAN			F NO.	SPECIMEN	REMARKS
				PL	PRI	GATE	GAIN	MODE	INT.	TIME			
U-1	Imm.	1-Way	On-Axis	3	1K	159-207	-10	2	6	44	5.6	Alcoa #4	
-2	↓	↓	↓	6	↓	↓	↓	↓	↓	47	↓	↓	
-3	↓	↓	↓	6	↓	↓	↓	↓	↓	45	↓	Alcoa #1	
-4	↓	↓	↓	16	↓	↓	-9	↓	↓	45	↓	↓	
-5	↓	↓	↓	6	↓	167-207	-9.5	↓	↓	45	↓	Coverage Block	1/4" Edge on Top
-6	↓	↓	↓	↓	↓	↓	↓	↓	↓	47	↓	↓	3/4" Edge on Top
-7	↓	↓	↓	3	↓	162-207	↓	↓	↓	45	↓	Resolution Block	
-8	↓	↓	↓	6	↓	↓	-9	↓	↓	45	↓	↓	Ditto U-7 6μsec Pulse
-9	↓	2-Way	↓	3	↓	106-121	-10	↓	3	90	↓	↓	
-10	↓	↓	↓	10	↓	165-189	-10	↓	6	50	↓	Lens Piece	
-11	↓	↓	↓	11	↓	167-177	-10	↓	6	45	↓	Flat Plate	Alum. Side Up

A12

A15

A16

B11

B14

B15

B16

C3

D1

D2

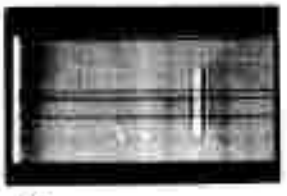

D3

E1

E2

E4

F1

F3

F4

F5

F6

Figure 27. Ultrasonic Holograms Generated on Program (See Table I). (six pages)

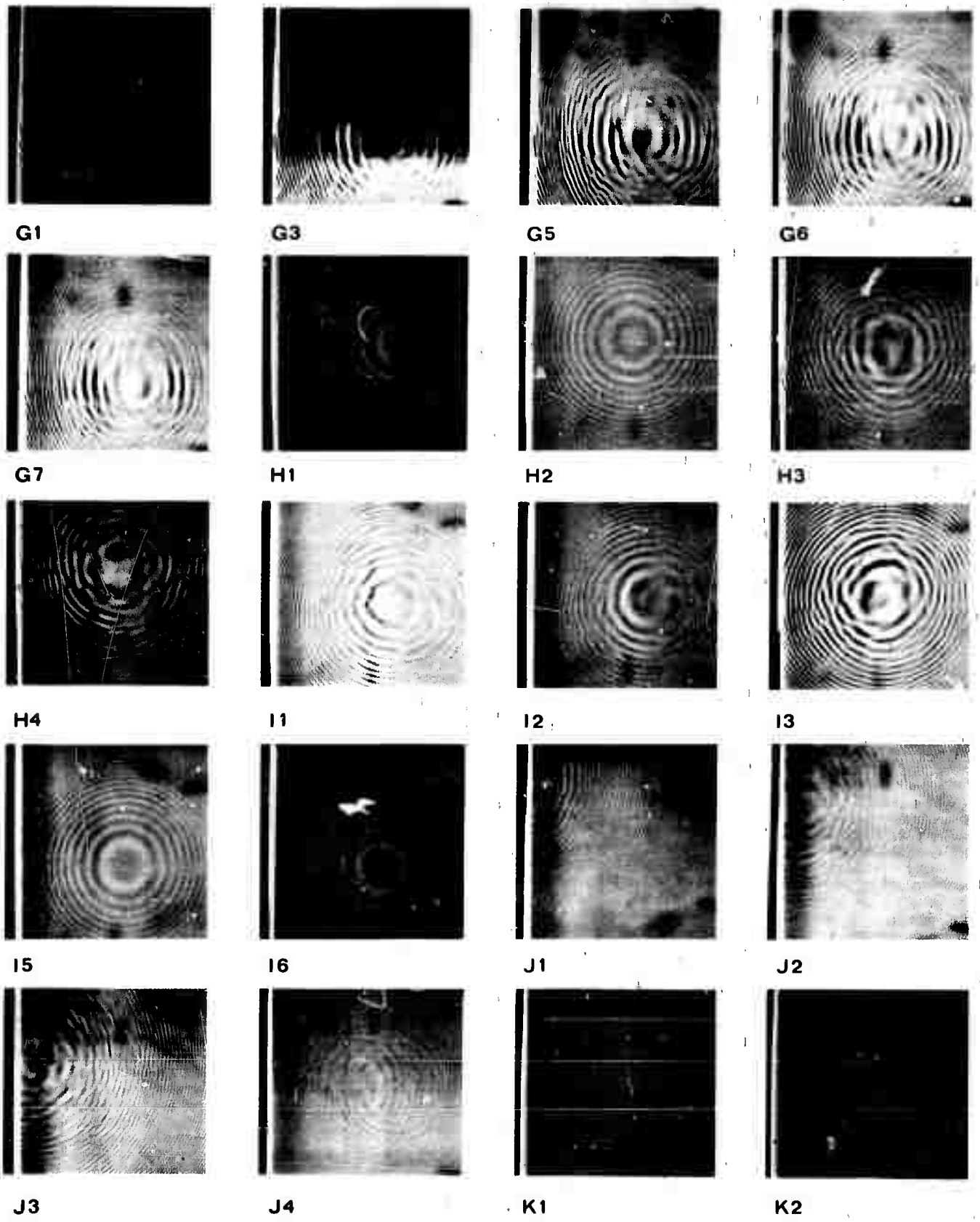

Figure 27. (Cont.)

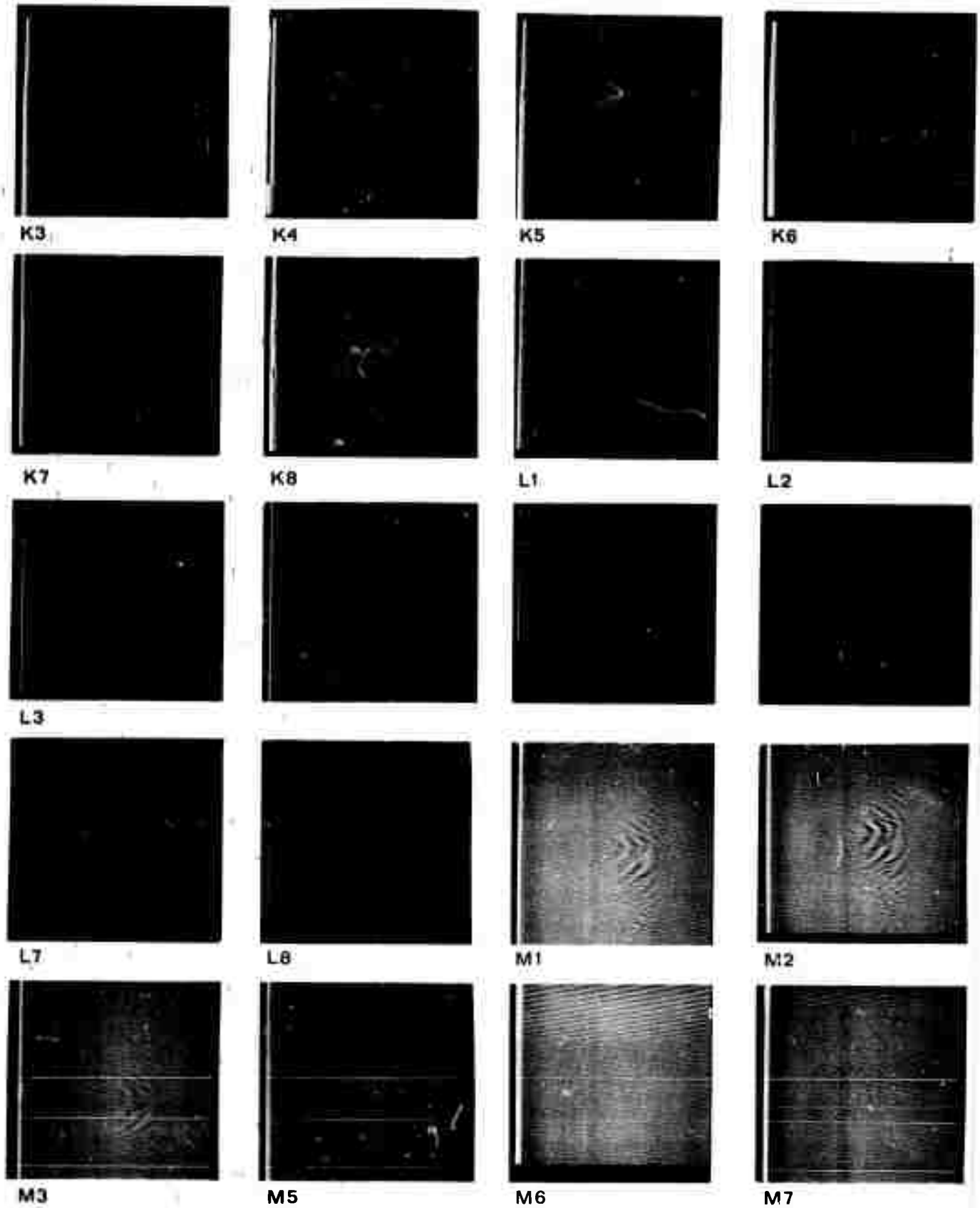

Figure 27. (Cont.)

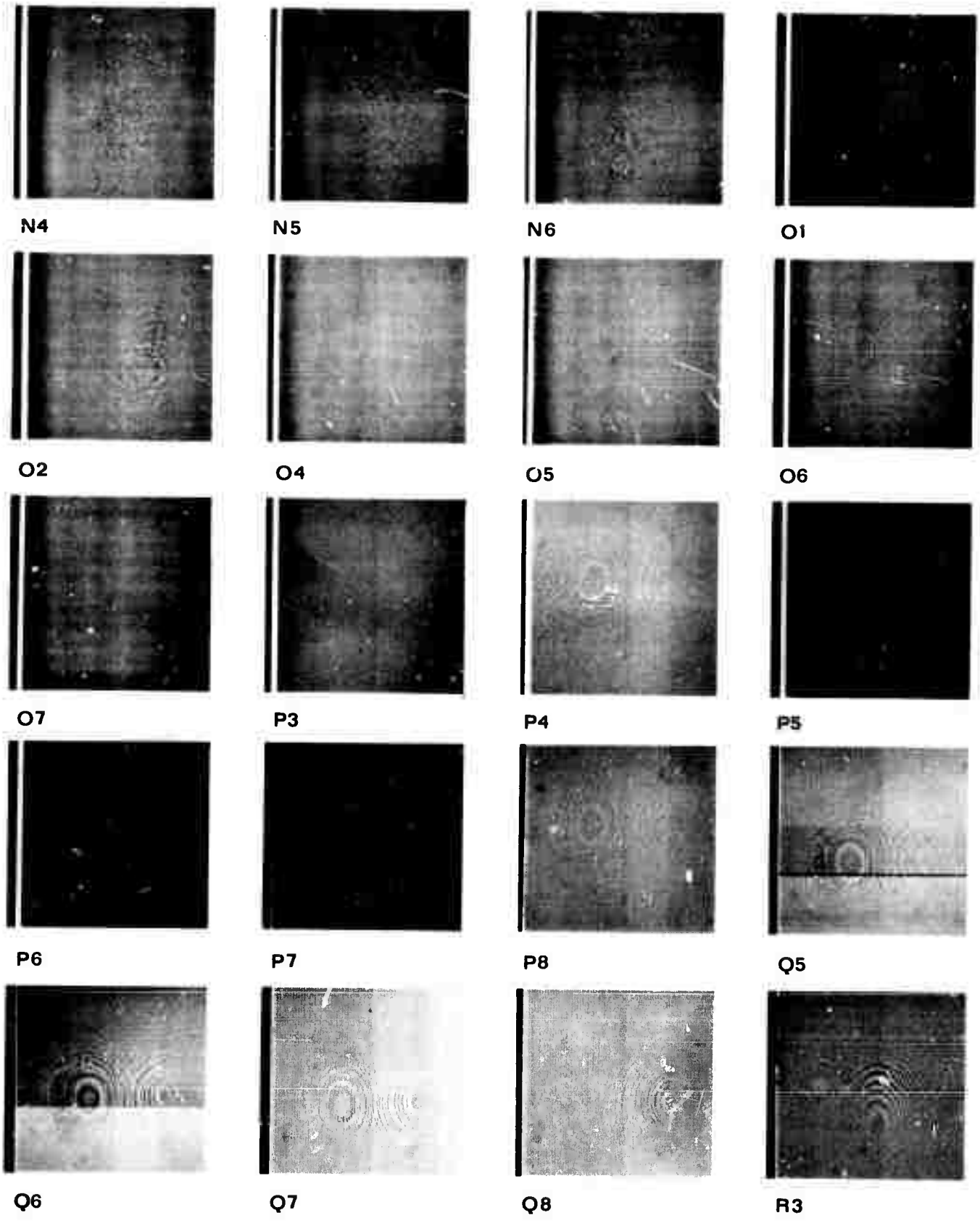

Figure 27. (Cont.)

R4

R5

R6

R7

R9

R10

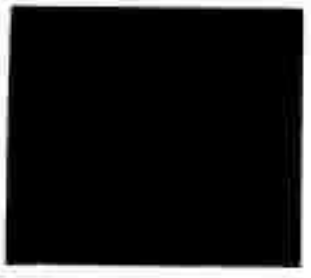

R11

S1

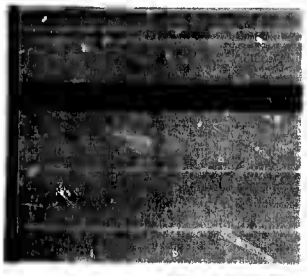

S2

S6

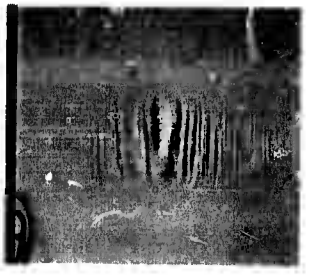

S7

S8

T1

T2

T3

T5

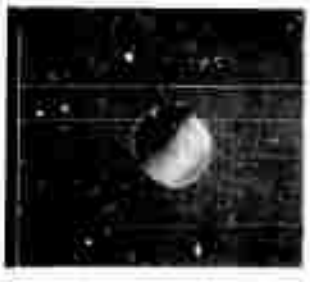

T6

U1

U2

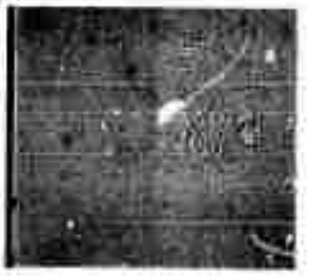

U3

Figure 27. (Cont.)

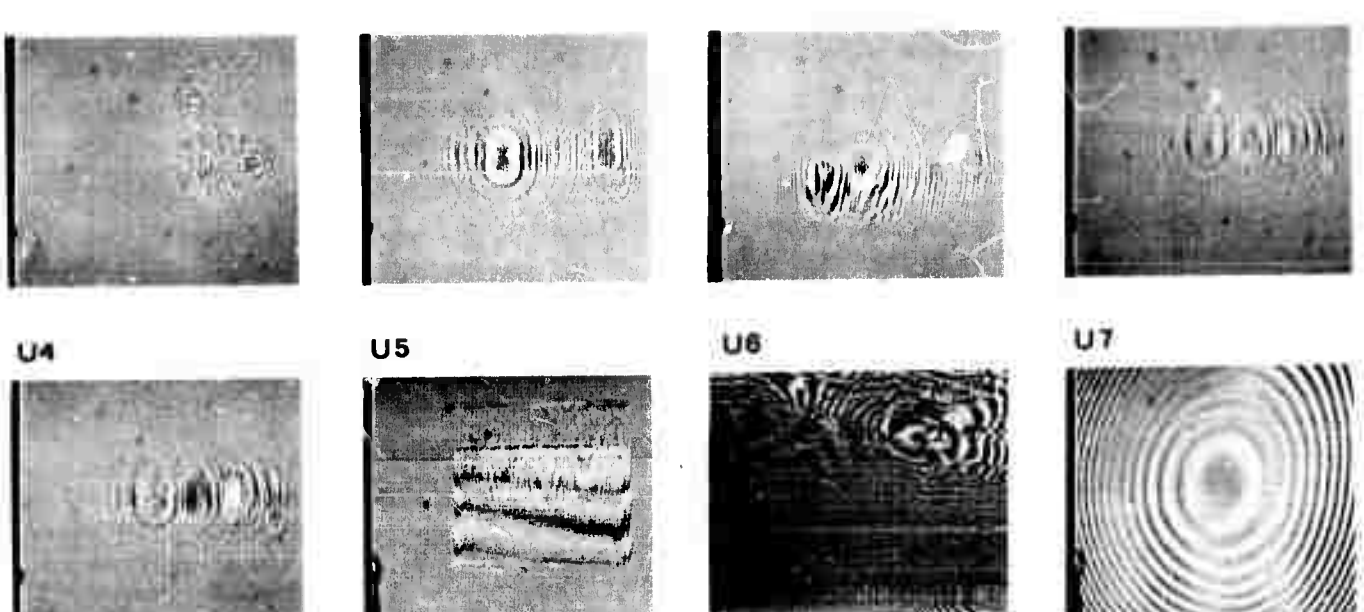

Figure 27. (Cont.)

through series J were carried out on a Perkin-Elmer related IR&D program, but the results obtained were of considerable value during the remainder of the work on the NDT program.

The holograms made at long range of the steel balls (G-1, particularly) were especially valuable for calibration and analysis work (See Reference 3, page A-4, Figure A-1), since they behaved as almost perfect point scatterers. G-1, the hologram of a one-inch diameter ball was also used for the computer generated image reported in Appendix B of reference 3, and summarized in Appendix B of this report.

Holograms made of other small targets at the long range produced surprisingly good images upon reconstruction (see Figures 28 and 29, for example), but emphasized immediately the prevailing problem of high frequency underwater imaging - the effects of specular reflection. Most objects appear very smooth at an acoustic wavelength of 0.3mm (5MHz frequency). and reflect an image of the illuminating transducer at target aspect angles which direct the reflection into the receiver. The reconstructed image of a small coin illustrated in Figure 29 demonstrates this effect. The coin was approximately one inch in diameter and located at range of 40 inches from the receiving transducer.

The K-series of holograms covered some experiments in which the targets were placed close to the receiving antenna (on the acoustic mirror in the tank), and on the use of diffuse scatterers. The L-series were made using two small balls to check resolution capabilities at the long range, and using one small ball at various ranges from the receiving antenna. The remaining series of holograms, M through U, were made for NDT evaluation at shorter ranges.

Commencing with the M series of holograms and continuing through R-4 all of the experimental testing was concentrated on the difference in performance between the contact technique of illuminating the specimen and the immersion technique. Since the results of this work were covered thoroughly in the third semi-annual technical report. reference 3, they will be only summarized at this point.

The difference between the contact and immersion techniques was illustrated in Figure 19 in Section III of this report. It would be very desirable if most holographic NDT work could be done without altering the specimen or fastening a transducer onto the specimen. It was especially important, therefore, to investigate these two techniques.

1. Contact Technique

When a wide-angle illuminating transducer was fastened to one end of either the blank test block or the one having the single hole, two strong pulse signals were observed as the receiving transducer was scanned along the block from X to Y in Figure 30. One of the signals had a delay time of 92 microseconds when the receiving transducer was directly over the edge of the block where the transmitting transducer was fastened (front), and increased in delay time to approximately 108 microseconds as the receiving transducer scanned

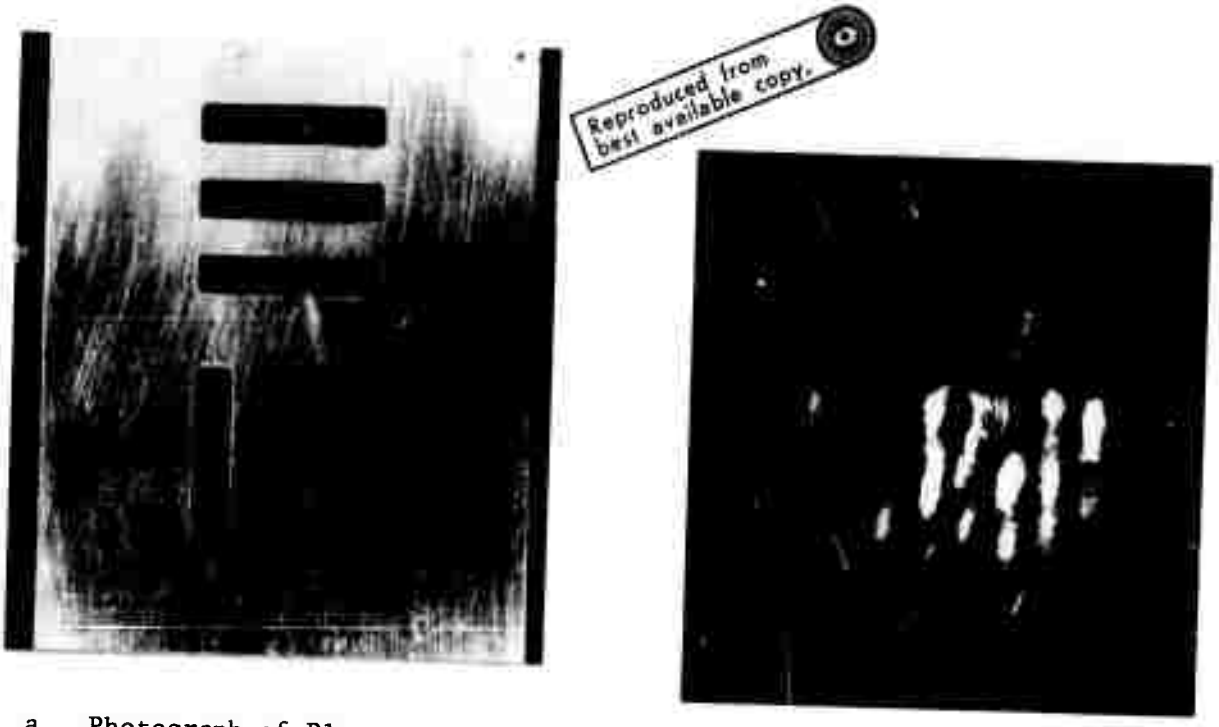

a. Photograph of Plate

b. Reconstructed Image

Figure 28. Reconstructed Image of 3/16-Inch Wide Slits in Aluminum Plate (range approximately 40 inches)

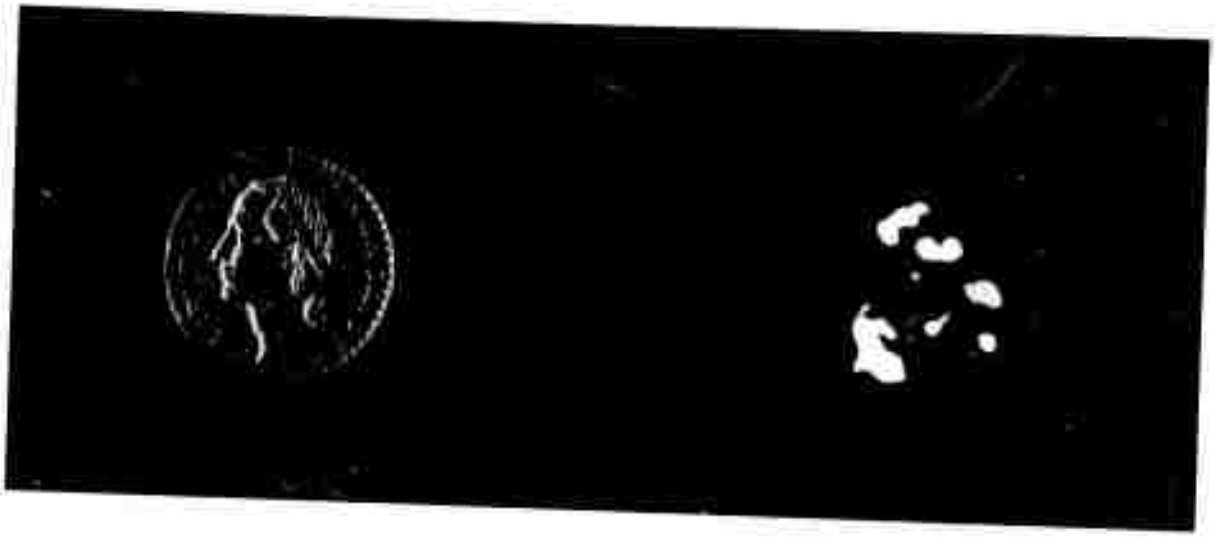

a. Photograph of Coin

b. Reconstructed Image

Figure 29. Reconstructed Image of 1-Inch Diameter Coin (range approximately 40 inches)

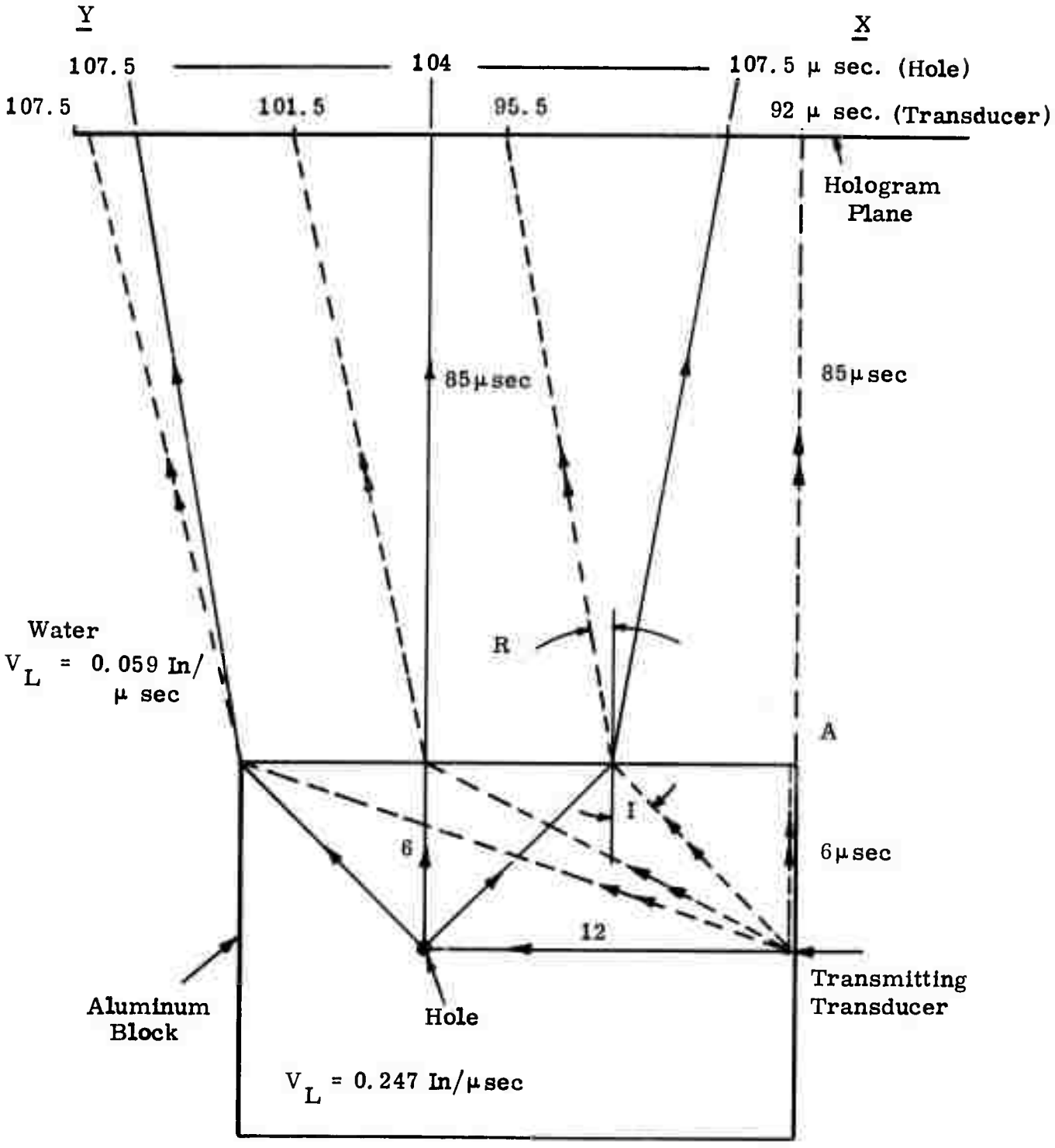

Figure 30. Calculated Signal Paths and Delay Times (Hole Defect and Direct Transducer)

along the block to a position about one inch beyond the rear edge. The second signal did not appear until the scanner was approximately over the center of the test block, and was larger than the first. Its delay time went from 105 microseconds, when the signal first appeared, to approximately 130 microseconds at the end of the scan.

Oscilloscope photographs of the two received signals are shown in Figure 31. Figure 31a was taken with the transmitting transducer fastened to the clear aluminum block, while Figure 31b was taken with the transducer fastened to the block with the single hole. A three-microsecond transmitted pulse was used. The time scale in the photographs is 10 microseconds per centimeter, and the two small pips at the third and seventh centimeter locations are markers that define the start and finish of the receive gate, which was set from 90 to 130 microseconds. The receiving transducer was located approximately over the hole in the block, and at this point the first signal had a time delay of approximately 98 microseconds, and the second signal a time delay of approximately 110 microseconds, as may be seen in the photographs. A signal from the hole should be present within the 104- to 107.5-microsecond range.

Since the two strong signals occur at time delays which overlap the expected time delay of the hole defect, it was not possible to positively identify the signal from the hole at any location of the receiving transducer. Figures 31a and 31b indicate very little difference between the signals received from the block with the hole and the block without the hole.

By plotting the possible propagation paths and calculating the delay times graphically, as shown in Figure 30, the first interfering signal was identified as the direct pulse from the transmitting transducer. This signal is propagated as a longitudinal wave in the aluminum and the water, as indicated by the dotted lines in Figure 30, with refractive bending at the aluminum-to-water boundary in accordance with Snell's law. The source of the second large pulse signal was found to be the reflection of the transmitted signal from the bottom of the block.

Figures 32a and 32b are enlargements of the acoustic holograms made from the two block specimens just described. Figure 32a was made by illuminating the block without the hole, while Figure 32b was made by illuminating the block with a single hole. Although the pulse signals observed from each were essentially identical, as shown in Figures 31a and 31b, the holograms were decidedly different. The hologram of the clear block (Figure 32a) shows the zone plate originating over the leading edge of the block and the fine fringes toward the rear edge of the block where the bottom echo signal predominated. The hologram of Figure 32b has, in addition to these zone plates, a new zone plate with its zero phase area located over the region of the hole. Thus, even though the pulse echo of the hole was not readily discernible in the clutter, the zone plate it created was made visible by the coherent detection processing.

Reconstructed images made from the holograms of Figures 32a and 32b are illustrated in Figures 33a and 33b, respectively. In these holograms the direct image of the transmitting transducer fastened to the block specimen is shown as a bright point at the right center of the photograph. The image of the

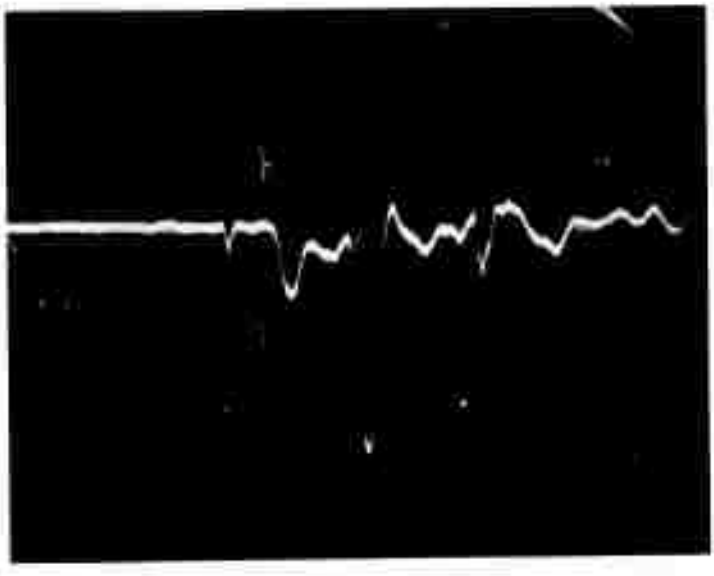

a. Aluminum Block Without Hole
(Scale 10μsec/cm

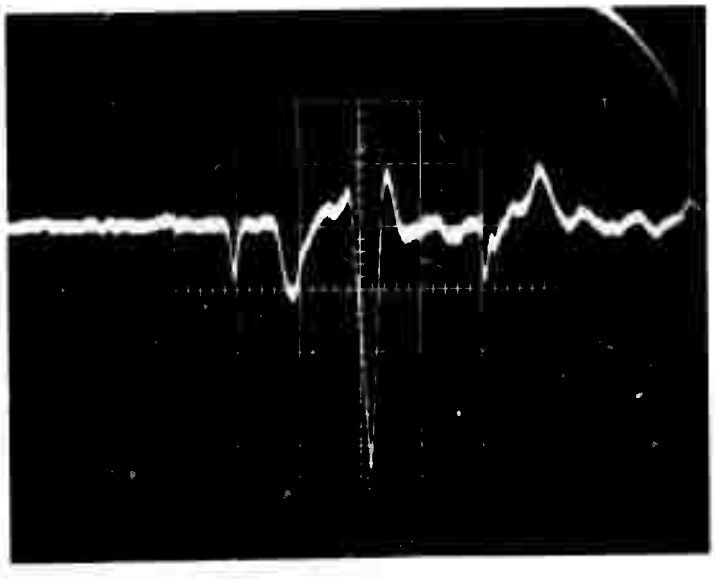

b. Aluminum Block with Single Hole
(Scale 10μsec/cm

Figure 31. Received Signals - Contact Technique

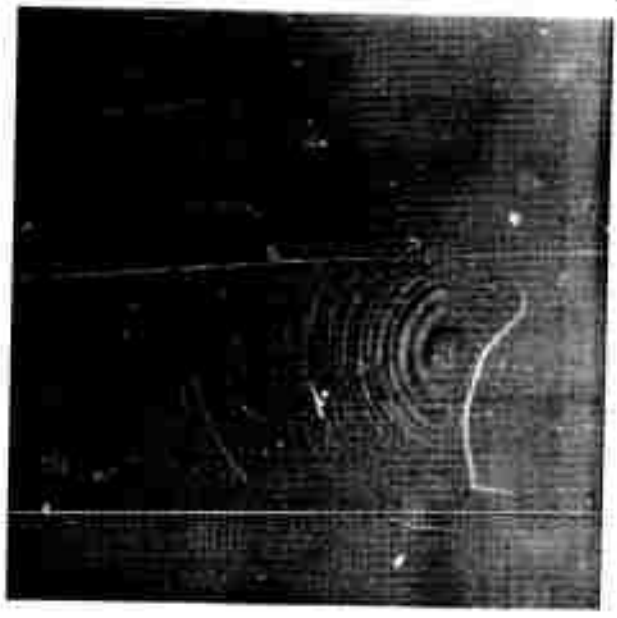

a. Aluminum Test Block Without Hole

b. Aluminum Test Block With Single Hole

Figure 32. Acoustic Holograms - Contact Technique

a. Aluminum Test Block Without Hole

b. Aluminum Test Block With Single Hole

Figure 33. Reconstructed Images - Contact Technique

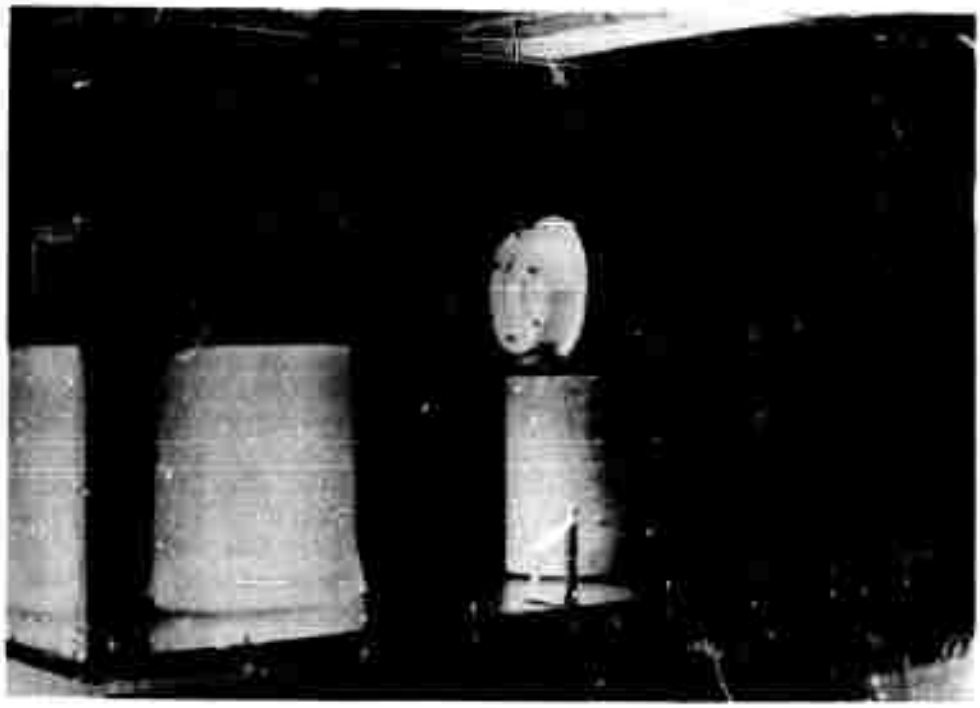

Figure 34. Immersion Testing Technique Setup in Tank

hole may be seen to the left of the transmitting transducer in Figure 33a, but is not seen in Figure 33b.

2. Immersion Technique

In implementing this technique, a high-gain transmitting transducer was placed about 4 inches away from one end of the test specimens, as shown in Figure 34 (also visible in a 90-degree rotated orientation in the photograph of the overall system, Figure 10). It was hoped that sufficient energy could be transmitted into the block and scattered from a defect to produce a useful hologram at the scanning plane. Difficulties were anticipated in obtaining good results with this technique because of the high percentage of acoustic energy reflected away from a water-to-metal (aluminum) interface, the large refractive angles experienced by the longitudinal and transverse waves propagating in the block from the point of incidence of the illuminating beam, and the relatively narrow beam of the illuminating transducer.

When the test blocks are illuminated by the high-gain transducer, using the immersion technique, the signals received from known defects within the blocks are much stronger than those received from the same defects when the small, low-gain transducer is used in contact with the block. At the same time, spurious signals from multiple reflections within the specimen (occurring within the range of expected defect signals) are not as prevalent or as large in amplitude as when the contact technique is used. This is undoubtedly the result of the higher gain and increased directivity of the illuminating transducer.

According to the plot of signal paths and time-delays the signal from the single hole should appear at a time delay of 168 to 177 microseconds and indicate a zero change in phase directly over the hole. This was verified experimentally, as shown by the photograph of the signal received from the hole in Figure 35b. In the photograph the time scale is 10 microseconds per centimeter, and the receive gate marker pips occur at 162 and 202 microseconds. The signal from the hole may be seen as the strong 3-microsecond-long negative pulse-starting at 168 microseconds in Figure 35b. Note that the signal from the hole is clearly discernible and not obscured by noise and clutter, as was the case for the contact technique. Figure 35a is the corresponding photograph of the signals received from the block without a hole.

Holograms made from the clear and single-hole blocks under these conditions are illustrated in Figures 36a and 36b, respectively. Because of the strong signal return from the hole and the relatively weak returns from spurious reflections, the zone plate from the hole predominates in the hologram of the single-hole block (Figure 36b). However, it may be noted in the hologram that the zone plate produced by the hole is not complete and the lower fringes are not present. This is probably caused by refraction of the collimated illuminating source away from a portion of the hole and not by any tilt of the hole with respect to the sampling plane.

The reconstructed images made from the holograms of Figure 36 are shown in Figure 37. The hologram of the clear block, of course, produces no image, Figure 37a, while the hologram of the block with the single hole produces

a. Aluminum Block Without Hole
(Scale: 10μsec/cm)

b. Aluminum Block With Single Hole
(Scale: 10μsec/cm)

Figure 35. Received Signals - Immersion Technique

a. Aluminum Test Block Without Hole

b. Aluminum Test Block With Single Hole

Figure 36. Acoustic Holograms - Immersion Technique

a. Aluminum Test Block Without Hole

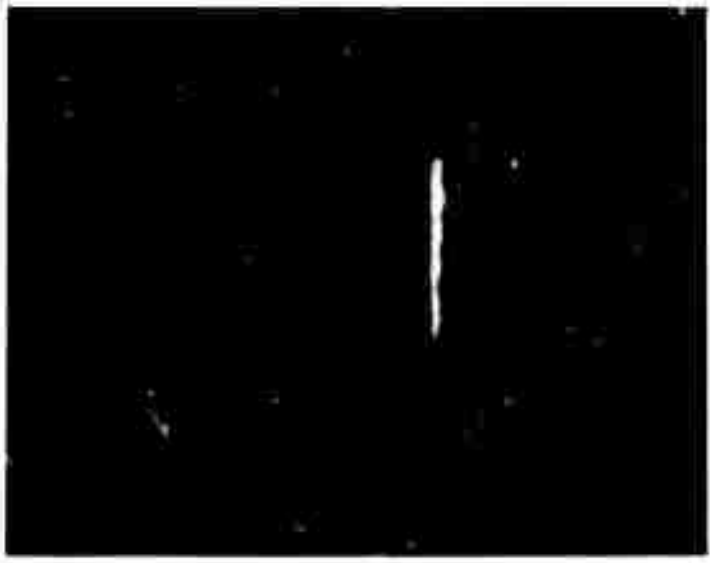

b. Aluminum Block With Single Hole

Figure 37. Reconstructed Images - Immersion Technique

a strong image of the hole. Figure 37b. Because of the lack of strong interfering signals within the range-gated interval encompassing the hole signal, the hole image is exceptionally clear of extraneous background caused by defocused images of the transducer received either directly, or by reflection from the internal surfaces of the block specimen. The image focuses sharply and the signal-to-noise ratio of the output image is high.

Although the tests performed to date demonstrate that better results are obtained by not fastening the transmitting transducer to the specimen to be tested, it must be recognized that a much smaller transmitting transducer was mounted on the block for the contact tests than was used in the water for the immersion tests. The transducer fastened to the block was only 10 wavelengths (1/8 inch) in diameter, while the one used for the immersion testing was 170 wavelengths (2 inches) in diameter. The difference in power gain between the two is approximately 25 dB. The smaller transducer was used on the block to provide wide angular coverage which would illuminate the entire interior of the specimen. The larger one was used for the immersion testing to make up for the additional water path attenuation and the loss due to reflection at the block face. If a larger transducer were mounted on the block, the image of the single hole defect obtained with the contact technique would probably be as good or better than that obtained with the immersion technique. Holograms made of the same single-hole block earlier in the program using a one-half inch diameter transducer mounted on the block produced images comparable to those obtained with the immersion technique.

After completing the analysis of the contact and immersion techniques, all remaining testing was done using the immersion technique. Since only the clear and single-hole blocks had been used in that analysis, the more complicated three-hole block was chosen next and it provided excellent holograms (S-6 and S-7). These were analyzed thoroughly in the reconstruction phase.

At the same time, a small transmitting transducer was mounted directly alongside the receiving transducer on the scanner carriage, so that monostatic (two-way) transmission could be employed (holograms R5 through S-1).

Reconstructed images of the three-hole block using the immersion technique were strong and focused well according to their depth in the block. However, multiple reflections of the holes from the bottom, top, and sides of the specimen (internal) were quite numerous and strong at several focusing positions within the range of interest. Figures 38a through 38ℓ illustrate what was attained with this reconstruction.

The images reconstructed in Figure 38 were made by focusing the optical system to provide 10 equal intervals of depth within the block between its top and bottom surfaces. To obtain these calculated depths, the distance between the hologram plane and the image plane being examined was varied from 20cm to 48cm in ten 2.8cm steps. Figure 38a, made just below the top surface of the block at 22.8cm, illustrates the multiple reflections which can be present. The holes in this block (see Figure 38) are located so that the one in the center of the reconstruction is above the others, the one to the left of the top one is midway between the top and bottom holes, and the bottom hole is

(a) b = 22.8cm

(b) b = 25.6cm

(c) b = 28.4cm
ND = 0.6

(d) b = 28.4cm

(e) b = 31.2cm

(f) b = 34.0cm

(g) b = 36.8cm
ND = 0.6

(h) b = 36.8cm
ND = 1.0

(i) b = 39.6cm

(j) b = 42.4cm

(k) b = 45.2cm

(l) b = 48.0cm

Figure 38. Reconstructed Images from 3-Hole Block, Immersion Technique

directly under the top one. In the reconstruction the top hole focuses first between 31.2 and 34.0cm, the left-hand hole around 34.0cm and the bottom hole just to the right of the top at 36.8cm. If shorter exposures are used. it will be noted that all three holes may be clearly seen at one time, both near the top of the block, Figure 38d, and near the bottom, Figure 38ℓ. Although it may appear from these photographs that it would be very difficult to locate the holes positively if their locations were not known, it is not that difficult when using the optical setup. Figure 39, for example, is an enlarged photograph of the top hole when it was focused precisely. However, care must be taken in interpreting the results, as is the case in conventional pulse-echo testing.

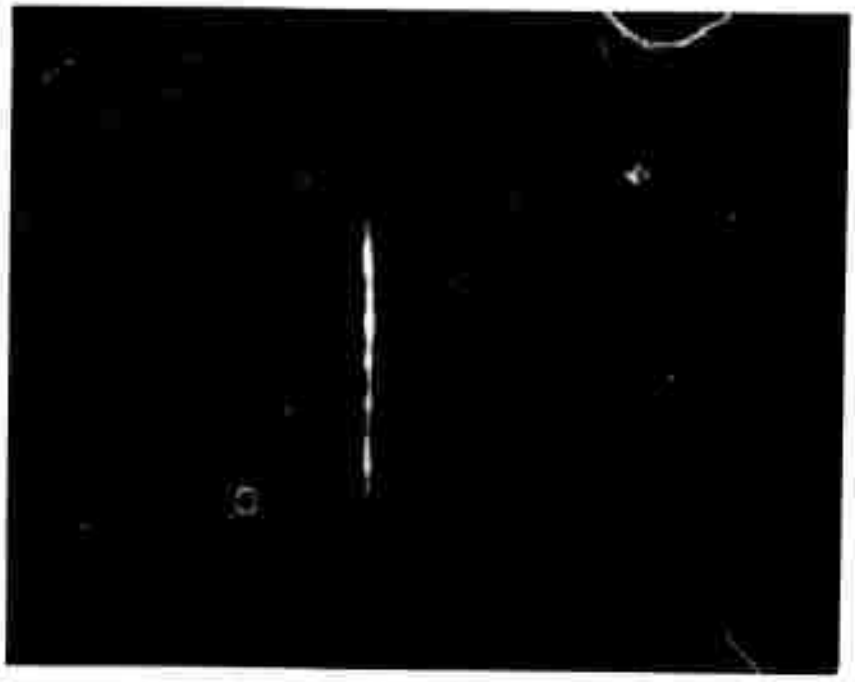

Figure 39. Enlarged Reconstructed Image of Top Hole in 3-Hole Blank (see Figure 38e)

3. Monostatic Transmission

Since good images were being produced by the immersion technique, it was expected that very good results would be obtained by mounting the transmitting transducer on the carriage of the scanner alongside the receiving transducer and transmitting and receiving from the scanner. It was reasoned that, since the transmitted energy was directed throughout all portions of the specimen by the scanning action, this mode of transmission would at least duplicate the results of the previous immersion testing. Also, it had been found during the immersion testing that the backscatter from the defect was much stronger than the forward scatter (see the third semi-annual technical report, reference (3), page 20) which would favor this mode of transmission. Then, there is a doubling of the theoretical resolution obtainable from two-way illumination, since the phase and amplitude of a signal are affected by the position of both the transmitting and receiving transducers.

The holographic scanner was modified for monostatic transmission by mounting a small transducer on a metal plate alongside the receiving transducer. The same transducer that was mounted on the specimens for the contact experiments was used. It was a piece of PZT material about 1/16-inch in diameter mounted on a 1/32-inch thick piece of aluminum, so that transmission was downward through the aluminum mounting strip. The spacing between the transmitting and receiving transducers was approximately one quarter inch, but the coupling between the two was very slight.

Although the holograms generated by this technique appear to be excellent (see holograms R-5 through S-1, and T-6), the results upon reconstruction were very disappointing. When making the holograms, it was recognized immediately that the top surface of each specimen reflected a very strong signal which would have to be gated out. Consequently, the receiver gate was set to open immediately after the echo return from the top surface of the specimen was completed. Recall, however, that the velocity of sound in aluminum is approximately 1/4 inch per microsecond, so that receive gate would have to be opened within 8 microseconds after completion of the leading edge return pulse in order to see a defect 1 inch below the surface (4 usec transmission time each way). Despite this precaution, some of the surface scattering generally leaked through. However, no signals internal to the specimens were discerned.

Figure 40a is typical of the results obtained on the block specimens with the monostatic technique. The specimen was the single-hole block, and it had 1/8-inch thick rubber pieces glued to the top edges of the block to inhibit radiation from all but the top flat surface of the block. The hologram for this case is R-7. It is interesting to note that although these rubber strips were essentially perfect attenuators for any acoustic propagation through them (transmission), they were excellent reflectors of normally-incident radiation. The reconstructed image of Figure 40a clearly shows the rubber strips glued around the block. However, no image could be focused at any depth within the block. Figure 40b is a similar reconstruction of the single-hole block with the rubber pieces removed. Again the interferogram of the surface may be seen with no sign of the hole.

The same results were obtained later, when a set of ALCOA-A series test blocks were also tested with the two-way transmission. The ALCOA-A series blocks are aluminum cylinders 1½ inches in diameter, and 4 inches long, with holes of varying diameter bored in from one end. The holes have accurately ground flat bottoms, so that when the blocks are placed on end and "looked at" from the top they appear as void defects of different sizes. The voids, varying in size from 1/64 inch to 1/16 inch in the blocks we had, produce very strong echo returns when tested with a conventional pulse-echo two-way transducer in contact with the end opposite the hole. However, as may be seen in the reconstruction of hologram T-6, Figure 41, the 1/16 inch diameter hole cannot be seen.

a. Rubber Pieces Glued to Edges (No Image of Hole)

b. Rubber Pieces Removed (No Image of Hole)

Figure 40. Reconstructed Image of Single-Hole Block-Monostatic Transmission (No Image of Hole)

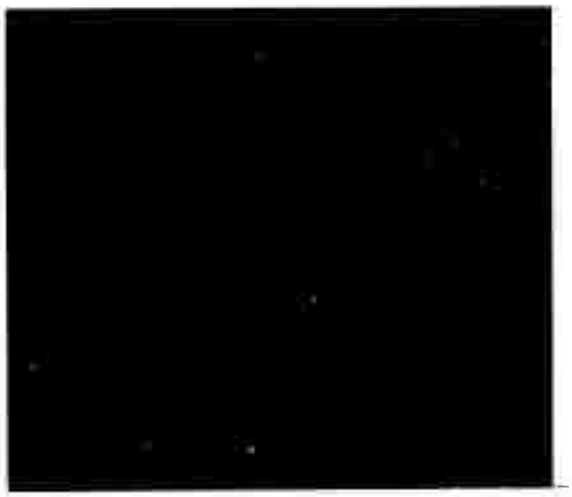

Figure 41. Reconstructed Image ALCOA - Series A Test Block No. 4 - 1/16 Inch Diameter Void, Monostatic Transmission (No Image of Hole)

Care again was taken to gate out the surface return, but just a faint outline of the cylinder may be seen. Focusing through the block also produced no image.

It is reasonable to expect that the greater signal strength received by the pulse-echo test equipment, as compared with the holographic scanner, is a result of the much larger transmitting/receiving transducer used with the pulse-echo equipment. Wide-angle transducers must be used with the holographic scanner in order to attain the full resolution capability of the scanned aperture size. This results in extremely low transmitting and receiving gain (2 to 3 dB gain each way), as compared to the 20 to 30 dB gain each way for the pulse-echo transducers. If higher gain (larger) transducers were used, the simulated voids would have been seen, but at a sacrifice of overall system resolution.

4. Off-Axis Reference

The next system tests were accomplished with an off-axis reference signal. As explained earlier in this report, a reference signal with a linear phase change across the aperture is equivalent to superimposing the interference pattern from the defect on a "carrier" frequency. After transformation of the signal by a lens during reconstruction, the "spectrum" of the defect (its image) is displaced to one side of the optical axis. The interfering conjugate image is likewide displaced, but to the opposite side of the optical axis. Thus, the reconstructed image may be easily separated from the undiffracted light on the optical axis, and the interfering conjugate image, which lies on top of the reconstructed image (but out of focus), when the on-axis reference is used.

The holograms of T-1, 2, and 5 are typical of those made with the off-axis reference. T-1 and T-2 are from the 3-hole block, and T-5 from the single-hole block. Because of the 90-degree phase shift from line to line, the holograms do not have the characteristic patterns of the on-axis holograms, and appear to be more uniform with less contrast. The reconstructions, however, have less clutter than the on-axis ones, and, in general, are somewhat superior. Figure 42 is the reconstruction for hologram T-5, showing the hole in the single-hole

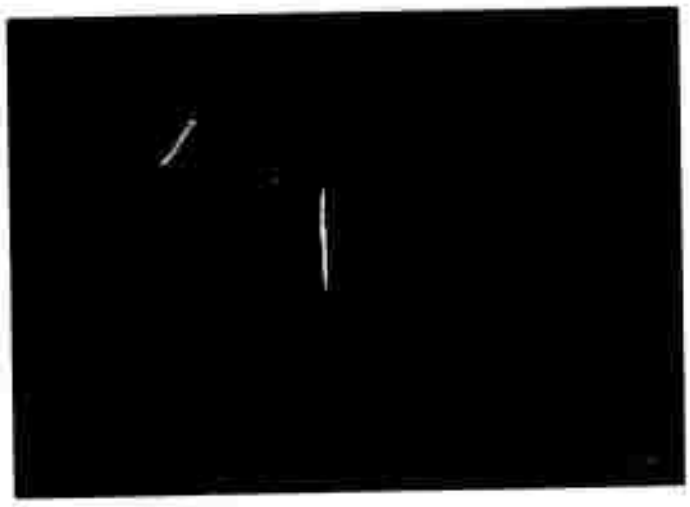

Figure 42. Reconstructed Image, 1-Hole Block, Off-Axis Reference, Immersion Technical

block. Although the exposure of Figure 42 was long enough to show some background clutter near the hole, the overall reconstruction has much less interference than those done on-axis.

Reconstruction of the 3-hole block, hologram T-2, was done by focusing in steps through the block as had been done for the 3-hole block on-axis, in Figure 43. The three reconstructions illustrated in Figure are not as bright as those obtained by the on-axis technique, but show the top, left, and bottom holes in Figure 43a, b, and c, respectively.

The last series of holograms, U-1 through U-11, were made primarily from the last remaining test specimens, although the first four, U-1 through U-4, were another attempt to see the voids in the ALCOA blocks by illuminating from the side with the large transducer, rather than from the top in the monostatic mode.

The largest hole in the ALCOA Series A block #1 was 1/16 inch in diameter, and its image from hologram U-4 may be seen in Figure 44, as a single focused point. It appears, therefore, that with additional power to compensate for the very low-gain transducers used, the two-way transmission would also give good results. This fact was emphasized again on hologram U-9, when the two-way transmission was tried on the resultion block. Some of the resolution holes are faintly visible in the reconstruction of that hologram. This will be discussed later with the resolution block.

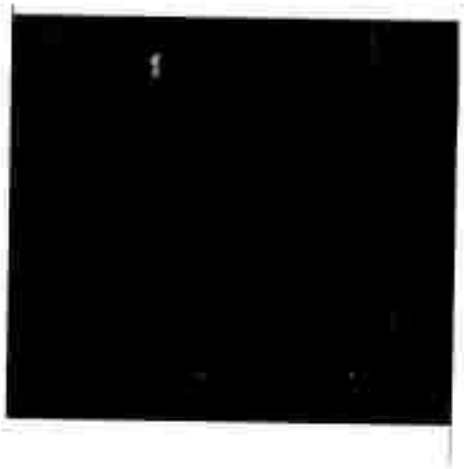

a. Hole at Top of Block

b. Hole Midway in Block to Left of Top Hole

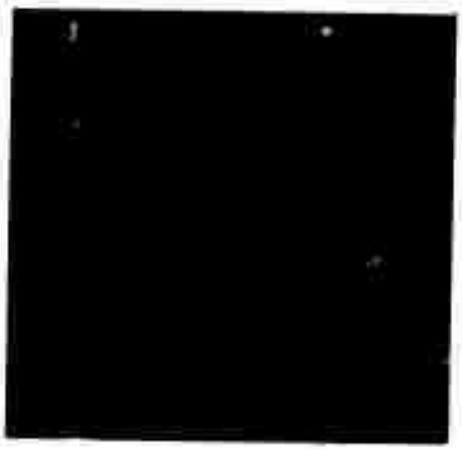

c. Hole at Bottom of Block, Directly Below Top Hole

Figure 43. Reconstructed Images, 3-Hole Block Off-Axis Reference, Immersion Technique

Figure 44. Reconstructed Image of ALCOA - Series A Test Block No. 4 - 1/16 Inch Diameter Void Monostatic Transmission (Void Focuses at Left Center of Photo)

5. Coverage and Resolution

The test specimen made to check internal coverage has 0.040-inch diameter holes drilled into the side of the block very near two of the corners. One hole was drilled 1/4 inch away from the edges at one corner, as shown in Figure 22, while the other was 1/2 inch away from the edges at the diametrically opposite corner. The specimen was made to test whether the corners of the specimen would mask or distort the images from defects in these locations. This specimen also had a broken 0.040-inch diameter drill imbedded in its side at the same location as the hole in the single-hole block.

Hologram U-5 was made of the coverage block with the hole within 1/4 inch of the corner at the top of the block nearest to the illuminating transducer at the right. The hologram plainly shows the zone-plate fringes over the broken drill at the center and the bottom hole at the extreme left. However, there are no fringes to be seen over the top hole, which was closest to the illuminating transducer at the right hand side. Reconstruction of the image from U-5, shown in Figure 45a and b bears out the interpretation of the hologram, showing the bottom hole at the extreme left and the broken drill discontinuity near the center. The top hole to the right cannot be seen clearly.

The hologram of U-6 was made by turning the block over so that the hole 1/4 inch away from the corner was at the bottom nearest the transmitting transducer at the right, and the hole 1/2 inch from the corner at the top furthest from the transducer. The hologram for this configuration shows the fringes for the drill point at the center and the fringes for the bottom hole just to the right of the drill point. The very weak fringes at the extreme left were also present in the hologram U-5, and are not from the top left-hand hole. The reconstruction of this hologram in Figure 45c and d also shows the broken drill and the bottom hole, this time to the right of the drill. The top hole at the left was only seen faintly.

a. Focused on Bottom Hole at Left (1/2 Inch from Corner of Block)

b. Focused on Broken Drill Embedded in Center of Block

c. Block Turned Over, Focused on Broken Drill Embedded in Center of Block

d. Block Turned Over, Focused on Bottom Hole at Right (1/4 Inch from Corner of Block)

Figure 45. Reconstructed Images from Coverage Test Block (see Figure 22e)

It is apparent from the reconstructions of U-5 and U-6, just discussed, that the transmitting transducer was illuminating the center and bottom regions of the test specimen, but not the top. The bottom hole was, thus, adequately illuminated and provided an image regardless of whether it was near or far from the illuminating transducer, or placed directly in a corner. The top hole, not being illuminated, produced a very faint or no image.

Tests made of the resolution test specimen clearly show the six 0.040-inch diameter holes bored into the block. Recall from Figure 22 that the holes in each pair were drilled 1/16, 1/8, and 3/16 inch apart, and the pairs separated by approximately 1 inch from each other. The holograms U-7 and U-8 show the fringe patterns for each pair of holes, and the images of all six holes may be seen in the reconstruction, Figure 46a. All of the images are very close to being in focus at one time since they were all at the same depth from the top of the block. However, there is some difference in depth as may be seen by focusing on only the two end holes in Figure 46b. Since the closest spaced holes were 3 wavelengths in diameter, and spaced on 6 wavelength centers, there was approximately 1-1/2 wavelengths of "land" between the aluminum-to-air discontinuities. The demonstrated resolution is, therefore, very close to the theoretical value of approximately 1 wavelength*.

While the resolution block was in place for the last experiments, a test was made again with the monostatic system, using the small transmitting transducer mounted alongside the receiving transducer on the carriage. The hologram is U-9. This time, more of the top surface of the block was range-gated out, and some of the resolution holes are clearly visible in the reconstructed image. A photograph made of the images is available, but is of too poor a quality to reproduce well in this report.

6. Other Specimens

The final holograms made on this program, U-10 and U-11 were of the bonded specimens described earlier in Figure 23 . Neither of the reconstructed images was useful for NDT analysis. The reflectivity and attenuation of the teflon was such that no energy was intercepted from the intermediate aluminum-to-teflon bond layer. (A test illuminating from the aluminum side was inadvertently not made.) The image of the bonded glass lens showed portions of the hexagonal honeycomb lattice, but not in enough detail to be able to examine the cell bonds.

---

* For a 7.437-inch aperture at 6-inch range and 5MHz frequency.

a. Focused on Center Pair of Holes (Spacing = 1/8 Inch)

b. Focused at Left-Hand Pair of Holes (Spacing = 1/16 Inch)

Figure 46. Reconstructed Images of Resolution Test Block (See Figure 22d) Immersion Technique

SECTION V

BRAGG DIFFRACTION MICROSCOPE

During the investigation and test of the ultrasonic holographic scanner on this program, a brief investigation was also made of ultrasonic imaging by means of the Bragg diffraction technique. This technique utilizes the direct interaction between sound and light fields in a fluid to generate a real-time image of an object illuminated by the sound. Several Bragg imaging systems were built and tested on the program, the final system providing rather good real-time images on a TV receiver monitor. System details and a summary of the results are provided in Appendix A of this report. Additional details are available in the semi-annual technical reports, particularly reference (3).

SECTION VI

ACOUSTIC ARRAY INVESTIGATION

Although the generation of acoustic holograms by means of a mechanical scanner is entirely adequate for experimental work in the laboratory, the length of time required to scan the required aperture mechanically might be prohibitive for many NDT applications. An obvious method of reducing the scanning time is to use an array of acoustic receiving transducers in place of the mechanically scanned single transducer and sample the elements of the array electronically. It was never intended to develop or build such an array on this program, but a brief investigation of imaging by means of an array was made. The results of the study, summarized in Appendix B, indicate that real-time imaging from an ultrasonic holographic system is entirely feasible. Most of the work on this investigation was accomplished on a related Perkin-Elmer IR&D program.

REFERENCES

[1]Preston, K., Jr., Investigation of the Application of Coherent Acoustic Imaging to Nondestructive Testing, Army Materials and Mechanics Research Center, Watertown, Massachusetts, First Semi-Annual Technical Report (27 June 1969) Perkin-Elmer Eng. Report No. 9668.

[2]Arndt, W.R. and Kreuzer, J.L., Investigation of the Application of Coherent Acoustic Imaging to Nondestructive Testing, AMMRC-CR-70-14 Army Materials and Mechanics Research Center, Watertown, Massachusetts, Second Semi-Annual Technical Report (April 1970) Perkin-Elmer Eng. Report 9725.

[3]Arndt, W.R. and Kreuzer, J.L., Investigation of the Application of Coherent Acoustic Imaging to Nondestructive Testing, AMMRC-CR 70-14/2, Army Materials and Mechanics Research Center, Watertown, Massachusetts, Third Semi-Annual Technical Report (September 1970), Perkin-Elmer Eng. Report No. 10332.

[4]Kreuzer, J.L., Ultrasonic Three Dimensional Imaging Using Holographic Techniques, AMRA CR-12F Army Materials and Mechanics Research Agency, Watertown, Massachusetts, Final Report (31 March 1967).

[5]Kreuzer, J.L., Ultrasonic Holographic Imaging in Solids, AMMRC CR 69-05(F) Army Materials and Mechanics Research Center, Final Report (30 September 1969).

[6]Preston, K., Jr. and Kreuzer, J.L., Ultrasonic Imaging Using a Synthetic Holographic Technique, Applied Physics Letter, Vol. 10, No. 5, 1 March 1967, pp 150-152.

[7]Kreuzer, J.L., Proceedings of the Symposium on Modern Optics, Polytechnic Press, Vol. XVII, March 1967, p. 91.

[8]Kreuzer, J.L., and Vogel, P.E., Edited by Metherell, A.F., et al., Acoustical Holography, Plenum Press, (1969).

[9]Stroke, G.W., An Introduction to Coherent Optics and Holography, Second Edition, Academic Press, New York, 1969, p. xi.

[10]Korpel, A., "Visualization of the Cross Section of a Sound Beam by Bragg Diffraction of Light," Applied Physics Letters, Vol. 9, No. 12, 1966, p. 425.

[11] Korpel, A., "Acoustic Imaging by Diffracted Light 1. Two Dimensional Interaction," IEEE Transactions on Sonics and Ultrasonics, Vol. SU-15, No. 3, 1966 p. 153.

[12] Tsai, Chen S., and Hance, A.V., "Optical Imaging of the Cross Section of a Microwave Acoustic Beam in Rutile by Bragg Diffraction of a Laser Beam," the Jour. of the Acoustical Society of America, Vol. 42, No. 6, (1967) p. 1345.

[13] Landry, K., Powers, J., and Wade, G., "Ultrasonic Imaging of Internal Structure by Bragg Diffraction," Applied Physics Letters, Vol. 15, No. 6, (1969), p. 186.

APPENDIX A

ULTRASONIC DIFFRACTION MICROSCOPE

1. Theory

The ultrasonic diffraction microscope uses the linear Bragg angle diffraction of light by the ultrasonic field to form an optical "image" or map of the ultrasonic field.[10-13] Figure 1 illustrates the principle of operation in two dimensions. A point source of light (ℓ) is weakly diffracted by the ultrasonic waves emanating from a point-source of sound (s) in a material transparent to both waves, such as water. The ultrasonic field is weak enough so that only a small amount of the light source (ℓ) is diffracted. This makes the interaction linear. Thus, the optical and acoustic fields can be expanded into sums (integrals) of plane waves, and each differential plane-wave component treated alone. Each point source is expanded as a uniform distribution of plane waves propagating in all directions and whose relative phases are the same at the center of the point. This is represented by the "rays" starting from the point sources. These rays are actually the propagation vectors of the plane-wave components of the point sources. Wherever rays intersect, the corresponding plane waves have similar phases. Where many plane wave components have similar phases, they interfere constructively to produce a bright point image.

Each ultrasonic plane-wave component diffracts a small portion of an optical plane wave only if the two waves are at the Bragg angle. The diffracted wave is also a plane wave propagating at the diffraction Bragg angle. The fraction of the optical plane wave diffracted is proportional to the ultrasonic plane-wave component involved. The temporal frequency of the diffracted optical plane waves differs from the incident optical plane waves by the ultrasonic temporal frequency. This frequency shift will be ignored for now. The ultrasonically diffracted optical field contains one optical plane-wave component for each ultrasonic plane-wave component and, thus, produces an image of the ultrasonic field.

In Figure 1, the large circle (C_1) has a radius (d), where (d) is the distance from (ℓ) to (s), and is centered at the point (s). The small circle (C_2) has a diameter (g) and passes through the points (ℓ) and (s). A mathematical analysis of Bragg angle diffraction based on this diagram will show that the optical plane-wave components leaving the optical point source (ℓ) and diffracted by the ultrasonic point source(s), appear to have originated from point (i). This implies that (i) is the image of (s).

If the imaging process is considered in three dimensions, there are two cases of special interest:

(1) The light source (ℓ) is a coherent line source emitting cylindrical waves, and

(2) The light source (ℓ) is a coherent point source emitting spherical waves.

First we will consider the case where (ℓ) is a line source. In the third dimension the image (i) is actually a slightly curved coherent line perpendicular to the plane of Figure 1. The acoustic point source (s) has been mapped into a line. A suitable set of high quality cylindrical lenses can be used to compress this line image into a point, to form a one-to-one ultrasonic imaging system.

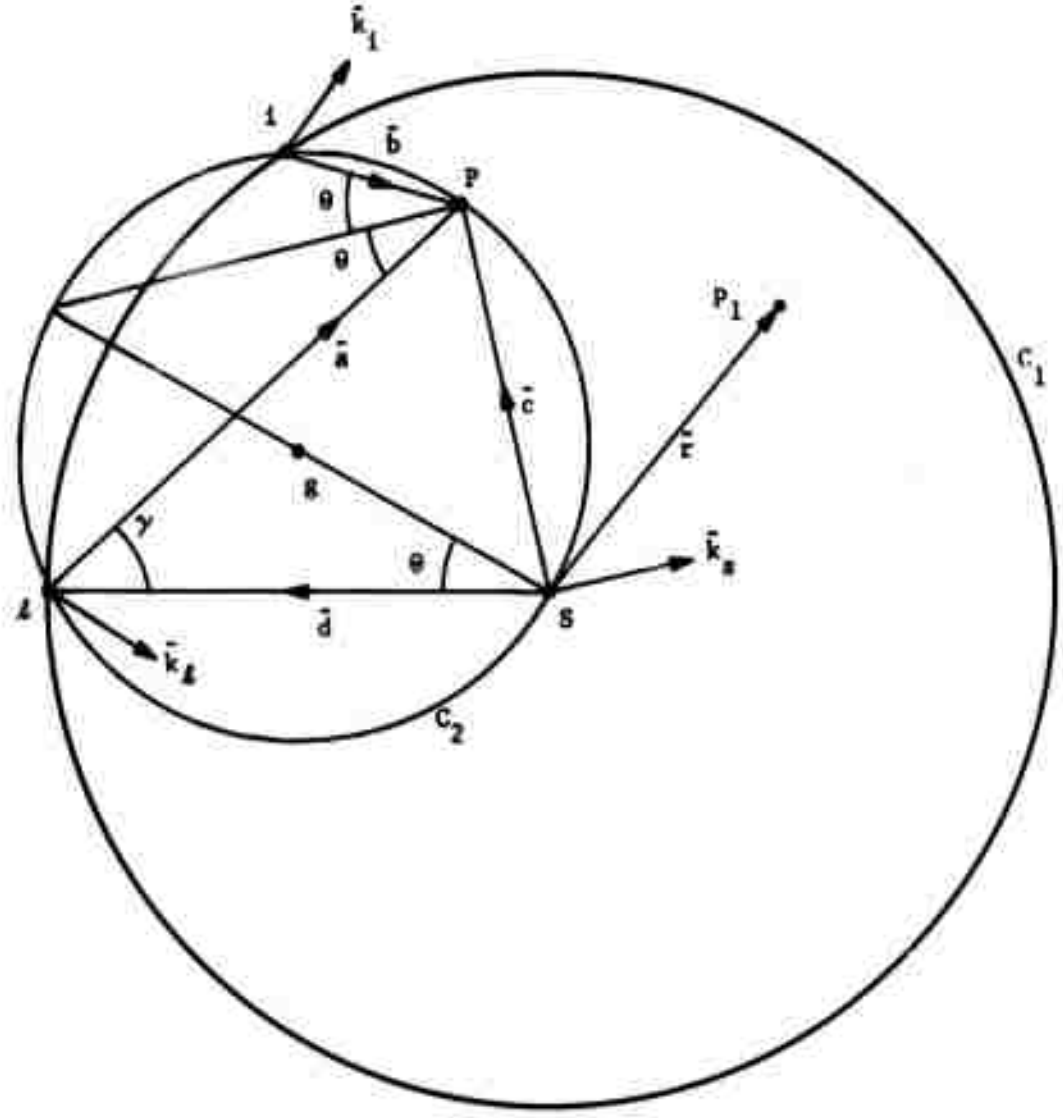

Figure 1. Bragg Angle Imaging Relations

In the second case, (ℓ) is a coherent optical point source emitting spherical waves. Figure 1 thus has rotational symmetry about the line (d). Therefore, we may rotate Figure 1 about line (d) as an axis to find that the image (i) becomes a circle centered about the line (d). Circle (C_1) has become a sphere, and circle C_2 has become a doughnut without a hole. The optical image of an acoustic point source is a circle centered on the straight line drawn through the illuminating optical point source and the acoustic point source, and lying on the intersection of the sphere (C_1) and the holeless doughnut (C_2). Acoustic points are mapped into a unique family of circles. It is possible to compress these circles back into point images by optical holographic techniques, using an acoustic point source, or transparent holographic filter.

2. Experiments

Preliminary experiments were done with lens and mirror breadboard systems using a spherical point source. A one-milliwatt fundamental transverse-mode helium-neon laser with a wavelength of 0.63μm provided the light source. The ultrasonic point source was formed by a one-centimeter diameter quartz transducer crystal radiating into a 7-cm diameter, 7-cm radius-of-curvature glass mirror. The ultrasonic frequency was 5MHz, and the acoustic power was approximately 0.25 watts. Both lens and reflecting mirror optics were used to read out the final image.

Figure 2 is a photograph of the ring pattern produced by a point acoustic source on the optical axis. Only part of the diffraction ring image shows, because the acoustic point source formed in the tank is not a true point source emitting spherical waves, but only a small part of a spherical wave. Only sound rays with angles corresponding to the waves emitted by the one-centimeter diameter transducer are present.

Figure 2. Light Intensity Distribution in Diffraction Plane of Ultrasonic Diffraction Microscope

Upon completion of these early experiments, a Bragg ultrasonic imaging system was built, based upon a line source of light. The system was a modification of the basic system that has been used by others. The major difference is that in this system the light line source was placed within the cell near the object to be imaged, whereas others have this source placed external to the cell. The reason for doing this is that resolution in the direction perpendicular to the line source is a function of the angle subtended by the rays forming the source in this direction. The resolution is essentially proportional to the sine of the half angle subtended by the aberration-free rays. It is difficult to get an aberration-free line-source subtending a large angle without using specially designed lenses. If we use only simple single-element plano-cylindrical lenses, the lowest-aberration large-angle line source is produced by using the shortest focal length lenses possible, rather than trying to project the line source outside of the tank as has previously been done. Resolution in the other direction is a function of the angle subtended by the length of the line source and the point in the sound field.

We can note the nature of the image formed by the optical line source and an acoustic point within the Bragg cell with the aid, again, of Figure 1. The line source can be synthesized by the principle of linear superposition by placing a point source on top of a point source until we have synthesized a vertical line source to the required length. Each of these point sources will form a ring image, as previously described, centered on the line through the point-source sound source. All of the point sources are assumed to be in phase to form the equiphase line source. The rings are equiphase circles, except for a relative phase term which we will neglect at this time. Piling point source upon point source merely approximates convolution in order to form the line source. The corresponding convolution of the image rings produces two curved lines. The two curved lines are approximately in the plane that contains the line source and is perpendicular to the shortest line between the point of sound and the line source. The ends of the image curve away from the line source, and are closest to the line source at the point where the line source is closest to the acoustic point source. These curved lines form an astigmatic point image. That is, the best horizontal focus is different from the best focus in the vertical direction.

The scale of the optical image in the Bragg cell is: 1) the ratio of the optical to the acoustic wavelength in the cell, perpendicular to the line source, and 2) unity in the direction parallel to the line source. The optical image in the cell, thus, has both a distorted scale and astigmatic focus.

Figure 3 shows a top and side view of our experimental line source imaging system. Laser light is incident from the left. The lenses served the following purposes. Lens L1 was a microscope objective that diverges the laser beam. Lens L2 recollimates the expanded beam. Cylindrical lens C1 forms the equiphase line source in the center of the Bragg imaging cell. Cylindrical lens C2 recollimates the line source. The collimated light then falls on lens L3, and is focused to a point. The power axis of the cylindrical lenses are parallel. Lens L4 relays the optical image onto a closed-circuit television vidicon connected to a monitor as a convenient display. The spherical lenses were inexpensive, but good quality, commercial microscope objectives for lenses

L1 and L4, and telescope objectives of 5-cm diameter for lenses L2 and L3. The general quality of the spherical and cylindrical lenses, Bragg cell, and alignment was such that the overall system was close to diffraction limited for the non-imaging light with the stops in place. The cylindrical lenses, C1 and C2, were single-element plano-cylindrical lenses.

The optical system contains three major stops. Stop S1 is a small pinhole, 25μm in diameter, that passes the main laser beam and blocks scattered light. Stop S2 is used to restrict the angular content of the line source. Stop S2 is an adjustable rectangular slit 1 to 4 cm long parallel to the line source, and 0.5 and 1.5 cm wide perpendicular to the line source. Most of the pictures were made with Stop S2 set to a width of about 1 cm, and a length of 4 cm. The focal length of the cylinder when measured in the water is about 7 cm, so that the 1-cm-wide slit corresponds to an f number of 7. This was presumably the diffraction-limited aperture of the combined system in this direction, because enlarging the aperture improved the resolution until the 1-cm limit was reached.

Stop S3 is a razor blade placed at the focus of lens L3, as shown in the lower half of Figure 3. The prime purpose of Stop S3 is to remove the undiffracted, or zero order light, which does not contribute to the image. The focal point of lens L3 should contain all of the light from the line source that has not been diffracted in forming an image. This stop could have been a single spot to block the undiffracted point of light focused by lens L3.

The source of sound was a 5-cm-diameter X-cut quartz transducer backed by silicone rubber. The backing provided strength, and repaired a crack in the transducer. It was not possible to monitor the voltage directly at the transducer. However, the total acoustic power radiated was about 1 watt. The transducer was operated continuously at a frequency of 5MHz. This frequency was chosen to provide low attenuation through various moderate lossy materials. The total laser beam energy in the apertured line source in the Bragg cell was attenuated to between approximately 10 and 100 microwatts. The laser was a helium neon laser operating in the fundamental Gaussian spatial mode. The laser wavelength was 0.6328μm. The image on the face of the vidicon contains about 0.1 microwatt of light.

The optical image was projected directly onto the face of the vidicon from a standard commercial closed-circuit television system. The television operated at 30 complete frames per second with the scan lines interlaced in the conventional method.

3. Experimental Results

One of the advantages of ultrasonic Bragg diffraction imaging is that it is a real-time imaging technique. In our system, objects to be imaged could be moved around within a cubic volume of approximately 5 cm on a side on either side of the line source. Objects on the transducer side of the line source are imaged by transmission or shadowing, whereas objects on the other side of the line source are imaged by sound reflected from the object. The pictures shown in this section are Polaroid photographs of the closed-circuit

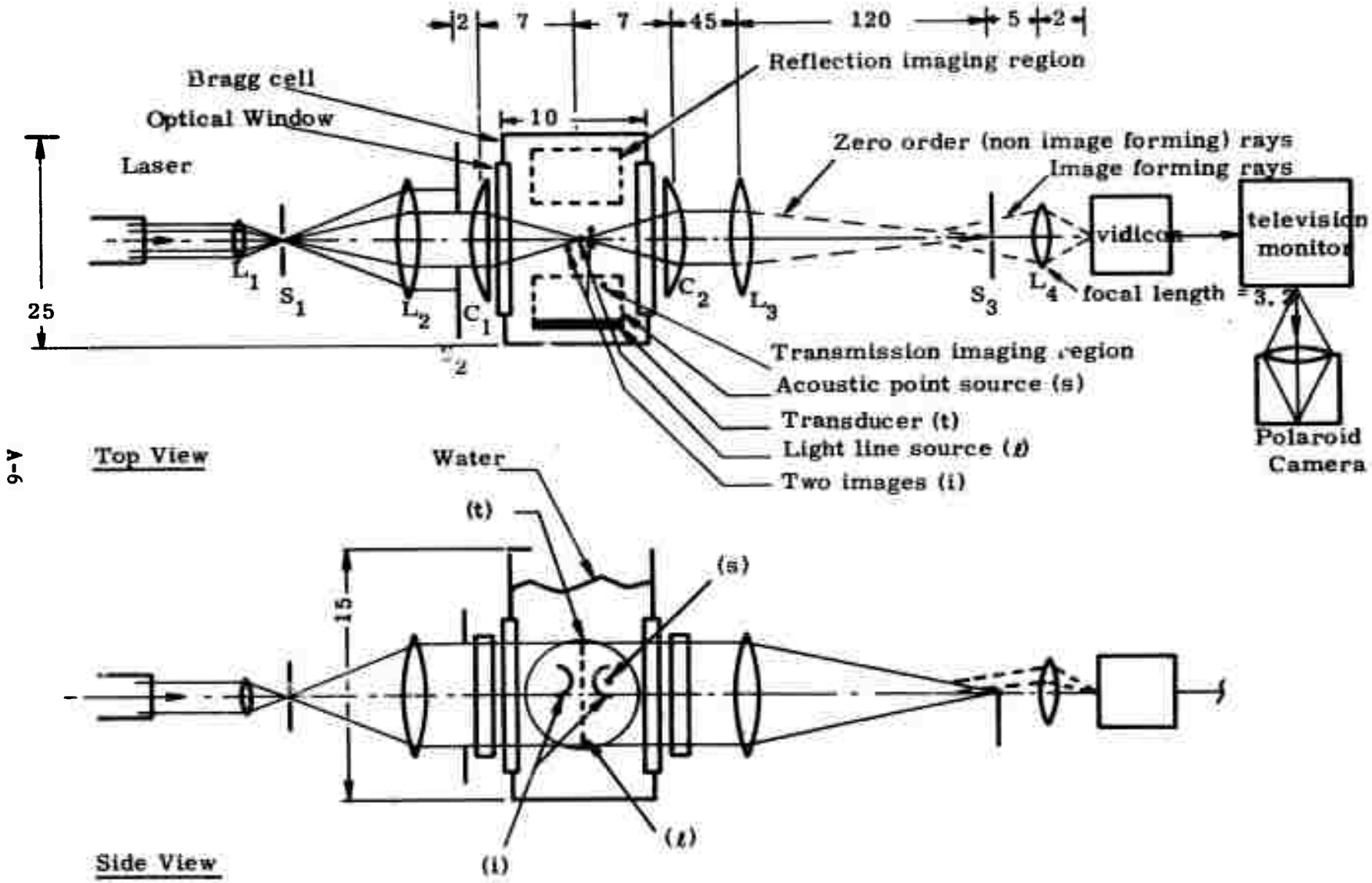

A-6

Figure 3. Experimental Line Source Bragg Angle Diffraction Imaging System

This sketch is not drawn to scale. All numbers are in centimeters. System details are discussed in the text.

a.

b.

c.

Figure 4. Acoustic Images of Thin Wires.
(Details are in the text.)

a. Image in transmission (shadow) made by the experimental Bragg imaging system.

b. Image made by reflection by the original holographic camera of reference 8 in 1966.

c. The wire object. The letters are about 3 cm tall.

television monitor. The low spatial frequency intensity variations and the small bright dots are defects of the closed-circuit television system. White in these pictures corresponds to the presence of sonic energy, and black to the absence of sonic energy. The bright background from the transducer on the pictures made by transmission is restricted in the vertical direction by the length of the line source, which was less than the length of the transducer. The transducer was moved around so that sometimes the top, bottom, or a region of both was truncated. In general, the images were best when the transducer was approximately parallel to the optical axis, but tilted one to ten degrees with respect to the line source.

Figure 4a is an image of the wire letters P-E made by transmitted sound. Figure 4b is the image made of the same letters made by reflected sound with the original holographic camera in 1966. The missing portions of the letters from the holographic camera image are due to specular reflection of the incident sound. The Bragg diffraction image is a shadow image made in transmission, whereas the holographic camera image is a reflection image. In each case, the letters are parallel to the prime image-forming plane. Both systems operated at 5MHz and, as can be seen in the pictures, have similar resolution. If the image of the letters P-E were repeated with the currently improved camera system, it would be slightly better. The resolution in the horizontal direction was measured experimentally to be about the same as the horizontal resolution. Figure 4c shows the metal wire letters P-E.

Figure 5a is the transmission image of two glass discs 5 cm in diameter. Each disc was 9 mm thick. The two blocks were bonded face to face, except in the two semiconductor regions visible in Figure 5a. The glass block was oriented so that sound coming directly from the transducer that hit the front face was reflected so that it did not enter into the image formation. The block was thus at a slight angle in the vertical direction to both the ultrasonic transducer and the line source. Very small tilts were made about this angle until the sound transmission was a maximum. This indicated that sound was bouncing back and forth within the bonded glass discs. The image changes very rapidly as the block is tipped, depending upon whether the block is tipped so that the multiple sound fields are reenforcing or cancelling. The large defect is on the left; the smaller defect is on the right. The bright region at the upper right of Figure 5a is diffraction from the illuminating transducer where the sound passed around the edge of the disc. The circular disc is distorted because the horizontal and vertical magnifications were different, as previously mentioned. The glass disc dramatically illustrates the advantage of real-time imaging, because it was possible to manipulate the piece and observe the different images from different angular orientations. A single still picture cannot adequately illustrate the value of the real-time image that can be observed as the part is moved.

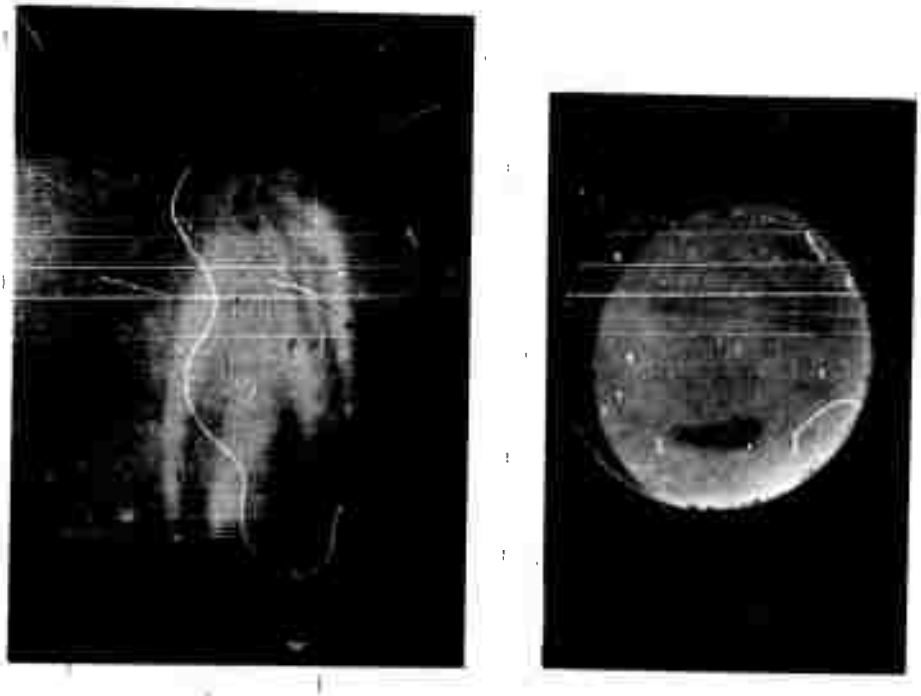

a. image b. object

Figure 5. Transmission Image of Bonded Glass Discs. The Discs are 5cm in Diameter and 9mm Thick. There are two Unbonded Regions to the Left and Right of the Center that Appear Darker in Each Photo. More details are in the text.

Figure 6a is the image made of a microwave stripline circuit board by reflection. Figure 6b is a similar picture made by transmission. Figure 6c is a photograph of the copper side of the stripline. The stripline board is a 3-layer laminate consisting of a backplate of aluminum 0.8mm thick, an intermediate layer of polyolefin 0.8mm thick, and a top layer of copper which is 36μm thick. Copper has been removed to form the stripline pattern shown. The copper strips are 2.4mm wide. The gap between the top bar and bottom U-shaped strip is 0.4mm. The copper plating thickness is approximately 1/8 of the acoustic wavelength in water. Both the copper and the polyolefin reflect the sound in the reflection image of Figure 6a. The copper side was facing the transducer for the reflection image. Both the polyolefin and copper have similar brightness in the image of Figure 6a, and hence reflect the same amount of sound. However, the copper is outlined as a black line. The outline of the copper, including the narrow 0.4mm gap, is probably caused by diffraction produced by the acoustic phase discontinuity at the polyolefin-copper edge. There is probably a phase change due to both different material acoustic properties and the mechanical step. Figure 6c which shows the object in transmission, also shows an approximately similar amount of sound passing through the copper clad and unclad regions. Again, the edge of the copper seems to be visible due to diffraction.

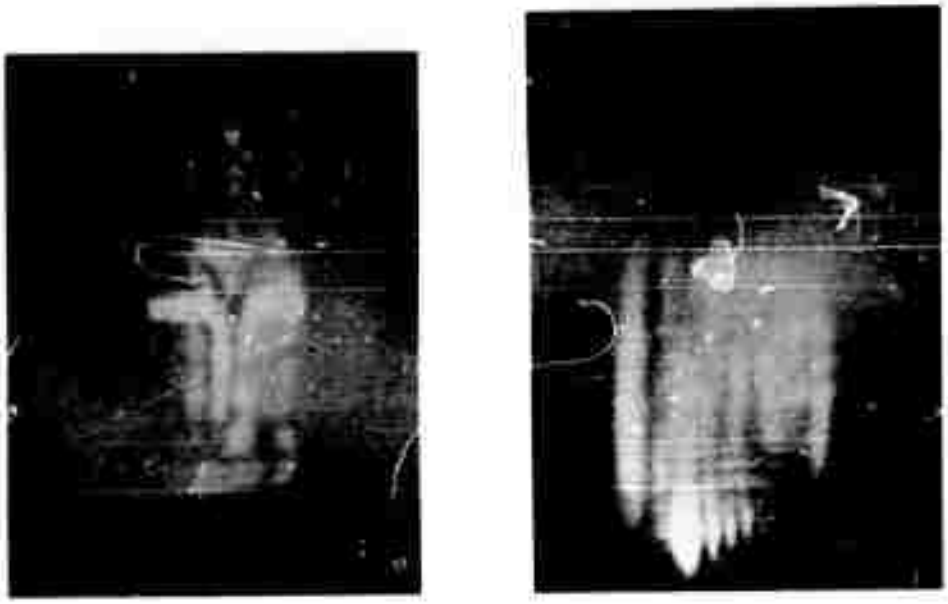

a. b.

c.

Figure 6. Images of a Clad Plate

The object is a printed circuit board consisting of a 0.8mm aluminum backing, 0.8mm polyolefin center and 36μm copper etched to the pattern shown. The board is 38mm wide. More details are in the text.

a. The image by reflection

b. The image by transmission

c. The object

These pictures were not very sensitive to alignment. Thus, there seems to be no problem about sound bouncing around within the object due to attenuation within the polyolefin region. This attenuation reduced the intensity of the transmission image. Thus, the imagery is impaired by background light scattered by the water and optics, and light diffracted by the stop. This scattered light is most visible at the bottom of the image.

4. Conclusions

The advantage of working in real time with an acoustic imaging system becomes very apparent after only a few minutes of experimenting on a real-time Bragg imaging system. Unfortunately, after a few minutes of experimenting, some of the difficulties become apparent, also. It appears that there is need for further work in both theoretical and experimental exploration of alternate imaging geometries and schemes. Some experimental difficulties include the following: diffraction speckles and specular reflections due to the spatial coherence of the illuminating sound become very apparent, and are a nuisance. This imaging system requires a quasi-monochromatic, or temporally-coherent sound source, but a large-angle, spatially incoherent source could be used to eliminate and minimize some of the specular reflection problems. It would be desirable to develop such a source for a Bragg angle imaging cell.

A second problem stems from acoustic reflections within the object. It would be desirable to be able to gate the sound which forms an image for the Bragg diffraction microscope, in the same way that we gate the image-forming sound in the holographic camera. This implies both gating the sound incident on the object and the laser beam so that the laser beam coincides with the desired region of the sound that we wish to form an image. No change should be required for the television monitor system. The television vidicon tube is an image storing device that can store the transitory image and scan it off in real time, so that we would still be able to have a real-time imaging system.

A third troublesome phenomenon is scattered light. Non-image-forming light is scattered by the optical surfaces and the water cell. Most of the undesired scattered light came from the water within the cell. In our system, the object to be imaged went directly into the water through which the light beam also passed. It should be possible to place a thin membrane divider which would keep contaminants from the object out of the region where the light passes. Even if this were done, there would still be a problem with scattered light.

The problem of scattered light can be minimized by keeping the acoustic level within the Bragg imaging cell high enough so that an appreciable amount of light is diffracted. Appropriate apertures, some of which were used here, can minimize scattered light. It is naturally assumed that clean distilled water, and good quality, low-scatter optical surfaces are used in this system. Distilled water will stay clean longer than tap water. The higher the frequency, the smaller the acoustic wavelength and the larger the image diffraction angle is, so that scattered light becomes less of a problem because most of the scattered light is diffracted at small angles. It is also possible to conceive of a heterodyne type of system to minimize the effect of scattered light because the scattered light has the same temporal frequency as the laser, while the image-forming light is either raised or depressed by the acoustic frequency. In general, a heterodyne imaging system would not work with the unmodified vidicon closed-circuit television.

Although any wavelength can be used with the Bragg imaging technique, it should be most useful for small objects at high frequencies, and hence for high resolution, because the small objects have lower total attenuation than large objects, and, in general, a higher acoustic power level is required to interact with a laser beam for Bragg imaging than would normally be required with a piezoelectric transducer.

A Bragg angle diffraction imaging system should be capable of operating over a wide range of wavelengths and of the parameters, to provide real-time acoustic imaging.

APPENDIX B

ACOUSTIC ARRAY INVESTIGATION

1. General

Although the generation of acoustic holograms by means of a mechanical scanner is entirely adequate for experimental work in the laboratory, the length of time required to scan the required aperture mechanically might be prohibitive for many NDT applications. It takes from 30 minutes to 1 hour, depending on the spacing used between scan lines, to scan a $7\frac{1}{4} \times 7\frac{1}{4}$ -inch aperture with the scanner used on this contract. In order to scan such an aperture in near real time, some type of electronic scanning is required. An obvious method of accomplishing this is to use an array of acoustic receiving transducers in place of the scanned transducer and sample the elements of the array electronically. Although it was never intended to build such an array on this contract, it was planned to investigate briefly their capabilities and limitations as related to holographic imaging and make recommendations for their use in the NDT application. The remainder of this Appendix summarizes the results of this investigation. A more complete analysis was given in Appendix B of the third semi-annual technical report, reference 3.

2. Technical Considerations

A method of attacking the design of an acoustic array to be used for image formation is to consider the array as a two-dimensional sampling system. The elements of the array sample the acoustic pressure field scattered from an illuminated object, and if the samples are properly spaced and processed, a true replica of the image can be produced from the sampled data. The procedure is similar to the one-dimensional sampling of a band-limited temporal waveform by a train of sampling pulses in telemetry and communications applications, and the subsequent reconstruction of the original waveform by proper filtering of the sampled spectrum. In that case, it is well-known that if the sampling frequency exceeds twice the highest signal frequency contained in the band-limited function, a faithful reproduction of the object can be obtained. A similar relationship exists for the image produced by an imaging array.

The philosophy behind the sampling technique and its application to an imaging system may be understood by examination of Figure 1. Figure 1 illustrates the waveforms and functional relationships existing at various stages of the sampling/reconstruction process. Although the diagram has been simplified to cover only one dimension, the indicated relationships are equally valid for two dimensions. Other assumptions made in the analysis are that the magnification factors between the various planes are equal to unity, and that the distances between them are such that the Fraunhofer field conditions prevail. Although the

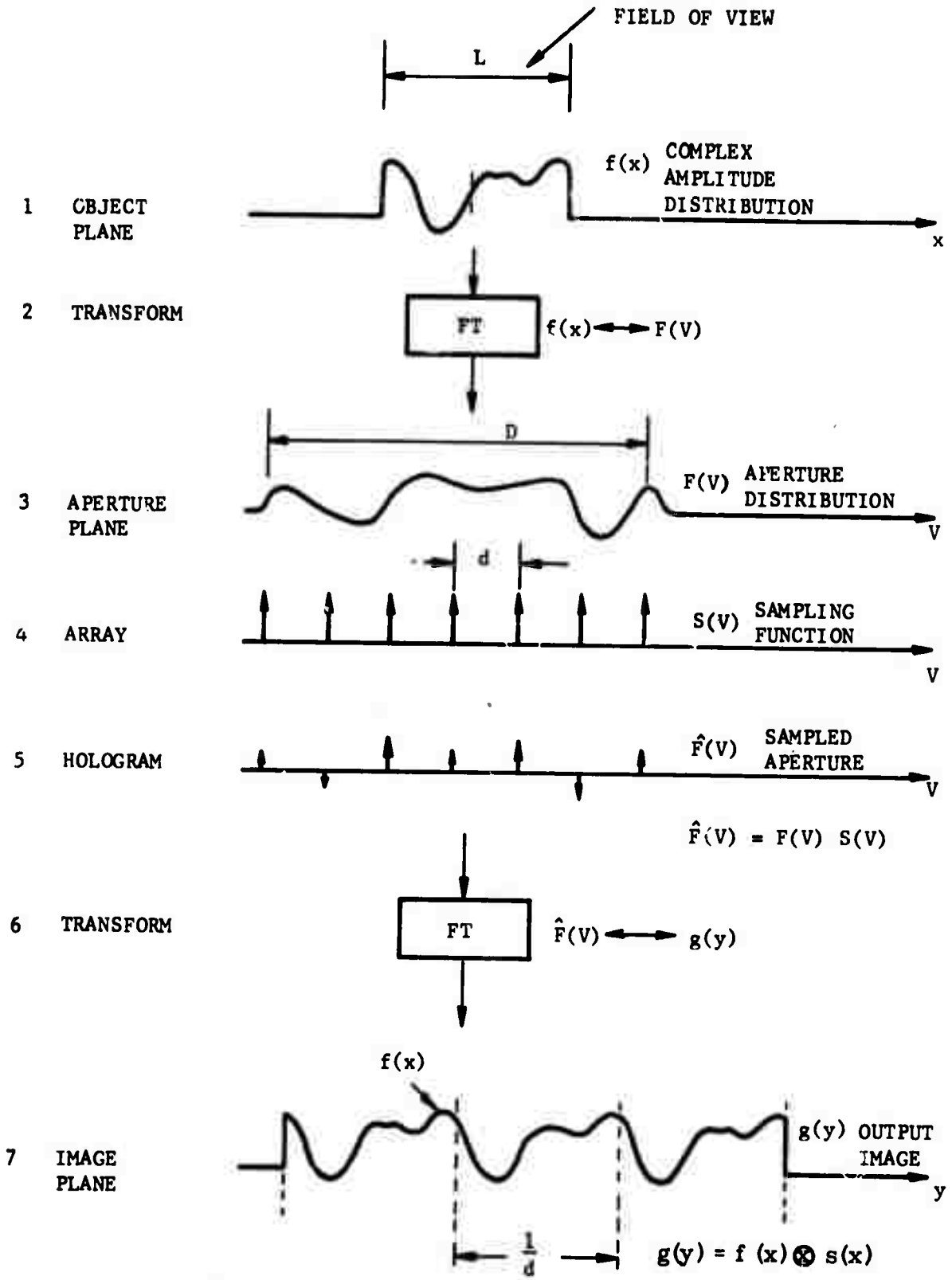

Figure 1. Imaging Array - Functional Relations

aperture size for an imaging array may place the object in the Fresnel region of the array, thereby invalidating the last assumption, the basic theory is not affected appreciably by this difference, especially if the Fresnel zone array is focused.

The top line in Figure 1 indicates the signal waveform f(x) scattered by an object or target. The signal exists only over the L dimension, and is zero elsewhere. It is f(x) that we wish to produce faithfully in the final image by the sampling and imaging system. The signal is a complex signal, having phase and amplitude characteristics. When f(x) is intercepted within the Fraunhofer region of an aperture, the signal waveform, F(V), in the aperture plane is the Fourier transform of the object function f(x). It is shown on line 3 of Figure 1. In general, a reciprocal relationship exists between the object and aperture planes, such that a small dimension in x transforms as a large dimension in V, and vice versa.

Although the signal, F(V), is continuous in the aperture plane, it becomes a discontinuous signal, $\hat{F}(V)$, if the aperture is sampled by the elements of an array. The array element sampling is indicated by the uniformly periodic series of N delta functions, $S(V) = \sum_{N} \delta(V-nd)$, on line 4, and the sampled data output by the function $\hat{F}(V)$ on line 5. If the sampled output of the aperture indicated on line 5 is stored on a film, the record is called a hologram, and the remainder of the sampling-reconstruction process would be accomplished optically. The sampled output can be processed in other ways, however, such as in near real time by a computer.

Reconstruction of the sampled aperture function, $\hat{F}(V)$, is obtained by taking the inverse Fourier transform of the sampled function by optical or computer means. Because of the fact that the transform of a train of delta functions, $\delta(V-nd)$, is also a train of delta functions, $1/d\delta(y-n/d)$, separated by 1/d (the reciprocal of the spacing d of the sampling train in the aperture plane), the resultant output consists of displaced copies of the original object function, f(x), separated by a distance 1/d, as shown on line 7 of Figure 1. This result may be readily derived from the relationship between the input and output signals of a linear system.

3. Experimental Results

Since the hologram transparency produced by the scanning system is a permanent record of the acoustic field sampled by the receiving transducer in the water, array imaging experiments may be conducted very conveniently by using the hologram instead of a physical array. This is accomplished by sampling the hologram transparency according to the desired array configuration as shown in Figure 2, and then taking the transform of the sampled hologram to produce the image. Experiments were performed using both the optical reconstruction system (lens) and a digital computer to take the transform and form the image. However, most of the work was done with the computer.

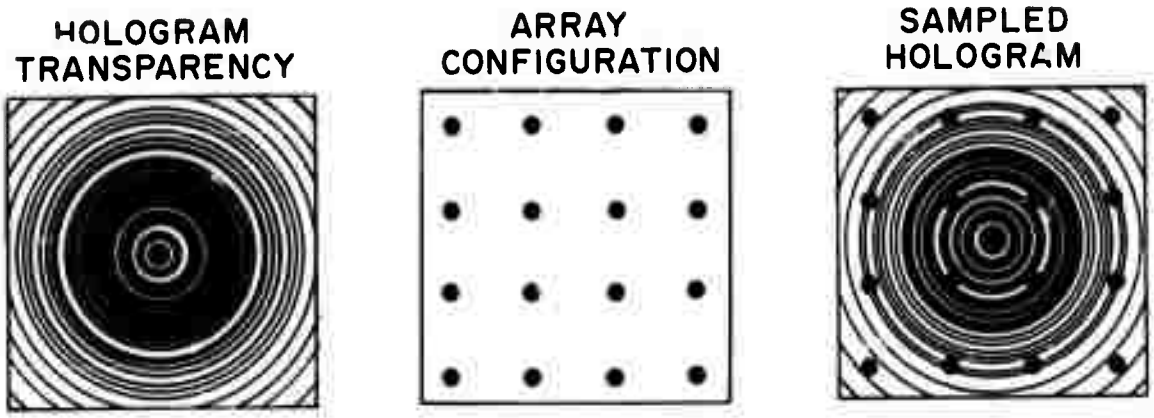

Figure 2. Optical Imaging-Acoustic Array Simulation

Because a sampling array breaks dowr. the hologram image into a set of discrete data points, the image may be formed by taking the Fourier transform with a digital computer. Although this would have been impractical several years ago because of the long computer processing time required to make the transform, it is now very practical and economical using a Fast Fourier Transform (FFT) algorithm. The FFT algorithms allow discrete Fourier Transforms to be accomplished in times proportional to the size of the array instead of in proportion to the square of the size.

Experiments were performed on the production of images from array-sampled holograms, using a FFT algorithm on a digital computer. The input data for the computer image was obtained by sampling the transmissivity of an actual hologram transparency in an array pattern. The computer output image was plotted as a perspective plot on a standard two-axis plotter. A block diagram of the technique is shown in Figure 3.

The first hologram chosen for the computer imaging experiment was the acoustic image of a 1-inch diameter steel ball made at a range of 40 inches. To obtain the longer range with our horizontal scanner, an acoustic reflector was installed at a 45-degree angle beneath the scanner, as indicated in Figure 4. The ball object was placed at point 0 in the tank and illuminated by the transmitting transducer, T, located at the bottom of the tank near the reflector.

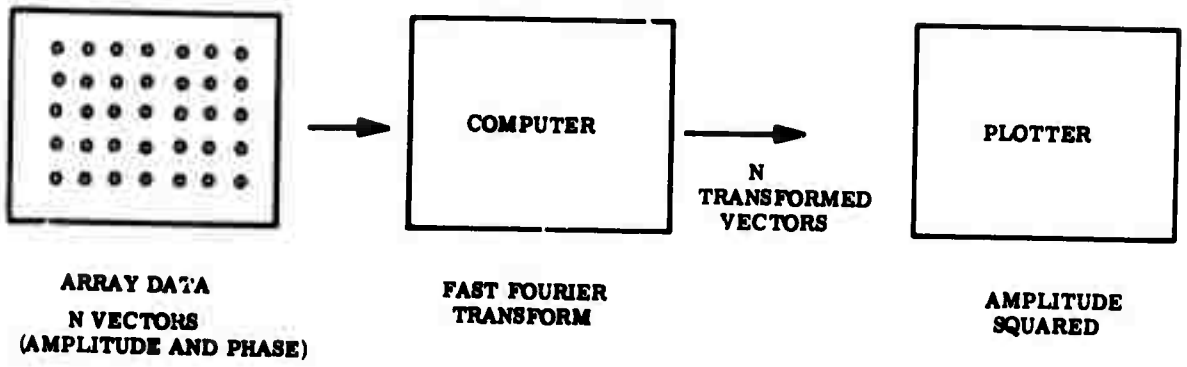

Figure 3. Computer Imaging - Acoustic Array Simulation

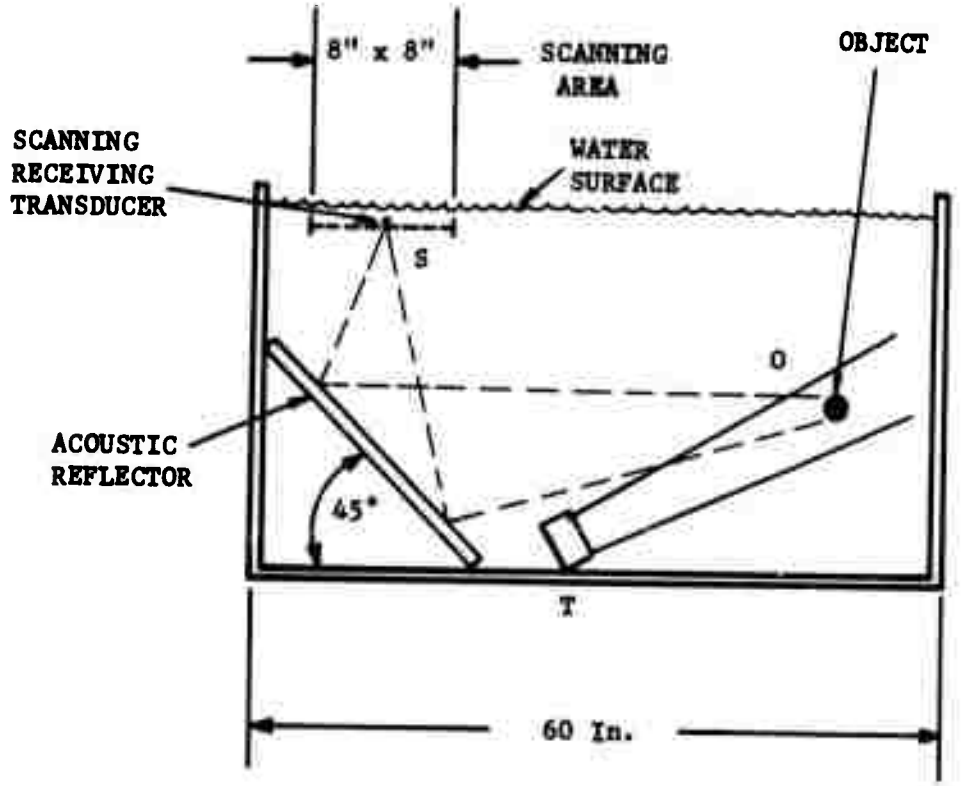

Figure 4. Acoustic Reflector in Water Tank to Extend Range

The hologram generated from the one-inch diameter steel ball is shown in Figure 5. Note that it is a "text-book" copy of the Fresnel zone plate generated by the interference of spherical and plane wave sources in optics. The ball, behaving as a point-source radiator, scatters a spherical wave front that interferes with the transmitted reference signal in the receiver. The reference signal is equivalent to a plane wave.

The image reconstructed from the ball by the optical system is a single bright pin-point of light, focusing sharply at a range equivalent to 40 inches in the water. When the image is greatly magnified, it is found to be the two-dimensional transform of the square hologram aperture.

To form the computer image of the ball hologram, the optical transmissivity of the hologram was sampled at 1024 points by an automatic scanner (Line Scan Image Generator - LSIG). An 8x10-inch enlargement of the hologram negative was used in the LSIG and transmissivity samples taken over a 32x32-inch square matrix. The transmissivity data samples were encoded on magnetic tape for use by the computer.

Before taking the FFT of the sampled hologram data on the IBM-360/67 computer to obtain the image, some additional programming had to be done. The additional programming was required to "focus" the image and center it on the plotter. The focusing was entirely analogous to the optical focusing of the hologram and consisted of introducing a quadrature phase change into the array elements which shifted the phase of the input data vectors radially outward from the center of the hologram. The introduced phase change just cancelled the phase change caused by the spherical wavefront. Programming to center the plot was accomplished by introducing a linear phase shift of the proper magnitude across the array elements in each dimension. The centering is required because of the nature of the FFT algorithm, which places the center of the output transform at one corner of the output data array.

The output image of the ball hologram plotted by the computer is illustrated in Figure 6. The plot is a three-dimensional plot of the output amplitude squared (intensity), and is displayed in perspective on a conventional two-axis plotter by means of a plotting program. The plotting program removed all hidden lines automatically during the plot to enhance the display.

The reconstruction of an image from an acoustic hologram by computer has demonstrated the feasibility of this technique for future real-time acoustic holographic imaging systems.

Figure 5. Acoustic Hologram of 1-inch Steel Ball at 40-Inches Range

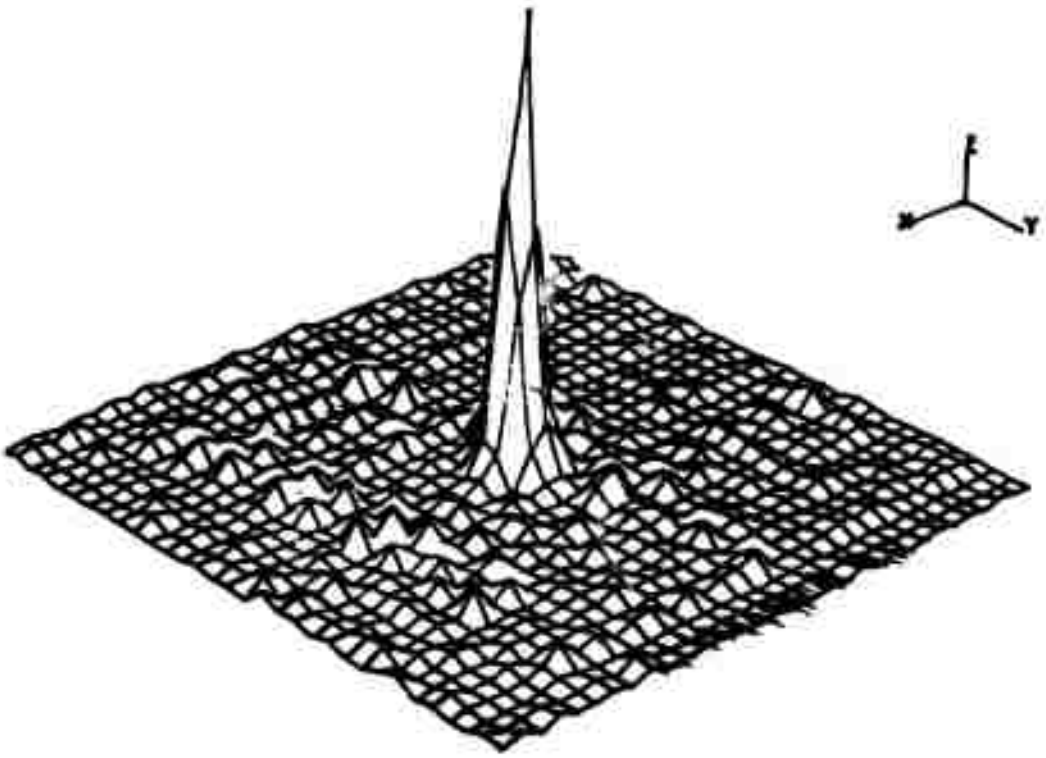

Figure 6. Perspective Plot of Ball Image Generated by Computer